

Old Dominion University  
**ODU Digital Commons**

---

Mathematics & Statistics Theses &  
Dissertations

Mathematics & Statistics


---

Summer 2009

## An Adaptive Method for Calculating Blow-Up Solutions

Charles F. Touron  
*Old Dominion University*

Follow this and additional works at: [https://digitalcommons.odu.edu/mathstat\\_etds](https://digitalcommons.odu.edu/mathstat_etds)

 Part of the [Algebraic Geometry Commons](#), and the [Ordinary Differential Equations and Applied Dynamics Commons](#)

---

### Recommended Citation

Touron, Charles F. "An Adaptive Method for Calculating Blow-Up Solutions" (2009). Doctor of Philosophy (PhD), Dissertation, Mathematics & Statistics, Old Dominion University, DOI: 10.25777/1vgh-ev86  
[https://digitalcommons.odu.edu/mathstat\\_etds/62](https://digitalcommons.odu.edu/mathstat_etds/62)

This Dissertation is brought to you for free and open access by the Mathematics & Statistics at ODU Digital Commons. It has been accepted for inclusion in Mathematics & Statistics Theses & Dissertations by an authorized administrator of ODU Digital Commons. For more information, please contact [digitalcommons@odu.edu](mailto:digitalcommons@odu.edu).

**AN ADAPTIVE METHOD FOR CALCULATING  
BLOW-UP SOLUTIONS**

by

Charles F. Touron  
A.B./B.S. May 1994, Elon College  
M.A. July 1999, East Carolina University  
M.S. May 2002, Old Dominion University

A Dissertation Submitted to the Faculty of  
Old Dominion University in Partial Fulfillment of the  
Requirement for the Degree of

DOCTOR OF PHILOSOPHY

COMPUTATIONAL AND APPLIED MATHEMATICS

OLD DOMINION UNIVERSITY

August 2009

Approved by:

---

David G. Lasseigne (Director)

---

John Adam (Member)

---

Richard Norton (Member)

---

Robert Ash (Member)

## ABSTRACT

### AN ADAPTIVE METHOD FOR CALCULATING BLOW-UP SOLUTIONS

Charles F. Touron  
Old Dominion University, 2009  
Director: Dr. David G. Lasseigne

Reactive-diffusive systems modeling physical phenomena in certain situations develop a singularity at a finite value of the independent variable referred to as "blow-up." The attempt to find the blow-up time analytically is most often impossible, thus requiring a numerical determination of the value. The numerical methods often use *a priori* knowledge of the blow-up solution such as monotonicity or self-similarity. For equations where such *a priori* knowledge is unavailable, *ad hoc* methods were constructed. The object of this research is to develop a simple and consistent approach to find numerically the blow-up solution without having *a priori* knowledge or resorting to other *ad hoc* methods. The proposed method allows the investigator the ability to distinguish whether a singular solution or a non-singular solution exists on a given interval. Step size in the vicinity of a singular solution is automatically adjusted. The programming of the proposed method is simple and uses well-developed software for most of the auxiliary routines. The proposed numerical method is mainly concerned with the integration of nonlinear integral equations with Abel-type kernels developed from combustion problems, but may be used on similar equations from other fields. To demonstrate the flexibility of the proposed method, it is applied to ordinary differential equations with blow-up solutions or to ordinary differential equations which exhibit extremely stiff structure.

## ACKNOWLEDGEMENTS

I would like to express my thanks first to my wife, Julie, and children: Jaclyn, Alexandria, Bayley and Abbey. They kept me grounded. Thank you also to my advisor, D. Glenn Lasseigne, for his guidance and patience throughout my graduate study. I would also like to thank my fellow graduate students Terri Grant, Roy Sabo and Caleb Adams for their friendship, discussions and general help.

I am thankful to the professors John Adam, Richard Noren and Robert Ash for reading this dissertation and their many suggestions and comments. I am grateful to professors David Pravica, Mike Spurr, Cynthia DeBisschop, Li-Shi Luo, Mark Dorrepaal and the numerous other professors, instructors, teachers and fellow classmates that have supported me in my mathematical research. I am also thankful for the great help of the administrative assistants, Barbara M. Jeffrey-Dixon and Gayle P. Tarkelsen for their many efforts to assist me in completing this project.

I am grateful to my parents, Frank and Jan, for all their love and support and their faith and trust in allowing me to follow the path that I have chosen. Much thanks to my extended family members. Their support and prayers helped me in this process. Lastly, I am thankful for the prayers of my mother-in-law, Doris Mays. May she rest in peace after her long battle with lung cancer.

## TABLE OF CONTENTS

	Page
LIST OF TABLES . . . . .	vii
LIST OF FIGURES . . . . .	viii
Chapter	
I. INTRODUCTION . . . . .	1
II. BACKGROUND INFORMATION . . . . .	4
II.1 Blow-Up . . . . .	4
II.1.1 ODE Examples . . . . .	4
II.1.2 Partial Differential Equation Examples . . . . .	6
II.1.2.1 Reaction-Diffusion Equations . . . . .	6
II.1.2.2 The Nonlinear Heat Equation . . . . .	6
II.1.2.3 The Keller-Segel model for Chemotaxis . . . . .	8
II.1.2.4 The Nonlinear Schrödinger Equation . . . . .	9
II.2 Volterra Integral Equation Example . . . . .	11
II.2.1 Reaction-Diffusion Problem . . . . .	11
II.3 Integral Equations . . . . .	12
II.4 A Short History of Volterra Integral Equations . . . . .	13
II.5 Numerical Schemes for Volterra Integral Equations . . . . .	15
II.5.1 Grid . . . . .	16
II.5.2 Quadrature . . . . .	16
II.5.2.1 Primitive Solution Schemes . . . . .	17
II.5.2.2 Schemes Based on ODE Methods . . . . .	19
II.5.3 Runge-Kutta Methods for Integral Equations . . . . .	22
II.5.4 Collocation . . . . .	23
II.6 Blow-up Problems . . . . .	24
III. VOLTERRA INTEGRAL EQUATIONS . . . . .	26
III.1 Introduction . . . . .	26
III.2 Numerical Routine . . . . .	27
III.3 Numerical Solution of Benchmark Equation . . . . .	35
III.3.1 Convergence and Accuracy Analysis of Numerical Routine . . . . .	40
III.3.1.1 Derivative Evaluation . . . . .	40
III.3.1.2 Spline Fit . . . . .	44
III.3.1.3 Numerical Integration . . . . .	45
III.3.1.4 Extrapolation . . . . .	47
III.3.2 Determining If the Solution is Singular on the Active Interval . . . . .	53
III.4 Solution of Second Benchmark Problem . . . . .	53

Chapter	Page
III.5 Solution of Third Benchmark Problem . . . . .	60
IV. ORDINARY DIFFERENTIAL EQUATIONS . . . . .	70
IV.1 Introduction . . . . .	70
IV.2 Runge-Kutta . . . . .	71
IV.3 Initial Value Problem Examples . . . . .	73
IV.3.1 Blow-up Conditions . . . . .	73
IV.4 Solution to the Exponential Growth Equation . . . . .	76
IV.5 Solution to the <i>p</i> th-order Growth Equation . . . . .	76
IV.6 Solution to Kassoy's Thermal Explosion Problem . . . . .	77
IV.6.1 Unique Solution of Initial Value Problem . . . . .	78
IV.6.2 The Numerical Solution for the Initial Value Problem . . . . .	78
IV.6.3 Comparison of the Numerical Solution and the Analytic Solution	81
V. CONCLUSIONS . . . . .	86
REFERENCES . . . . .	94
VITA . . . . .	95

## LIST OF TABLES

Table	Page
1. Integral equations solved. . . . .	28
2. Relative errors of spline approximation in $\eta$ variable. . . . .	46
3. Relative tolerance of the extrapolation $10^{-9}$ with $j_{max} = 1000$ . . . . .	50
4. Relative tolerance of the extrapolation $10^{-9}$ with $j_{max} = 1250$ . . . . .	51
5. Relative tolerance of the extrapolation $10^{-7}$ with $j_{max} = 1250$ . . . . .	52
6. The blowup value $\eta^*$ vs $\lambda < \lambda_c$ . . . . .	62
7. Ordinary differential equations solved. . . . .	70
8. Number of coarse grid refinements vs $\epsilon$ . . . . .	80
9. The "blow-up" time vs $\epsilon$ . . . . .	81

## LIST OF FIGURES

Figure		Page
1.	Solution of benchmark equation in $\rho$ variable. . . . .	32
2.	Benchmark solution as function of fine-grid variable $\rho$ for each coarse-grid interval. . . . .	36
3.	Schematic showing fine and coarse grids for benchmark solution. . . . .	39
4.	Relative error in derivative approximations and absolute error near blowup for $\delta\rho = .05$ , $j_{max} = 1000$ . . . . .	42
5.	Relative error in derivative approximations and absolute error near blowup for $\delta\rho = .005$ , $j_{max} = 10000$ . . . . .	43
6.	Investigation of numerical integration routines. . . . .	48
7.	Second benchmark solution as a function of $\eta$ depending on $\gamma$ . (a) $\gamma \in (0, 3.0)$ by $\Delta\gamma = -0.5$ , (b) $\gamma \in (0, 1.0)$ by $\Delta\gamma = -0.1$ . . . . .	55
8.	Second benchmark solution as a function of $\eta$ depending on $\gamma$ . (a) $\gamma \in (0.46, 0.5)$ by $\Delta\gamma = -0.01$ and $\Delta\gamma = -0.001$ , (b) $\gamma \in (0.4631, 0.46305)$ by $\Delta\gamma = -0.0001$ . . . . .	56
9.	Second benchmark solution as a function of $\eta$ depending on $\gamma$ . (a) $\gamma \in (0.46307, 0.46306)$ by $\Delta\gamma = -0.00001$ , (b) $\gamma \in (0.463066, 0.463065)$ by $\Delta\gamma = -0.000001$ . . . . .	57
10.	Second benchmark solution as a function of $\eta$ depending on $\gamma$ . $\gamma \in (0.463065, 0.4630652824)$ by $\Delta\gamma = -0.000001$ , $\Delta\gamma = -0.0000001$ and $\Delta\gamma = -0.00000001$ . . . . .	58
11.	Plot of the blow-up time $\eta^*$ vs the parameter $\gamma$ . . . . .	59
12.	Investigation scheme's fit to $\eta^*(\gamma) \sim A \ln(\gamma - \gamma_c)$ . . . . .	61
13.	Third benchmark solution as a function of $\eta$ depending on $\lambda$ . (a) $\lambda \in (0, 3.0)$ , (b) $\lambda \in (1.0, 1.5)$ . . . . .	63
14.	Third benchmark solution as a function of $\eta$ depending on $\lambda$ . (a) $\lambda \in (1.08, 1.09)$ , (b) $\lambda \in (1.088, 1.089)$ . . . . .	64



Figure	Page
15. Third benchmark solution as a function of $\eta$ depending on $\lambda$ for $\lambda \in (1.0883, 1.08822322)$ . . . . .	66
16. Plot of the blow-up time $\eta^*$ vs the parameter $\lambda$ . . . . .	67
17. Investigation scheme's fit to $\eta^*(\lambda) \sim A \ln(\lambda_c - \lambda)$ . . . . .	69
18. Self-similar solutions to the exponential and <i>p</i> th-order growth equations.	75
19. Solutions of Kasso problem. (a) Solutions with $\beta = 2$ and $\varepsilon = \{2, 1, .5, .2, .1\}$ on the interval $t \in (0, 5)$ . . . . .	79
20. Solutions of Kasso problem. (a) Solutions with $\beta = 2$ and $\varepsilon = \{.01, .005, .001\}$ on the interval $t \in (0, 1.2)$ . . . . .	82
21. Comparison of numerical and analytical solution to the Kasso problem for $\beta = 2, \varepsilon = .1, \delta t_i = .1$ . . . . .	84
22. Comparison of numerical and analytical solution to the Kasso problem for $\beta = 2, \varepsilon = .05, \delta t_i = .1$ . . . . .	85

# CHAPTER I

## INTRODUCTION

This monograph describes a simple and consistent approach to the numerical integration of a class of nonlinear integral equations with Abel-type kernels formed from reactive-diffusive systems. In certain situations, the solution develops a singularity referred to as blow-up. Solving such integral equations employing standard finite-difference time-marching schemes is a difficult task because of complexities caused by the singularity in the solution.

Time-marching the numerical scheme assumes that the solution exists at each specified value of the independent variable. This assumption is not valid when the singularity is contained in the interval under consideration. However, in the special case where the solution is known to be monotone, solving the inverse problem eliminates the inherent difficulties by interchanging the independent and dependent variables. In the context of combustion and ignition problems, the interchange of variables converts the time-marching scheme into a temperature-marching scheme, with the temperature being prescribed and the time value associated with the temperature being sought. The advantage of this approach is its ability to avoid time-stepping past the singularity in the solution and automatically adjusting the temporal step-size to be sufficiently small near the singularity.

The use of the inverse problem to find the solution is justified only for solutions known to be monotone. Switching the independent and dependent variables fails to work in the cases where the monotonicity of the solution is unknown, omitting a large class of reactive-diffusive systems. A nonlinear integral equation for which solving the inverse problem is justified results from investigating the ignition problem in reactive media. The solution of this nonlinear integral equation represents the temperature perturbation above the temperature solution in a similar but unreactive media. This problem was formulated in Linan and Williams [52], "The ignition of a reactive solid by a constant energy flux." Olmstead [56] used analytical techniques to prove that the solution to the nonlinear Volterra integral equation derived by Linan and Williams [52] is both monotone and singular. The singularity in the integral equation solution occurs at a finite time, and this decisive event unambiguously defines the ignition time. Although the singularity is proven to exist, the integral equation must be solved numerically in order to determine the value of this "blow-up" time.

Solving the inverse problem is unjustified for the integral equation developed by Lasseigne and Olmstead [49]. The one-parameter nonlinear integral equation includes the effects of reactant consumption in the problem of ignition by a constant energy flux. The parameter is a measure of the heat release of the reaction and a measure of the initial reactant level. The analytical techniques used by Olmstead to provide *a priori* knowledge of the monotonicity of the solution when reactant consumption is excluded fail to provide the same *a priori* knowledge when reactant consumption is included. Furthermore, these analytic techniques fail to prove that the solution to the new one-parameter integral equation is singular for all values of the parameter. Upon numerical integration, a critical value of the parameter is determined such that no singularity in the solution exists for small values of the heat release. This absence of a singularity is interpreted as a non-ignition event. Lasseigne and Olmstead [49] took an *ad hoc* numerical approach by seeking a solution using the interchange of independent and dependent variables previously described and monitoring the process for the possibility of a non-singular solution. If a non-singular solution is found, then the calculation is redone without the interchange of independent and dependent variables to verify the original result.

Recent numerical methods by Haynes and Turner [68] to determine blow-up in differential or partial differential equations use a Sundman transformation so that the finite blow-up time is transferred to infinity in the new variable. One drawback of the Sundman transformation is that the new fictive temporal variable depends on the solution as does the arc length transformation used by Hirota and Ozawa [34] and Shoheile and Stockie [67]. C.J. Budd and others use a Sundman-like transformation in their solutions of partial differential equations exhibiting blow-up behavior [20, 19, 17, 18]. These methods use adaptive spatial meshes that depend on the solution much like time depends on the solution in the Sundman transformation.

The proposed method of solving the temporal blow-up problem, unlike the Sundman transformation methods, is independent of the solution. If applied to a partial differential equation, the proposed method would be compatible with spatial mesh adaptation that is independent of the solution, e.g., Wavelet Optimized Finite Difference [32, 22]. The simple and consistent numerical scheme proposed here allows the investigator the ability to determine whether the solution is singular or not singular, avoiding *ad hoc* methods to determine the solution's characteristics. The solution is found by using the natural variables of temperature perturbation as the dependent variable and time as the independent variable. When a singular solution is found, the time-step is adjusted appropriately to

maintain accuracy. The numerical scheme allows the use of well-developed software to interpolate the solution and integrate accurately within the presence of Abel-type kernels. The programming is straightforward and does not introduce complex or low-order finite-difference schemes.

The thesis is organized as follows: In Chapter II background information, definitions, examples of blow up, and Volterra integral equations are presented. Three of the main numerical methods used to solve Volterra integral equations: quadrature methods, Runge-Kutta methods, and collocation, are also summarized in Chapter II. A reader interested in the main results of the proposed method may wish to skip Chapter II altogether and begin directly with Chapter III. The proposed method of solving the blow-up problem is applied to test Volterra integral equations in Chapter III. In Chapter IV the proposed method of solving the blow-up problem is applied to test ordinary differential equations (ODE's). Concluding remarks are given in Chapter V.

## CHAPTER II

### BACKGROUND INFORMATION

#### II.1 Blow-Up

Linear and non-linear evolution equations are used to model many different physical situations, such as the dynamics of chemical reactions, the dynamics of biological systems, and the motion of waves in fluids and electromagnetic fields. The evolution equations take the form of systems of ordinary differential equations (ODE's), partial differential equations, or integral equations. This paper is mostly concerned about the numerical solution of blow-up problems developed as Volterra integral equations and ODE's from reaction-diffusion problems.

Blow-up is the explosive growth in the solution or a derivative of the solution in a finite time. Mathematically, blow-up manifests itself as a singularity in the solution. Other terms describing blow-up, depending on context, are *thermal runaway*, *finite escape time*, *first infinity*, *self-focusing*, *wave collapse*, *chemotactic collapse* and *gravitational collapse*. The following questions naturally arise while investigating blow-up:

- Does blow-up occur?
- If blow-up occurs, when, where, and how does it occur?
- How does the blow-up point change when the problem is perturbed?
- How is the blow-up point computed numerically?

The following subsections contain examples are know to exhibit blow-up phenomena.

A reader interested in the proposed method may skip Chapter II altogether and begin directly with Chapter III.

#### II.1.1 ODE Examples

Some very simple ODE's demonstrate the blow-up phenomenon and allow us to develop the basic tools and intuition required to study blow-up. These ODE's have explicit formulas defining the blow-up point and blow-up behavior. The scalar *quadratic growth* equation,

$$\frac{du}{dt} = u^2, \quad t \geq 0, \quad u(0) = u_0 \geq 0, \quad (\text{II.1.1})$$

has the unique solution,

$$u(t) = \frac{1}{t^* - t}, \quad t < t^*, \quad (\text{II.1.2})$$

where  $t^* = 1/u_0$  gives the dependence of the blow-up time on the initial value. The solution smoothly evolves for time  $t < t^*$  and approaches infinity as  $t \rightarrow t^*$ .

The  $p$ th-order growth equation,

$$\frac{du}{dt} = u^p, \quad t \geq 0, \quad u(0) = u_0 \geq 0, \quad (\text{II.1.3})$$

has the solution

$$u(t) = \begin{cases} \left(\frac{\beta}{t^* - t}\right)^\beta, & \beta = \frac{1}{p-1} \quad p > 1, \\ \frac{1}{((1-p)t + u_0^{1-p})^{\frac{1}{1-p}}}, & p < 1. \end{cases} \quad (\text{II.1.4})$$

When  $p > 1$ , the solution approaches infinity as  $t$  approaches  $t^*$  where  $t^*$  is the blow-up time given by

$$t^* = \frac{u_0^{1-p}}{p-1}. \quad (\text{II.1.5})$$

Blow-up does not occur when  $0 < p < 1$ , and the solution exists for all time.

Upon generalizing, the growth equation is given by

$$\frac{du}{dt} = f(u), \quad t \geq 0, \quad u(0) = u_0 \geq 0, \quad (\text{II.1.6})$$

for any positive and continuous function  $f$ . The growth equation has solution

$$\int_{u_0}^u \frac{d\hat{u}}{f(\hat{u})} = t. \quad (\text{II.1.7})$$

Blow-up occurs if the function  $f$  fulfills the *Osgood's condition* [57],

$$\int_{u_0}^{\infty} \frac{ds}{f(s)} < \infty, \quad (\text{II.1.8})$$

a necessary and sufficient condition formulated around 1898 for positive initial data. If  $f(u) = \exp(u)$  in (II.1.6), the solution is

$$u(t) = -\ln|t^* - t|, \quad (\text{II.1.9})$$

where  $t^* = \exp(u_0)$  is the blow-up time. The solution grows logarithmically as  $t \rightarrow t^*$ . This logarithmic blow-up behavior is especially challenging to capture numerically.

## II.1.2 Partial Differential Equation Examples

### II.1.2.1 Reaction-Diffusion Equations

Reaction-diffusion systems describe how the concentration of one or more substances, which are distributed in space, change under the influence of two processes: a) local chemical reactions in which reactants are transformed into products while possibly generating or conserving thermal energy, and b) diffusion which attempts to eliminate the spatial distribution of reactants along with the spatial distribution of the thermal energy products.

As this description implies, reaction-diffusion systems are naturally applied in chemistry. However, reaction-diffusion equations also describe dynamical processes of non-chemical nature in fields such as biology, geology, physics and ecology. Mathematically, reaction-diffusion systems take the form of semi-linear parabolic partial differential equations such as

$$\frac{\partial \vec{q}}{\partial t} = D\Delta\vec{q} + R(\vec{q}) \quad (\text{II.1.10})$$

where each component of the vector  $\vec{q}(x, t)$  represents the concentration of one substance or the thermal energy,  $D$  is a matrix of diffusion coefficients, and  $R$  accounts for all local reactions. The solutions of reaction-diffusion equations display a wide range of behaviors, including the formation of traveling waves, wave-like phenomena, and self-organizing patterns like stripes, hexagons or more intricate structure like dissipative solitons [1, 66]. Solitons are self-localized nonlinear waves maintained by equilibrium between dispersion and nonlinearity. Dissipative solitons are soliton-like localized modes in dissipative systems that are distant from thermal equilibrium, i.e., hydrodynamics, granular media, gas discharges and nonlinear optics.

### II.1.2.2 The Nonlinear Heat Equation

The nonlinear heat equation, a scalar semilinear parabolic reaction-diffusion equation modeling explosive phenomena, is given by

$$\frac{\partial u}{\partial t} = \Delta u + f(u), \quad t \geq 0, \quad u(0) = u_0. \quad (\text{II.1.11})$$

The Laplacian term is dissipative, giving a negative contribution to the time derivative at the local spatial maximum. Thus, the Laplacian tends to drive the solution towards a constant value. The positive and increasing nonlinear term contributes the most to the temporal derivative when  $u$  is large, leading to possible blow-up behavior. Omitting the Laplacian term and leaving the nonlinear and time-derivative terms model a spatially uniform solution which assumes the use of no-flux boundary conditions. These conditions result in the ODE examples previously discussed. Conversely, omitting the time-derivative term and leaving the nonlinear and Laplacian terms model a steady non-uniform solution, which requires energy to be lost at the boundary to dissipate heat from the reaction.

In particular, if  $f(u) = \delta \exp(u)$ , the *exponential reaction model* or the Frank-Kamenetskii equation, models solid (rigid) fuel ignition. Bebernes and Eberly [7] investigated the initial-value problem subject to Dirichlet boundary conditions and the related steady-state problem. Their book is a summary of the works of Ball [4], Bellout [11], Bebernes [8, 9, 10], Kassoy [40, 41, 42, 43], Kaplan [38], Kapila [36], Lacey [46, 47], Frank-Kamenetskii [24], Friedman [25, 26, 27], Fujita [28], Weissler [72] and others. Specifically, they studied

$$\frac{du}{dt} - \Delta u = \delta \exp(u), \quad (x, t) \in \Omega \times (0, T), \quad (\text{II.1.12})$$

$$u(x, 0) = 0, \quad x \in \Omega, \quad (\text{II.1.13})$$

$$u(x, t) = 0, \quad (x, t) \in \partial\Omega \times (0, T), \quad (\text{II.1.14})$$

and the related steady-state problem

$$-\Delta u = \delta \exp(u), \quad x \in \Omega, \quad (\text{II.1.15})$$

$$u(x) = 0, \quad x \in \partial\Omega. \quad (\text{II.1.16})$$

When solutions to (II.1.12)-(II.1.14) exist for all time, they converge to the steady-state solution. Investigating the steady-state solution leads to the determination of the domain-dependent *Frank-Kamenetskii* parameter,  $\delta_{FK}$ . When  $\delta < \delta_{FK}$ , the temporal solution evolves toward the steady-state solution as time approaches infinity. When  $\delta > \delta_{FK}$ , blow-up (thermal runaway) occurs since there is no steady state toward which to evolve.



Bebernes and Eberly also investigate the solid fuel ignition model [7] using a general reaction-rate term  $f(u)$  subject to general initial conditions and various boundary conditions. Their investigation included the requirements on the function  $f(u)$  in a given domain that causes blow-up to occur.

The  $p$ -th order growth reaction model where  $f(u) = u^p$  with  $p > 1$  models the inclusion of reactant consumption during the ignition process. The  $p$ -th order growth reaction model is also used in the biological and social science fields as a population model describing the population change given an amount of species  $u$ . In 1966, Fujita [28] showed that the only positive steady-state solution of the  $p$ -th order growth reaction model with a Cauchy domain  $D = R^N$  is the trivial one,  $u = 0$ , if  $1 < p < 1 + 2/N$ . Fujita also proved that solutions blow-up in finite time  $t$  when the initial condition is sufficiently large and if  $p > 1 + 2/N$ . In 1973, Hayakawa [31] showed that all solutions blow-up if the initial data are sufficiently large and if  $p = 1 + 2/N$ . The investigation of blow-up has been extended to other domains and functions, see [5, 6]. Analytic methods [7, 8, 47, 48, 70, 51] show that if the initial condition is large enough and has a single maximum in a closed interval, there is finite blow-up time for both, the exponential and  $p$ -th order growth reaction models.

### II.1.2.3 The Keller-Segel model for Chemotaxis

Chemotaxis is the movement of cells influenced by the spatial distribution of chemicals. The cells move toward favorable conditions and avoid unfavorable conditions. Chemotaxis occurs in embryogenesis, immune response, tumor growth, wound healing, amoebae aggregation, and the formation of patterns on animal skins. In 1953, Patlak [60] first developed a mathematical model for chemotaxis, and in 1970, Keller and Segel [44, 45] expanded the mathematical model. The Keller-Segel or Patlak-Keller-Segel chemotaxis model of slime mold (*Dictyostelium discoideum*) is an advection-diffusion system of two coupled parabolic equations:

$$\frac{\partial \rho}{\partial t} = \nabla \cdot (D \nabla \rho - \chi \rho \nabla S), \quad (\text{II.1.17})$$

$$\frac{\partial S}{\partial t} = D_0 \Delta S + \varphi(S, \rho), \quad (\text{II.1.18})$$

where  $\rho = \rho(x, t) \geq 0$  is the cell density at position  $x$  and time  $t$ ,  $S = S(x, t) \geq 0$  is the density of the chemoattractant, and  $\chi \geq 0$  is the chemotactic sensitivity. The diffusivity of the chemoattractant  $D_0$  and the diffusivity of the cells  $D$  are positive constants. Blow-up

in this context, referred to as *chemotactic collapse*, is the formation of dense aggregates of the predator population, i.e., mold or bacteria. Blow-up depends on the initial data and the spatial dimension  $d$ . It does not occur in one spatial dimension ( $d = 1$ ) but does arise with small initial conditions when  $d \geq 3$ . Borderline cases occur in two spatial dimension ( $d = 2$ ) where the solution may or may not blow-up depending on the size of the initial conditions.

The system of parabolic equations (II.1.17)-(II.1.18) can be used to study problem of *gravitational collapse* (Jeans instability). In this context,  $S$  is the gravitational potential,  $\chi$  is the gravitational sensitivity and  $\rho$  is the mass density. Equations (II.1.17)-(II.1.18) are the diffusive limit of a kinetic model [33, 58] and are either called a *gravitational drift-diffusion-Poisson* or *Smoluchowsky-Poisson* system [13].

#### II.1.2.4 The Nonlinear Schrödinger Equation

The nonlinear Schrödinger equation (NLS) models the propagation of waves such as the propagation of light in optical fibers, the vibrations of DNA molecules, water waves, continuous laser beams, and plasma waves. A specific NLS, given by the semi-linear Schrödinger equation

$$\frac{\partial u}{\partial t} = i\Delta u + i|u|^{p-1}u, \quad u = u(t, \mathbf{x}), \quad \mathbf{t} \in \mathbf{R}^+, \quad \mathbf{x} \in \mathbf{R}^d, \quad (\text{II.1.19})$$

is the simplest non-linear model of perturbations of the linear wave equation. The solution exhibits a magnifying envelope to the plane-wave solution. The nonlinear effect occurs through the dependence of the propagation speed on the wave amplitude, i.e., the speed decreases as amplitude decreases. In geometric optics, this leads to the extreme increase of the field amplitude called self-focusing.

Blow-up in this example is more subtle than blow-up in the nonlinear heat equation since the nonlinearity does not lead explicitly to blow-up. For example, the equation has conserved quantities, and under certain conditions, the existence of a global solution is guaranteed. If blow-up occurs, its structure is still unknown and remains an active area of research. Blow-up is best understood for the cubic nonlinear Schrödinger equation  $p = 3$  which describes the propagation of a laser beam in a medium whose index of refraction is sensitive to the wave amplitude; water waves at the free surface of an ideal fluid; or plasma waves. In one-dimension ( $d = 1$ ), the equation is well studied,

is known to be integrable, and has a global solution. For the case of  $d \geq 2$  with energy invariant initial conditions, the cubic NLS has solutions that become infinite at a single point in a finite time while conserving the two quantities: mass  $M = \int |u|^2 dx$  and energy  $E = \int |\nabla u|^2 - |u|^4/2 dx$ . In the 1970's, Vlasoc, Petritshev and Talanov [69] and Glassey [29] showed that the solution blows up when  $d \geq 2$  and the energy is negative. In 1983, Weinstein [71] proved that if the mass is suitably small,  $M < M_c$  where  $M_c$  is a critical mass, the solution exists globally showing that the *ground-state* of the cubic NLS is important in determining the blow-up.

Explicit equations for radially symmetric blow-up solutions when  $d \geq 2$  are written by using the dilation symmetry property,  $u(\mathbf{x}, t) \rightarrow \lambda u(\lambda \mathbf{x}, \lambda^2 t)$ , of the NLS equation. In particular, the blow-up solution has the form

$$u(r, t) = \frac{1}{t^* - t} \exp\left(\frac{-ir^2}{4(t^* - t)}\right) R\left(\frac{r}{t^* - t}\right), \quad (\text{II.1.20})$$

where  $R(r)$  is the unique positive solution (Townes soliton) of

$$-\left(R'' + \frac{1}{r}\right)R' + R - R^3 = 0, \quad R'(0) = 0. \quad (\text{II.1.21})$$

Radially symmetric blow-up solutions in the case  $d > 2$  have the form

$$u(r, t) = \frac{1}{[K(t^* - t)]^{1/2}} \exp\left(\frac{i}{K} \ln\left(\frac{t^*}{t^* - t}\right)\right) Q\left(\frac{r}{[K(t^* - t)]^{1/2}}\right), \quad (\text{II.1.22})$$

where  $K$  is a positive constant dependent on  $d$  and  $Q(r)$  is a solution of

$$-\left(Q'' + \frac{1}{r}Q'\right) + Q - |Q|^2Q + iK(Q + rQ') = 0, \quad Q'(0) = 0. \quad (\text{II.1.23})$$

These self-similar solutions show the structure and asymptotic behavior of the singular solutions near the blow-up. Self-similar solutions play an important role in the analysis of qualitative properties of the solution to several nonlinear problems, and numerical calculations taking advantage of self-similarity are more easily performed by converting a partial differential equation into a system of ODE's.

The method of lines or other transformation methods (Sundman, Fourier, etc.) convert partial differential equations into a system of ODE's that are solvable by an ODE solver. The behavior of the solution to a nonlinear system of partial differential equations is difficult to predict. The solution's complex behavior makes numerical computation nontrivial

even in ideal conditions and misleading results are easily generated. There is a danger in using similarity properties to develop a numerical scheme since this might force a certain behavior on the solution. It is always wise to verify the solution by using a method that is independent of the similarity properties.

## II.2 Volterra Integral Equation Example

### II.2.1 Reaction-Diffusion Problem

Blow-up in a chemical system describes a dramatic increase in temperature leading to ignition. Blow-up in the absence of external energy input is identified with self-ignition or explosion. Knowledge of when and how blow-up occurs might be the difference between life and death. The solution of many reaction-diffusion systems may be found by solving the inverse problem, i.e., the conversion of the initial value problem into an integral equation. Reaction-diffusion problems may also be formulated directly as integral equations. A class of Volterra integral equations modeling a diffusive media that may experience explosive behavior is given by

$$u(t) = Tu(t) \equiv \int_{t_0}^t k(t-s)G[u(s),s]ds, \quad t \geq t_0, \quad (\text{II.2.1})$$

where the nonlinearity is generally allowed to have the form

$$G[u(t),t] = r(t)g[u(t) + h(t)], \quad (\text{II.2.2})$$

with  $g(u)$  nonlinear and positive increasing. Commonly,  $g(u)$  either follows a power law or is an exponential function. The nontrivial functions  $r(t)$  and  $h(t)$  enhance the explosive behavior if they are nondecreasing. The kernel is also assumed to be nonnegative, decreasing and continuously differentiable except possibly at endpoint discontinuities. The most well known Volterra integral equation incorporating explosive behavior is given by Olmstead [56] as

$$u(t) = \int_{-\infty}^t \frac{e^{u(t)+s}}{\sqrt{\pi(t-s)}} ds, \quad t \geq -\infty. \quad (\text{II.2.3})$$

The solution depends on the interaction between the nonlinear function and the kernel. The nonlinear function corresponds to the source term imposed upon a linear parabolic partial differential equation. The kernel corresponds to the diffusive part and is a decreasing

function.

### II.3 Integral Equations

An *Integral equation* is any functional equation with the unknown function within an integration sign. Integral equations are found in many branches of science: potential theory, acoustics, elasticity, fluid mechanics, radiative transport, population theory, etc. The integral equation is often created by converting a boundary-value problem or an initial-value problem associated with a partial or ordinary differential equation. Other integral equations are formed directly because the physical problem cannot be formulated in terms of differential equations. Integral equations are derived from the global behavior of the system where differential equations are derived from the local behavior of the system. The Fredholm integral equation uses a fixed region of integration and is often considered analogous to a boundary-value ODE. The Volterra integral equation uses a variable integration region and is often considered analogous to an initial-value ODE.

A simple example of a Fredholm equation has the form

$$cy(x) = f(x) + \int_a^b K(x, \xi, y(\xi)) d\xi, \quad a \leq x \leq b, \quad (\text{II.3.1})$$

and a simple example of a Volterra equation has the form

$$cy(t) = f(t) + \int_a^t K(t, s, y(s)) ds, \quad a \leq t. \quad (\text{II.3.2})$$

The known functions are the forcing function  $f(t)$  and the *kernel* function  $K(t, s, y(s))$ . The unknown function is  $y(t)$ . When  $c$  is zero, the integral equation is said to be of the *first-kind*, and when  $c$  is nonzero, the integral equation is said to be of the *second-kind*. An integral equation is called *linear* when the kernel is  $K(t, s, y(s)) = k(t, s)y(s)$  and *nonlinear* otherwise. The kernel of a *convolution* integral equation has the form  $K(t, s, y(s)) = k(t - s)g(s, y(s))$ , and the integral equation is linear when  $g(s, y(s)) = y(s)$ . An integral equation is called *homogeneous* if the function  $f(t) = 0$  and is called *non-homogeneous* or *inhomogeneous* when  $f(t) \neq 0$ . A *singular* integral equation has a kernel containing a singularity or has an infinite integration range. A *weakly singular* integral equation has an unbounded but integrable kernel such that a suitable change of variables transforms the unbounded kernel into a bounded kernel. An *Abel* type integral equation belongs to a class of weakly singular Volterra integral equations first investigated by Niels Henrik Abel in 1823 while solving the problem of tautochronous motion. The Volterra

integral equations investigated in this thesis are nonlinear, non-homogeneous, of second kind, and with weakly singular kernels of Abel type.

#### II.4 A Short History of Volterra Integral Equations

This short history is taken from H. Brunner's books [14, 16] on the numerical solution of Volterra equations that enumerate the history of Volterra integral equations with a comprehensive bibliography of sources. Abel in the 19th century is credited with the first investigation of the quantitative theory of integral equations with variable upper limits of integration. He investigated the problem of finding the equation of the curve in the vertical plane such that the time taken for a mass point, under the influence of gravity, sliding along this curve is constant irrespective of the starting height. The first-type Abel Volterra integral equation modeling this motion is

$$\int_0^t \frac{y(s)}{\sqrt{(t-s)}} ds = g(t), \quad t > 0, \quad (\text{II.4.1})$$

and a generalization of equation (II.4.1) is

$$\int_0^t \frac{y(s) ds}{(t-s)^\alpha} = g(t), \quad t > 0. \quad (\text{II.4.2})$$

Abel's inversion formula when  $\alpha \in (0, 1)$  provides the solution

$$y(t) = \frac{\sin(\alpha\pi)}{\pi} \frac{d}{dt} \left[ \int_0^t g(s)(t-s)^{\alpha-1} ds \right], \quad t > 0. \quad (\text{II.4.3})$$

Liouville independently investigated the problem of inverting the generalized Abel equation (II.4.2) and second-kind integral equations in the late 1830's. A paper on electrostatics lead Volterra to investigate first-kind integral equations in 1884. Volterra in 1896 published a general theory on the inversion of linear integral equations of the first-kind –

$$\int_0^t K(t,s)y(s)ds = g(t), \quad g(0) = 0. \quad (\text{II.4.4})$$

The inversion requires transforming the equation by taking the derivative with respect to  $t$  in order to form a second-kind integral equation with kernel  $\hat{K}(t,s) = -(\partial K(t,s)/\partial t)/K(t,t)$  and forcing function  $\hat{g}(t) = g'(t)/K(t,t)$ . When  $K(t,t)$  does not vanish on the interval  $(0, T)$  and the derivatives of both the kernel and forcing function are continuous, the unique solution of equation (II.4.4) is given by the inversion formula

$$y(t) = g(t) + \int_0^t \hat{R}(t,s)g(s)ds, \quad t \in (0,T), \quad (\text{II.4.5})$$

where  $\hat{R}(t,s)$  is the resolvent kernel of  $\hat{K}(t,s)$  given by  $\hat{R}(t,s) = \lim_{n \rightarrow \infty} K_n(t,s)$  in terms of the iterated integrals,

$$\hat{K}_n(t,s) \equiv \int_0^t \hat{K}(t,u)\hat{K}_{n-1}(u,s)du, \quad n \geq 2, \quad (\text{II.4.6})$$

$$\hat{K}_1(t,s) \equiv \hat{K}(t,s). \quad (\text{II.4.7})$$

Volterra proved the above series is absolutely and uniformly convergent for any kernel satisfying the stated conditions.

Du Bois-Reymond in 1888 is given credit for first using the term "integral equations." Hilbert was first to use the terms first- and second-kind to describe integral equation types while investigating Fredholm integral equations. Lalesco in 1908 coined the term "Volterra integral equation." Lauricella in 1908 wrote a survey on integral equations with variable upper limits of integration. Sonine in 1884 extended the inversion formula to cover first-kind integral equations with convolution kernels. Volterra in 1896 extended his general ideas to linear integral equations of the first type with weakly singular kernels by using Abel's approach to develop the inversion formula (II.4.5) showing that the equation

$$\int_0^t \frac{K(t,s)y(s)ds}{(t-s)^\alpha} = g(t), \quad \alpha \in (0,1), \quad (\text{II.4.8})$$

is transformable into an equation of first type with a regular kernel.

G. C. Evan in 1910 and 1911 first investigated second-kind Volterra integral equation with weakly singular kernels. Hille and Tamarkin in 1930 used the Mittag-Leffler function to relate the solution to certain Volterra integral equation with weakly singular kernels. The unique solution  $y$  of the Volterra integral equation

$$y(t) = y_0 + \lambda \int_0^t (t-s)^{-\alpha} y(s)ds, \quad t \geq 0, \quad (\text{II.4.9})$$

for any interval  $[0, T]$  with  $0 < \alpha < 1$ , is

$$y(t) = E_{1-\alpha}(\lambda \Gamma(1-\alpha)t^{1-\alpha})y_0, \quad t \geq 0, \quad (\text{II.4.10})$$

where  $E_\beta(z)$  is the Mittag-Leffler function

$$E_\beta(z) \equiv \sum_{k=0}^{\infty} \frac{z^k}{\Gamma(1+k\beta)}, \quad \beta > 0, \quad (\text{II.4.11})$$

and  $\Gamma(s)$  is the gamma function. The function is an entire function of order  $p = 1/\beta$  for positive  $\beta$ . When  $\beta = 1$  the exponential function is recovered, and when  $\beta = 1/2$ , the Mittag-Leffler function is

$$E_{\frac{1}{2}}(\pm z^{\frac{1}{2}}) = \exp(z)[1 + \operatorname{erf}(\pm z^{\frac{1}{2}})] \quad (\text{II.4.12})$$

$$= \exp(z)\operatorname{erfc}(\pm z^{\frac{1}{2}}), \quad (\text{II.4.13})$$

where  $\operatorname{erf}(x)$  and  $\operatorname{erfc}(x)$  are the error and complementary error functions.

While the above examples are equations with analytic solutions, most equations of practical interest must be solved numerically.

## II.5 Numerical Schemes for Volterra Integral Equations

The literature on the numerical treatment and solution of integral equations is considerable owing to the many equations arising as models for different scientific problems. Linear operator theory allows the exact solution of many linear integral equations by analytical methods. Nonlinear or more elaborate linear integral equations often require numerical methods to find solutions.

Anderssen and De Hoog [2] conclude that using discrete methods to evaluate Abel's inversion formula is computationally difficult and simple mathematical transformations do not remove the associated difficulties. A perturbation analysis of the discretization leads to a step-size dependent amplification factor that demonstrates the difficulties, i.e., when using a finite difference scheme, the amplification factor has order  $h^{\frac{1}{2}}$ . Numerically, the amplification factor introduces a minimum grid spacing, where the step-size must not fall below the minimum spacing, in order for reliable approximations; otherwise, a loss in resolution occurs.

The details of the numerical methods outlined below mainly come from the works of Baker [3] and Brunner [14, 16]. Three main methods to solve Volterra integral equations are: quadrature methods, Runge-Kutta methods, and collocation. The specific solution strategy for each method develops after constructing a grid.



### II.5.1 Grid

A grid or mesh is built as

$$I := t_0 < t_1 < t_2 < \cdots < t_{n-1} < t_n < \cdots < t_N = T, \quad h_n := t_{n+1} - t_n. \quad (\text{II.5.1})$$

The *width* or *diameter* of the grid is  $h(I) := \sup_{t_n \in I} h_n$ . The grid is *uniform* if  $h_n = h = T/N$  for all  $n$  and *quasi-uniform* if there exists a finite  $k$  such that  $\sup h_n \leq k \inf h_n$ . The grid is *finite* if  $T_N := \max_n t_n = T < \infty$ . The finite grid is *graded with grading exponent*  $\alpha$  if  $t_n - t_0 = (n/N)^\alpha$  or *geometric* if  $t_n - t_0 = \beta^{N-n}(T - t_0)$  for some  $0 \leq \beta \leq 1$ . Volterra integral equations with weakly singular kernels often use graded meshes.

### II.5.2 Quadrature

Having defined a grid, each definite integral

$$\mathbf{I}[\phi] \equiv \int_a^b \phi(t) dt, \quad (\text{II.5.2})$$

where  $a$  and  $b$  are two not necessarily successive grid points, is numerically approximated by the  $(m+1)$ -point quadrature formula

$$\mathbf{I}_m[\phi] \equiv \sum_{j=0}^m c_{m,j} \phi(t_{m,j}), \quad (\text{II.5.3})$$

where  $t_{m,0} < t_{m,1} < \cdots < t_{m,m}$  are *points* or *abscissas*, not necessarily in  $[a, b]$ , and the  $c_{m,j}$  are the *coefficients*. The *approximation* or *quadrature error* is the difference between the integral and the numerical approximation  $\mathbf{E}[\phi] = \mathbf{I}[\phi] - \mathbf{I}_m[\phi]$ . The coefficients are chosen to make the quadrature error vanish for all test functions  $\phi$  in a test space. For example, the interpolatory quadrature formula of  $m$  polynomial test functions has coefficients

$$c_{m,j} = \int_a^b L_{m,j}(t) dt, \quad (\text{II.5.4})$$

where

$$L_{m,j}(t) = \prod_{i=0, i \neq j}^m \frac{t - t_{m,i}}{t_{m,j} - t_{m,i}}, \quad i \neq j. \quad (\text{II.5.5})$$

Newton-Cotes formulas are created when the points have equal spacing  $h = (t_{m,j} - t_{m,j-1})/m$  and the coefficients are defined by (II.5.4). A Newton-Cotes formula of closed

type uses  $a = t_{m,0}$  and  $b = t_{m,m}$ , a Newton-Cotes formula of open type uses  $a = t_{m,0} - h$  and  $b = t_{m,m} + h$ , and a Newton-Cotes formula half-open type uses either  $a = t_{m,0}$  and  $b = t_{m,m} + h$ , or  $a = t_{m,0} - h$  and  $b = t_{m,m}$ . The first three closed Newton-Cotes formulas are the trapezoidal rule ( $m = 1$ ), Simpson's rule ( $m = 2$ ), and Simpson's three-eighths rule ( $m = 3$ ). The trapezoidal rule is first-order accurate (i.e.,  $E[\phi]$  is proportional to  $h^2$ ) and both of the Simpson's rules are third-order accurate (i.e.,  $E[\phi]$  is proportional to  $h^4$ ).

The Gauss-Legendre formulas produce the greatest accuracy for fixed  $m$  by using the zeros of the Legendre polynomials  $z_{m,j}$  to generate the points

$$t_{m,j} = \frac{t_m - t_{m-1}}{2} z_{m,j} + \frac{t_{m-1} + t_m}{2}, \quad j = 0, 1, \dots, n, \quad (\text{II.5.6})$$

along with the coefficients

$$c_{m,j} = \frac{t_m - t_{m-1}}{(1 - z_{m,j})^2 [P'_{m+1}(z_{m,j})]^2}. \quad (\text{II.5.7})$$

For Gauss-Legendre formulas,  $E[\phi]$  is proportional to  $h^{2m+3}$ . Although, the Gauss-Legendre formulas produce the highest order of accuracy for a given  $m$ , the Gauss-Legendre formulas are *open* formulas that do not include evaluation at the endpoints. The Radau formulas include one of the endpoints and then maximize the precision by choosing appropriate abscissa. The Lobatto formulas include both endpoints and then maximize the precision by choosing appropriate abscissa. The order of accuracy are  $2m + 2$  and  $2m + 1$ , respectively. Applying the formulas involving evaluation of the function at points different from the grid points to solve a Volterra integral equation directly is difficult. Thus, Newton-Cotes formulas are the most common quadrature formulas used to solve Volterra integral equations.

### II.5.2.1 Primitive Solution Schemes

A family of methods that solve Volterra integral equations is defined by using a low-order Newton-Cotes quadrature rule on each grid interval

$$\int_{t_j}^{t_{j+1}} \phi(s) ds \approx h_j [(1 - \theta)\phi(t_j) + \theta\phi(t_{j+1})], \quad 0 \leq \theta \leq 1. \quad (\text{II.5.8})$$

The *Euler* rule is obtained when  $\theta = 0$ , the *backwards Euler* rule is obtained when  $\theta = 1$ , and the *trapezoid* rule is obtained when  $\theta = 1/2$ . A repeated application of equation (II.5.8) gives the relationship

$$\int_{t_0}^{t_n} \phi(s) ds \approx \sum_{j=0}^{n-1} h_j [(1-\theta)\phi(t_j) + \theta\phi(t_{j+1})], \quad (\text{II.5.9})$$

and discretizing the second-kind Volterra integral equation

$$y(t) = g(t) + \int_{t_0}^t K(t,s,y(s)) ds, \quad t_0 \leq t \leq T, \quad (\text{II.5.10})$$

with equation (II.5.9) produces the series of algebraic equations

$$\tilde{y}(t_{n+1}) = g(t_{n+1}) + \sum_{j=0}^n h_j [(1-\theta)K(t_{n+1},t_j,\tilde{y}(t_j)) + \theta K(t_{n+1},t_{j+1},\tilde{y}(t_{j+1}))] \quad (\text{II.5.11})$$

where, for each value of  $n$ , the approximate value  $\tilde{y}(t_{n+1})$  is the unknown. Equations (II.5.11) are recastable into a single summation

$$\tilde{y}(t_{n+1}) = g(t_{n+1}) + \sum_{j=0}^{n+1} W_{n+1,j} K(t_{n+1},t_j,\tilde{y}(t_j)) \quad (\text{II.5.12})$$

where  $W_{n+1,j}$  are referred to as the weights. The  $\theta$ -rules are low order requiring many functional evaluations to obtain an accurate approximation. Alternatively, higher-order methods such as the combination of Simpson's rule and Simpson's three-eighths rule require fewer functional evaluations for comparable accuracy. However, higher-order methods require more complex programming.

A primitive solution scheme to solve Abel-type Volterra integral equations is found by approximating

$$\Phi(t_n) = \int_{t_0}^{t_n} \frac{\phi(s)}{(t_n-s)^\alpha} ds, \quad (\text{II.5.13})$$

with one of the following formulas:

$$\Phi(t_n) \approx \sum_{j=0}^{n-1} \left\{ \int_{t_j}^{t_{j+1}} \frac{ds}{(t_n-s)^\alpha} \right\} \phi(t_j), \quad (\text{II.5.14})$$

$$\Phi(t_n) \approx \sum_{j=0}^{n-1} \left\{ \int_{t_j}^{t_{j+1}} \frac{ds}{(t_n-s)^\alpha} \right\} \phi(t_{j+1}), \quad (\text{II.5.15})$$

$$\Phi(t_n) \approx \sum_{j=0}^{n-1} \left\{ \int_{t_j}^{t_{j+1}} \frac{ds}{(t_n - s)^\alpha} \frac{t_{j+1} - s}{h_j} \phi(t_j) + \int_{t_j}^{t_{j+1}} \frac{ds}{(t_n - s)^\alpha} \frac{s - t_j}{h_j} \phi(t_{j+1}) \right\}, \quad (\text{II.5.16})$$

which generalize the Euler, backwards Euler and trapezoid rules, respectively. Extending (II.5.14) - (II.5.16) to higher order is more difficult than extending (II.5.9) to higher order.

### II.5.2.2 Schemes Based on ODE Methods

Methods solving the initial value ODE,

$$y'(t) = f(t, y(t)), \quad t \geq t_0, \quad y(t_0) = y_0, \quad (\text{II.5.17})$$

are connectible to methods of solving Volterra integral equations of the second-kind. The initial value ODE in integrated form is a second-kind Volterra integral equation

$$y(t) = y_0 + \int_{t_0}^t f(s, y(s)) ds, \quad t \geq t_0. \quad (\text{II.5.18})$$

Alternatively, Volterra integral equations (II.5.10) with separable kernels  $K(t, s, v) = \sum_{j=1}^N T_j(t) S_j(s, v)$  or exponential kernels  $K(t, s, v) = (t - s)^n \exp\{-\alpha(t - s)\} v$  reduce to a system of ODE's. For example, if  $K(t, s, v) = T_1(t) S_1(s, v) + T_2(t) S_2(s, v)$ , then, upon defining

$$u_1(t) = \int_0^t S_1(s, v) ds, \quad (\text{II.5.19})$$

$$u_2(t) = \int_0^t S_2(s, v) ds, \quad (\text{II.5.20})$$

the system of ODE's is

$$u_1'(t) = S_1(t, g(t) + T_1(t) u_1(t) + T_2(t) u_2(t)), \quad u_1(0) = 0, \quad (\text{II.5.21})$$

$$u_2'(t) = S_2(t, g(t) + T_1(t) u_1(t) + T_2(t) u_2(t)), \quad u_2(0) = 0. \quad (\text{II.5.22})$$

Numerical schemes to solve an ODE are often cast into the summation form

$$\sum_{j=0}^k \alpha_j y_{n-j} = h \sum_{j=0}^k \beta_j f_{n-j} \quad (\text{II.5.23})$$

which is similar to the primitive integral equation schemes (II.5.12).

A scheme is *explicit* when the calculation of the solution of an equation at the current time is found by using the solution at the previous times. Quadrature methods of the form (II.5.12) are explicit if  $W_{n+1,n+1} = 0$  and ODE methods of the form (II.5.23) are explicit if  $\beta_0 = 0$ . A scheme is *implicit* when the calculation of the solution of an equation at the current time is found by using both the solution at the current and previous times. Quadrature methods of the form (II.5.12) are implicit if  $W_{n+1,n+1} \neq 0$  and ODE methods of the form (II.5.23) are implicit if  $\beta_0 \neq 0$ . Implicit methods require a nonlinear algebraic solver and significantly more function evaluations. However, implicit methods usually lead to more accurate solutions and a more stable routine. Predictor-corrector schemes are simple methods to integrate ODE's that combine the advantages of implicit and explicit methods by first using an explicit formulation as a predictor and then using the predicted value in the implicit formula instead of an algebraic solver.

Single-step methods do not use information from the previous steps. Two popular high-order single-step methods are the Runge-Kutta method and the Taylor-series method. The simplest high-order single-step method uses the higher derivatives calculated from (II.5.17) in a truncated Taylor expansion. However, the Taylor-series method becomes problematic when expressions for the higher derivatives, derivable from (II.5.17), are overly complicated. Runge-Kutta methods provide a high-order scheme and do not require symbolic derivatives as in the Taylor-series method. Runge-Kutta methods also work when the right-hand side of (II.5.17) is only known numerically. The Runge-Kutta and the Taylor-series methods are not castible into the form of (II.5.23).

Multi-step methods use information from the previous integration steps to construct high-order approximations. Multi-step methods are more efficient than single-step methods, using fewer function evaluations per step for the same accuracy; however multi-step methods are less flexible than the single-step methods when changing step size. Furthermore, multi-step schemes require independent initial approximations at the desired accuracy for the first few initial steps, while single-step methods only require knowledge of the initial condition. Popular linear multi-step families of methods are the Adams and the

backwards-differentiation formula. For example, the 3-step explicit Adams method is

$$y_{n+1} = y_n + h \left\{ \frac{23}{12}f_n - \frac{16}{12}f_{n-1} + \frac{5}{12}f_{n-2} \right\}, \quad (\text{II.5.24})$$

and the 3-step implicit backwards-differentiation formula is

$$y_{n+1} - \frac{18}{11}y_n + \frac{9}{11}y_{n-1} - \frac{2}{11}y_{n-2} = \frac{6}{11}h f_{n+1}. \quad (\text{II.5.25})$$

Both are in the form of (II.5.23). In principle, every ODE method (multi-step methods, Runge-Kutta methods, and general linear methods) generates a corresponding integral equation method for second-kind Volterra integral equation. Likewise, every integral equation method for second-kind Volterra integral equation generates an ODE method. For example, a predictor-corrector method with variable order and variable step-size was developed by Jones and McKee [35] to solve Volterra integral equations with smooth kernels using a similar strategy to change the step-size as used in the ODE method.

Lubich [30, 54, 55] uses fractional powers of linear multi-step methods to numerically solve weakly singular Volterra integral equations. Lubich constructs *convolution quadratures for integrals of fractional order* from a linear multi-step method. The convolution quadrature has the same convergence properties and similar stability properties of the original multi-step method. The convolution quadratures for integrals of fractional order generate integration rules for constructing uniform meshes in discretizing Abel equations. Lubich approximates the fractional integrals of order  $1 - \nu$ ;

$$J^\nu[\phi](t_n) = \frac{1}{\Gamma(1-\nu)} \int_{t_0}^{t_n} \frac{\phi(s)}{(t_n-s)^\nu} ds, \quad 0 < \alpha < 1, \quad (\text{II.5.26})$$

with the sums

$$J^\nu[\phi](t_n) \approx h^{1-\nu} \sum_{j=0}^{n_0} w_{n,j}^{\{\nu\}} \phi(t_j) + h^{1-\nu} \sum_{j=n_0+1}^n w_{n-j}^{\{\nu\}} \phi(t_j), \quad (\text{II.5.27})$$

where  $t_n \equiv t_0 + nh$ . The second sum in the approximation is called the *convolution part*. The starting weights  $w_{n,j}$  are chosen so that the approximation is exact for

$$\phi(s) = (s - t_0)^{\mu_i}, \quad \mu_i \in \mathbb{R}, \quad (\text{II.5.28})$$

where

$$y(t) \sim a_0 + a_1(t-t_0)^{\mu_1} + a_2(t-t_0)^{\mu_2} + a_3(t-t_0)^{\mu_3} + \dots, \quad (\text{II.5.29})$$

as  $t \rightarrow t_0$ , with  $\mu_1 < \mu_2 < \mu_3 < \dots < \mu_m$ .

### II.5.3 Runge-Kutta Methods for Integral Equations

Runge-Kutta methods are popular choices for numerically solving ODE initial value problems. Runge-Kutta methods were first formulated around the 1900's, while modern Runge-Kutta methods using J.C. Butcher's theories date to the 1960's. In the 1960's, P. Pouzet [62] and B.A. Bel'tyukov [12] extended Runge-Kutta methods to second-kind Volterra integral equations. H. Brunner, E. Hairer, and S. Nørbert [15] systematically analyzed Runge-Kutta methods for second-kind Volterra integral equations in the 1980's.

To develop the Runge-Kutta method for Volterra integral equation rewrite the general equation (II.5.18) using a uniform mesh  $t_n = nh$  as

$$y(t) = F_n(t) + \int_{t_n}^t k(t,s,y(s))ds, \quad t \in [t_n, T], \quad (\text{II.5.30})$$

where  $F_n$  is the *lag* or *tail* term given by

$$F_n(t) = g(t) + \int_0^{t_n} k(t,s,y(s))ds, \quad n = 0, \dots, N-1, \quad (\text{II.5.31})$$

and the *increment function*  $\Phi(t)$  on the subinterval  $[t_n, t_{n+1}]$  is

$$h\Phi_n(t) = \int_{t_n}^t k(t,s,y(s))ds, \quad t \in [t_n, T], \quad n = 0, \dots, N-1. \quad (\text{II.5.32})$$

A Runge-Kutta method requires two independent approximation schemes: (i) an approximation scheme for the increment function on the subinterval  $[t_n, t_{n+1}]$  producing a discrete representation of the increment function  $\tilde{\Phi}(t)$  called the Volterra-Runge-Kutta formula and (ii) an approximation scheme for the lag term on the interval  $[0, t_n]$  producing a discrete lag term  $\tilde{F}_n(t)$ . The solution at  $t = t_{n+1} = t_n + h$  is approximated as

$$y_{n+1} = \tilde{F}_n(t_n + h) + h\tilde{\Phi}(t_n + h), \quad n = 0, \dots, N-1. \quad (\text{II.5.33})$$

For example, an *m-stage* Volterra-Runge-Kutta formula for the increment function has the form

$$\tilde{\Phi}_n(t) = \sum_{j=1}^m b_j k(t + (e_j - 1)h, t_n + c_j h, Y_{n,j}) \quad (\text{II.5.34})$$

where  $Y_{n,j}$  are approximations to  $y$  at points between  $t_n$  and  $t_{n+1}$  given by

$$Y_{n,j} = \tilde{F}_n(t_n + \theta_j h) + h \sum_{i=1}^m a_{j,i} k(t + d_{j,i} h, t_n + c_i h, Y_{n,i}), \quad j = 1, \dots, m. \quad (\text{II.5.35})$$

The constants  $a, b, c, d, e$  are suitably chosen to produce sufficient accuracy and to maintain stability. Other choices of approximation schemes are possible.

### II.5.4 Collocation

Collocation methods used to solve Volterra integral equations are often based on polynomial spline approximations. Let  $\tilde{y}_-(t)$  be the polynomial of degree  $m$  approximating  $y(t)$  to the left of  $t_n$  and  $\tilde{y}_+(t)$  be the polynomial of degree  $m$  approximating  $y(t)$  to the right of  $t_n$ . The spline of continuity class  $k$  with knots  $T_N \equiv \{t_n\}_1^N \subset T$  is created by setting

$$\tilde{y}_+(t_n) = \tilde{y}_-(t_n), \quad \tilde{y}'_+(t_n) = \tilde{y}'_-(t_n), \quad \dots, \quad \tilde{y}^{(k)}_+(t_n) = \tilde{y}^{(k)}_-(t_n). \quad (\text{II.5.36})$$

The polynomial spline is a *piecewise linear continuous* approximation when  $m = 1, k = 0$ , and the polynomial spline is a *classical cubic spline* approximation when  $m = 3, k = 2$ .

Any approximation  $\tilde{y}(t)$  to the solution to the second-kind Volterra integral equation,

$$y(t) = g(t) + \int_{t_0}^t K(t, s, y(s)) ds, \quad t \in [t_0, T], \quad (\text{II.5.37})$$

has a *defect*

$$\delta(\tilde{y}(\cdot); t) := \tilde{y}(t) - \left\{ g(t) + \int_{t_0}^t K(t, s, \tilde{y}(s)) ds \right\} \quad (t \in [t_0, T]). \quad (\text{II.5.38})$$

If equation (II.5.37) has a unique solution, then the defect is zero for all  $t$  if and only if  $\tilde{y}(\cdot) = y(\cdot)$ . This suggests that the best approximation would be one with the smallest defect. Collocation methods seek approximations with zero defect on the set of collocation points. The defect depends on the dimension  $d$  of the space and is uniquely determined by  $d$  parameters. The defect approximation satisfies  $k + 1$  continuity conditions (II.5.36) at



each point  $t_n$  and also satisfies  $Nm$  collocation conditions

$$\delta(\tilde{y}(\cdot); t_{n,r}) := 0, \quad n = 0, 1, 2, \dots, N-1; \quad r \in \{1, 2, \dots, m\}. \quad (\text{II.5.39})$$

The defect vanishes at the distinct collocation points  $t_{n,r} = t_n + \vartheta_r h_n$  and for  $t \in [t_n, t_{n+1}]$  is

$$\begin{aligned} \delta(\tilde{y}(\cdot); t) = \tilde{y}(t) - g(t) + & \left\{ \sum_{j=0}^{n-1} \int_{t_j}^{t_{j+1}} K(t, s, \tilde{y}(s)) ds \right. \\ & \left. + \int_{t_n}^t K(t, s, y_k(s)) ds \right\}, \end{aligned} \quad (\text{II.5.40})$$

where  $\tilde{y}(\cdot)$  is a polynomial of degree  $q_n$  in each interval  $(t_j, t_{j+1}]$ .

Spline collocation provides a continuous and smooth approximation as opposed to the approximation at a discrete set of points provided by Runge-Kutta and other finite difference schemes. However, spline collocation requires numerically evaluating  $n$  new integrals at each step. When the integral equations are generated by ODE's, spline collocation methods are equivalent to Runge-Kutta methods if the integrals are interpolated by quadratures. Uniform meshes cannot be used with polynomial collocation to solve Volterra integral equations with weakly singular kernels and smooth data, since the solutions' derivatives are unbounded at the left endpoint of the integration range. This problem is resolved by using graded meshes or uniform meshes with non-polynomial collocation as discussed in Brunner [14] and the works cited in that survey.

## II.6 Blow-up Problems

All of the previously mentioned non single-step integration techniques cannot be applied directly to integral equations with solutions that blow up at a finite time. These methods are based upon an *a priori* designated grid, and the appropriate grid for a blow-up solution cannot be known *a priori*. Runge-Kutta methods can be used if the step size is adjusted appropriately near the singularity. However, this still requires a monitoring of the solution to prevent time-stepping past the singularity. Furthermore, Runge-Kutta methods are more complicated for Able-type equations.

The purpose of this research is to utilize simple well-known numerical methods and ready-made software to numerically solve Volterra integral equations. A consistent method

of solution is presented in Chapter III that allows the investigator to easily distinguish between a singular solution and a non-singular solution, thus, avoiding the use of *ad hoc* approaches. Upon determining that a singular solution exists, the time step is appropriately adjusted to maintain accuracy. The technique uses well-developed software that interpolates the solution and that accurately integrates in the presence of an Abel singularity. The programming is straightforward and intuitive.

## CHAPTER III

### VOLTERRA INTEGRAL EQUATIONS

#### III.1 Introduction

The study of ignition problems in reactive media by deriving nonlinear integral equations whose solutions represent temperature perturbations above the temperature solutions in a similar but unreactive media started with two classic problems by Linan and Williams [52] & [53]: a) ignition of a reactive solid by a constant energy flux, and b) ignition of a reactive solid by a step in surface temperature. By using analytic techniques, Olmstead [56] proved that the solution to the nonlinear Volterra integral equation derived in Linan and Williams [52] is both monotone and singular. The singularity in the solution of the integral equation occurs at a finite time, and this decisive event unambiguously defines the ignition time for this problem. Although the singularity is proven to exist, the integral equation must be solved numerically in order to determine the value of this "blow-up" time. When approximating the solution of this nonlinear Volterra integral equation using a standard finite-difference time-marching scheme, significant difficulties arise owing to the singularity in the solution. Time marching requires assuming a solution exists at each specified value of the independent variable, but this assumption fails to hold when the singularity of the solution is on the interval under consideration. Interchanging the dependent and independent variables resolves the inherent difficulty when the solution is known to be monotone. Instead of time marching, the solution proceeds by "temperature marching", i.e., the temperature is prescribed and the time value corresponding to this temperature is sought. By using this interchange, time-stepping past the singularity in the solution is avoided, and the temporal step size automatically becomes appropriately small near the singularity.

Since Olmstead [56] proved that the solution to the integral equation derived in Linan and Williams [52] is both monotone and singular, solving the inverse problem instead of the direct problem is justified. However, interchanging the independent and dependent variables fails to determine numerically the solution for other integral equations resulting from reactive-diffusive systems. For example, Lasseigne and Olmstead [49] derive a one-parameter nonlinear integral equation by including the effects of reactant consumption in the problem of ignition using a constant energy flux. The parameter includes a measure of the heat release of the reaction and a measure of the initial reactant level. The analytical

techniques used by Olmstead to provide *a priori* knowledge of the monotonicity of the solution when reactant consumption is excluded fail to provide the same *a priori* knowledge as to the monotonicity of the solution when reactant consumption is included. Furthermore, these analytic techniques fail to prove that the solution to the new one-parameter integral equation is singular for all values of the parameter. Upon numerical integration, a critical value of the parameter is determined such that no singularity in the solution exists for small values of the heat release. This absence of a singularity is interpreted as a non-ignition event. Lasseigne and Olmstead [49] took an *ad hoc* approach by seeking a numerical solution using the interchange of independent and dependent variables previously described and monitoring the process for the possibility of a non-singular solution. If a non-singular solution is found, a recalculation without the interchange of independent and dependent variables verifies the result.

A consistent method of solution is presented below that allows the investigator to easily distinguish between a singular solution and a non-singular solution, thus, avoiding the *ad hoc* approach used in the past. Furthermore, the solution develops in the natural variables where the temperature perturbation is the dependent variable and time is the independent variable. Upon determining that a singular solution exists, the time step is appropriately adjusted to maintain accuracy. Another virtue of the present technique is the use of well-developed software that interpolates the solution and that accurately integrates in the presence of an Abel-type singularity. The programming is straightforward and intuitive without introducing the complexity and low-order of solving by finite differences. The solution method is used to solve all of the integral equations given in Table 1, and any necessary modifications for a particular equation is discussed in the text.

### III.2 Numerical Routine

When developing a numerical approximation of the solution to an equation, one usually looks for the simplest method that produces an accurate solution. For an integral equation with a non-singular kernel and a well-behaved solution, the method of finite differences provides a straightforward method to obtain an accurate approximation. The simplest versions of finite differences applied to an integral equation are equivalent to approximating the integral with the trapezoid rule or with Simpson's rule. The method of finite differences also provides a straightforward approximation scheme for integral equations having singular kernels, but with reduced accuracy compared with the same technique applied to integral equations with non-singular kernels.

TABLE 1  
Integral equations solved.

Description	Equation
Ignition of a Combustible Solid [56]	$u(\eta) = \int_{-\infty}^{\eta} \frac{1}{\sqrt{\pi(\eta - \xi)}} e^{u(\xi) + \xi} d\xi$
Ignition with Marginal Heating [50]	$u(\eta) = \gamma \int_{-\infty}^{\eta} \frac{1}{\sqrt{\pi(\eta - \xi)}} e^{u(\xi) - \xi^2} d\xi$
Ignition with Reactant Consumption[49]	$u(\eta) = \int_{-\infty}^{\eta} \frac{1}{\sqrt{\pi(\eta - \xi)}} e^{u(\xi) + \xi} F(\lambda v(\xi)) d\xi$ <p>where <math>F(x) = \frac{1 - e^{-x}}{x}</math> and <math>v(\xi) = \int_{-\infty}^{\xi} e^{u(\xi') + \xi'} d\xi'</math></p>

The finite-difference scheme that solves the general, nonlinear, Abel-like Volterra integral equation

$$u(\eta) = \int_{\eta_0}^{\eta} \frac{1}{\sqrt{\pi(\eta - \xi)}} F(u(\xi), \xi; \lambda_1, \lambda_2 \dots) d\xi \quad (\text{III.2.1})$$

is of the form

$$u(\eta_n) = \sum_{i=0}^n W_{in} F(u(\eta_i), \eta_i; \lambda_1, \lambda_2 \dots) \quad n \geq 1. \quad (\text{III.2.2})$$

Making appropriate approximations to  $F(u(\eta), \eta; \lambda_1, \lambda_2 \dots)$  on each sub-interval determines the weights  $W_{in}$ . The simplest (and lowest order) approximation replaces  $F$  by a straight line over each sub-interval. Replacing the function  $F$  with a parabola fitted through three points provides a higher-order approximation, but the square-root singularity in the kernel destroys the symmetry that makes Simpson's rule so accurate for non-singular kernels.

If the solution is well-behaved, using evenly spaced steps,  $\eta_{i+1} = \eta_i + \Delta\eta$ , keeps the

finite-difference scheme relatively simple. Time marching determines the solution at each successive point starting from  $u_0 = u(\eta_0) = 0$ . Upon assigning  $n = 1$ , equation (III.2.2) becomes a non-linear algebraic equation for the unknown  $u_1 = u(\eta_1)$  whose value is determined using a root finding program. The solution process continues by setting  $n = 2$  to obtain a non-linear algebraic equation for the unknown  $u_2 = u(\eta_2)$  which depends on the previously determined values  $u_0$  and  $u_1$ . The time marching continues until the solution is determined on the required interval. At each  $\eta_n$ , the non-linear algebraic equation explicitly depends on all of the previous solution points, i.e., the solution depends on  $u_0, u_1, \dots, u_{n-1}$ . For integral equations derived from reaction-diffusive systems, the *solution* might be singular at some finite point, say  $\eta^*$ . Thus, when using evenly spaced steps in a finite-difference scheme,  $\eta_{i+1} = \eta_i + \Delta\eta$ , the solution at the point  $\eta_N$  does not exist if  $\eta_{N-1} < \eta^* < \eta_N$ ; however, the value of  $N$  is unknown *a priori*. Thus, an attempt is made to find the nonexistent quantity  $u_N = u(\eta_N)$ . Since the non-linear algebraic equation is only an approximation to the integral equation, a false value for  $u_N$  might be found, and the time stepping would continue to search for the nonexistent solution  $u_{N+1}$ . Interchanging the independent and dependent variables prevents stepping past the singularity in the solution, but this interchange is inappropriate if the solution is not known to be monotone. If *a priori* knowledge of the monotonicity of the solution is unavailable, one is limited to using the time-stepping method, monitoring the solution, dynamically adjusting the step size to maintain accuracy, and preventing stepping past the singularity (if one exists). Since extending finite differences with unevenly spaced time steps to higher-order approximations is problematic from a programming perspective, using low-order methods is necessary. Thus, very small step sizes are required to accurately determine the solution near the point of singularity as the validity of the polynomial approximations becomes questionable. These difficulties are sometimes eliminated by exploiting the special (asymptotic) nature of the particular solution which produces an *ad hoc* approach to determining the blow-up point for each individual integral equation.

Lasseigne and Olmstead [49, 50] and others [64, 65] have taken this *ad hoc* approach in the past; however, the need to once again solve a similar problem justifies seeking a general approach. A general approach is developed here using the following integration criteria (IC):

- IC<sub>1</sub>: the integral is numerically approximated by existing software that accounts for the Abel-type singularity and adapts to a rapidly changing function;

- IC<sub>2</sub>: the singular or non-singular nature of the solution is unambiguously determined on a given time interval;
- IC<sub>3</sub>: if a point of singularity is determined to exist, the time step is adjusted in a straightforward manner to approximate the solution near this point accurately.

In order to satisfy the first criteria (IC<sub>1</sub>), a robust interpolation scheme is needed to provide a reasonable approximation to the unknown function for all values of the independent variable. In the interest of simplicity, as well as accuracy, a cubic-spline interpolation is a logical choice; however, because a singularity might exist in the solution, a cubic-spline interpolation directly applied to a discretized representation of the solution loses accuracy in the vicinity of the singularity. A specific change of variables is employed to satisfy the second criteria (IC<sub>2</sub>) and is key to the technique presented here. The change of variables is suggested by the asymptotic analysis of the nonlinear integral equation

$$u(\eta) = \int_{-\infty}^{\eta} \frac{1}{\sqrt{\pi(\eta - \xi)}} e^{u(\xi) + \xi} d\xi \quad (\text{III.2.3})$$

as developed by Olmstead [56]. Olmstead proved that a solution exists on the interval  $\eta \in (-\infty, -1)$  and that a solution cannot exist when  $\eta > 0$ . Thus, the solution is singular at some point  $\eta^* \in [-1, 0)$  which has been numerically determined to be  $\eta^* \approx -.431$ . The analysis proceeded by introducing the variables

$$\eta = \eta^0 - \frac{1}{\rho} \quad \xi = \eta^0 - \frac{1}{r} \quad \hat{u}(\rho) = u(\eta) \quad (\text{III.2.4})$$

and thereby, converting integral equation (III.2.3) to

$$\hat{u}(\rho) = \sqrt{\rho} e^{\eta^0} \int_0^{\rho} \frac{1}{\sqrt{\pi(\rho - r)}} e^{\hat{u}(r) - 1/r} r^{-3/2} dr. \quad (\text{III.2.5})$$

The lower limit changes from minus infinity to zero, and the variable  $\eta$  approaches  $\eta^0$  as  $\rho$  approaches infinity. Three possibilities for the value of  $\eta^0$  exist. If  $\eta^0 < \eta^*$ , it is easily determined that  $\hat{u}(\rho) \rightarrow u(\eta^0)$  as  $\rho \rightarrow \infty$ . If  $\eta^0$  is the ignition time (i.e.,  $\eta^0 = \eta^*$ ), then  $\hat{u}(\rho) \rightarrow \infty$  as  $\rho \rightarrow \infty$ . Finally, if  $\eta^0 > \eta^*$ , thermal runaway occurs for a *finite* value of  $\rho$  i.e.,  $\hat{u}(\rho) \rightarrow \infty$  as  $\rho \rightarrow \rho^*$ , and the analysis of (III.2.5) is as difficult as the analysis of (III.2.3). This last case is irrelevant to mathematical analysis developed by Olmstead [56]; however, considering  $\eta^0 > \eta^*$  is important in developing the numerical scheme satisfying integration criteria (IC<sub>1</sub>) and (IC<sub>2</sub>). The proposed method is illustrated

by a general discussion of the numerical solution of equations (III.2.3) and (III.2.5).

Upon using the asymptotic solution as  $\eta \rightarrow -\infty$  given by

$$u(\eta) \sim e^\eta + \dots \quad (\text{III.2.6})$$

equation (III.2.3) is approximated as

$$u(\eta) = \int_{-\infty}^{\eta_0} \frac{1}{\sqrt{\pi(\eta - \xi)}} e^\xi d\xi + \int_{\eta_0}^{\eta} \frac{1}{\sqrt{\pi(\eta - \xi)}} e^{u(\xi) + \xi} d\xi \quad (\text{III.2.7})$$

when  $\eta_0$  is chosen as a large negative number with large absolute value. A numerical solution to equation (III.2.7) has been successfully determined using a linear interpolation of the quantity  $e^{u(\xi) + \xi}$  in a finite-difference approximation to the second integral in (III.2.7) and interchanging the roles of the dependent and independent variables. Choosing a grid for values of  $u(\eta_i)$  results in a series of nonlinear algebraic equations to be solved for the values  $\eta_i$ . By using this interchange approach, stepping past the ignition point is *not* possible, and the temporal step size adjusts automatically near the ignition point. However, this exchange of dependent and independent variables is only valid when the solution is known to be one-to-one.

Now, imagine attempting to solve (III.2.7) while keeping time as the independent variable and using an adaptive numerical routine such as QUADPACK's D4QAWS [61] to approximate the integral with a square-root singularity. Using an adaptive numerical routine has the virtue of increasing the accuracy of the solution as opposed to the linear interpolation used previously. However, two problems exist. First, choosing a fixed, temporal step size leads to attempting to solve the discretized equations in a region where the solution does not exist (i.e., time-marching past the singularity). Second, the integrand is known only at the discretization points, and the adaptive numerical routine requires a value of  $u(\eta)$  for all  $\eta$ . A cubic-spline interpolation scheme provides values of  $u(\eta)$  between the discretization points. Away from the ignition point, the cubic spline is an excellent choice providing both accuracy and simplicity; however, even with the smaller and smaller step-sizes used near the ignition point, cubic-spline interpolation can fail in this crucial region.

Numerically approximating the solution to equation (III.2.5) instead of equation (III.2.3) resolves both difficulties. By using the asymptotic solution to take the first time



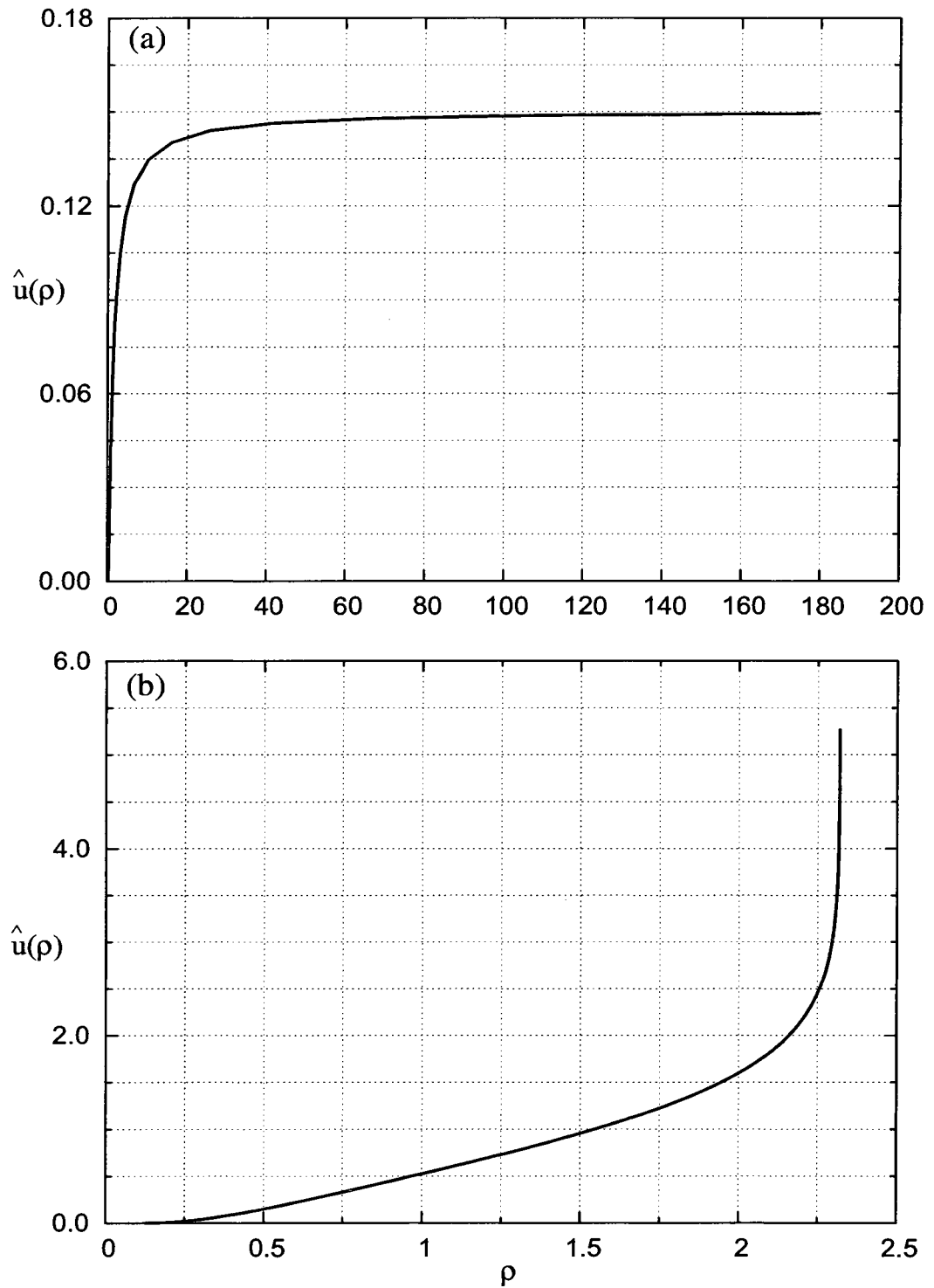


FIG. 1 Solution of benchmark equation in  $\rho$  variable. (a) Solution without a singularity,  $\eta^0 < \eta^*$ . (b) Solution with a singularity,  $\eta^0 > \eta^*$ .

step, the equation to solve numerically is

$$\begin{aligned} \hat{u}(\rho) = & \sqrt{\rho} e^{\eta^0} \int_0^{\rho_0} \frac{1}{\sqrt{\pi(\rho-r)}} e^{-1/r} r^{-3/2} dr \\ & + \sqrt{\rho} e^{\eta^0} \int_{\rho_0}^{\rho} \frac{1}{\sqrt{\pi(\rho-r)}} e^{\hat{u}(r)-1/r} r^{-3/2} dr, \end{aligned} \quad (\text{III.2.8})$$

with  $\rho_0$  some suitably small number. The numerical integration of (III.2.8) cannot begin until a choice is made for the parameter  $\eta^0$ . This choice affords the user control over the behavior of the solution. If  $\eta^0 < \eta^*$ , the solution in the  $\rho$  variable is similar to that seen in Figure 1(a), and approximating the integral by using QUADPACK's D4QAWS [61] routine and by interpolating the solution in the  $\rho$  variable with cubic splines produces excellent results. However, the solution is obtained on the interval  $(-\infty, \eta^0)$  and not the required interval  $(-\infty, \eta^*)$ . In fact, there is not yet any indication as to the value of  $\eta^*$ , which is the purpose of the numerical integration. A second (larger) choice of  $\eta^0$  must be made, and the solution to equation (III.2.8) is again determined numerically. Assuming that this time,  $\eta^0 > \eta^*$ , a singularity exists at some finite point  $\rho^*(\eta^0)$ , and the solution is as seen in Figure 1(b). Thus, a clear delineation exists between solutions which have singularities and solutions which do not have singularities. Upon determining that the solution with the second choice of  $\eta^0$  has a singularity, a search routine, e.g., bisection, can be constructed to find a value of  $\eta^0$  as close to  $\eta^*$  as possible. However, the integral equation must be solved numerous times, leading to a repetition of effort. In order to prevent this inefficiency, the following two-grid method is applied to equation (III.2.3):

- a coarse grid in the  $\eta$  variable is chosen as

$$\eta_{i+1} = \eta_i + \delta\eta_i \quad i = 0, 1, \dots; \quad (\text{III.2.9})$$

- the integral is written in three terms

$$\begin{aligned}
 u(\eta) = & \int_{-\infty}^{\eta_0} \frac{1}{\sqrt{\pi(\eta - \xi)}} e^{u(\xi) + \xi} d\xi \\
 & + \int_{\eta_0}^{\eta_i} \frac{1}{\sqrt{\pi(\eta - \xi)}} e^{u(\xi) + \xi} d\xi \\
 & + \int_{\eta_i}^{\eta} \frac{1}{\sqrt{\pi(\eta - \xi)}} e^{u(\xi) + \xi} d\xi;
 \end{aligned} \tag{III.2.10}$$

- the first integral is approximated by using the asymptotic value of the solution for the interval over  $(-\infty, \eta_0)$ ;
- the second integral is approximated by using a cubic spline interpolation in the  $\eta$  variable along with QUADPACK'S D4QAG [61] adaptive quadrature routine for the integral over  $(\eta_0, \eta_i)$ ;
- the change of variables

$$\eta = \eta_{i+1} - \frac{\delta\eta_i}{1 + \rho}, \quad \xi = \eta_{i+1} - \frac{\delta\eta_i}{1 + r}, \quad u(\eta) = \hat{u}(\rho) \tag{III.2.11}$$

is introduced in the third integral,

$$\int_{\eta_i}^{\eta} \frac{1}{\sqrt{\pi(\eta - \xi)}} e^{u(\xi) + \xi} d\xi = \tag{III.2.12}$$

$$\sqrt{\delta\eta_i(1 + \rho)} e^{\eta_{i+1}} \int_0^{\rho} \frac{1}{\sqrt{\pi(\rho - r)}} e^{\hat{u}(r) - \delta\eta_i/(1+r)} (1 + r)^{-3/2} dr,$$

and the numerical approximation proceeds on a fine grid chosen as

$$\rho_{j+1} = \rho_j(1 + \delta\rho), \quad \eta_{ij} = \eta_{i+1} - \frac{\delta\eta_i}{1 + \rho_j}, \quad 1 \leq j \leq j_{max}. \tag{III.2.13}$$

Thus, for each new interval  $(\eta_i, \eta_{i+1})$ , the solution is calculated on the fine grid,  $\eta_{ij}$ , by time stepping in the  $\rho$  variable. Using the  $\rho$  variable in lieu of the variable  $\eta$  provides a mechanism for satisfying integration criteria (IC<sub>2</sub>). If  $\eta_i < \eta^* < \eta_{i+1}$ , then  $u_{\rho\rho}$  becomes positive on the interval. Otherwise,  $u_{\rho\rho}$  remains negative for the entire interval, and  $\hat{u}(\rho)$

approaches  $u(\eta_{i+1})$  (a constant) as  $\rho$  approaches infinity. If the solution is determined to be singular on a given interval, the integration on this interval is discarded, and a smaller value of  $\delta\eta_i$  (i.e., a new value of  $\eta_{i+1}$ ) is chosen. The process continues until the interval with a singularity is found using the smaller  $\delta\eta_i$ . Again, the integration over the interval with the singularity is discarded, and an even smaller value of  $\delta\eta_i$  is chosen. Thus, the time step is adjusted in a straightforward manner near the point of singularity which satisfies integration criteria (IC<sub>3</sub>). The process is demonstrated in the next section by calculating the solution of integral equation (III.2.3).

### III.3 Numerical Solution of Benchmark Equation

The numerical solution of equation (III.2.3), restated here as

$$u(\eta) = \int_{-\infty}^{\eta} \frac{1}{\sqrt{\pi(\eta - \xi)}} e^{u(\xi) + \xi} d\xi, \quad (\text{III.3.1})$$

is sought. The solution exhibits a logarithmic singularity of the form

$$u \sim -\frac{1}{2} \ln(\eta^* - \eta) - \eta^* - \ln(2/\sqrt{\pi}) + O(\eta^* - \eta) \quad (\text{III.3.2})$$

where the finite blow-up time is  $\eta^* \approx -.431$ . Previous numerical integrations have determined this value by interchanging the dependent and independent variables during the numerical integration. While this interchange is certainly appropriate for this integral equation, it is inappropriate for other integral equations that are not known to be monotone *a priori*. Therefore, integral equation (III.3.1) provides a significant challenge (as well as a benchmark) to a general purpose solver that uses time marching.

To present our technique, we start with equation (III.2.10), the coarse grid given by (III.2.9), and the fine grid defined by (III.2.13). The asymptotic behavior of the solution is given by  $u(\eta) \sim e^\eta$  as  $\eta \rightarrow -\infty$ , and using this value to approximate the first integral gives

$$\int_{-\infty}^{\eta_0} \frac{1}{\sqrt{\pi(\eta - \xi)}} e^{u(\xi) + \xi} d\xi \sim e^\eta \operatorname{erfc}(\sqrt{\eta - \eta_0}). \quad (\text{III.3.3})$$

The second integral is zero if  $i = 1$ . For  $i > 1$ , the second integral is approximated using the numerical integration routine DQAG and interpolating  $u(\xi)$  with a cubic spline through the solution  $u_k$  and  $u_{kj}$  at the coarse grid points  $\eta_k$  and a subset of the fine grid points  $\eta_{kj}$ . The third integral is converted to the integral over the variable  $\rho$  on the interval  $(0, \rho_j)$  and

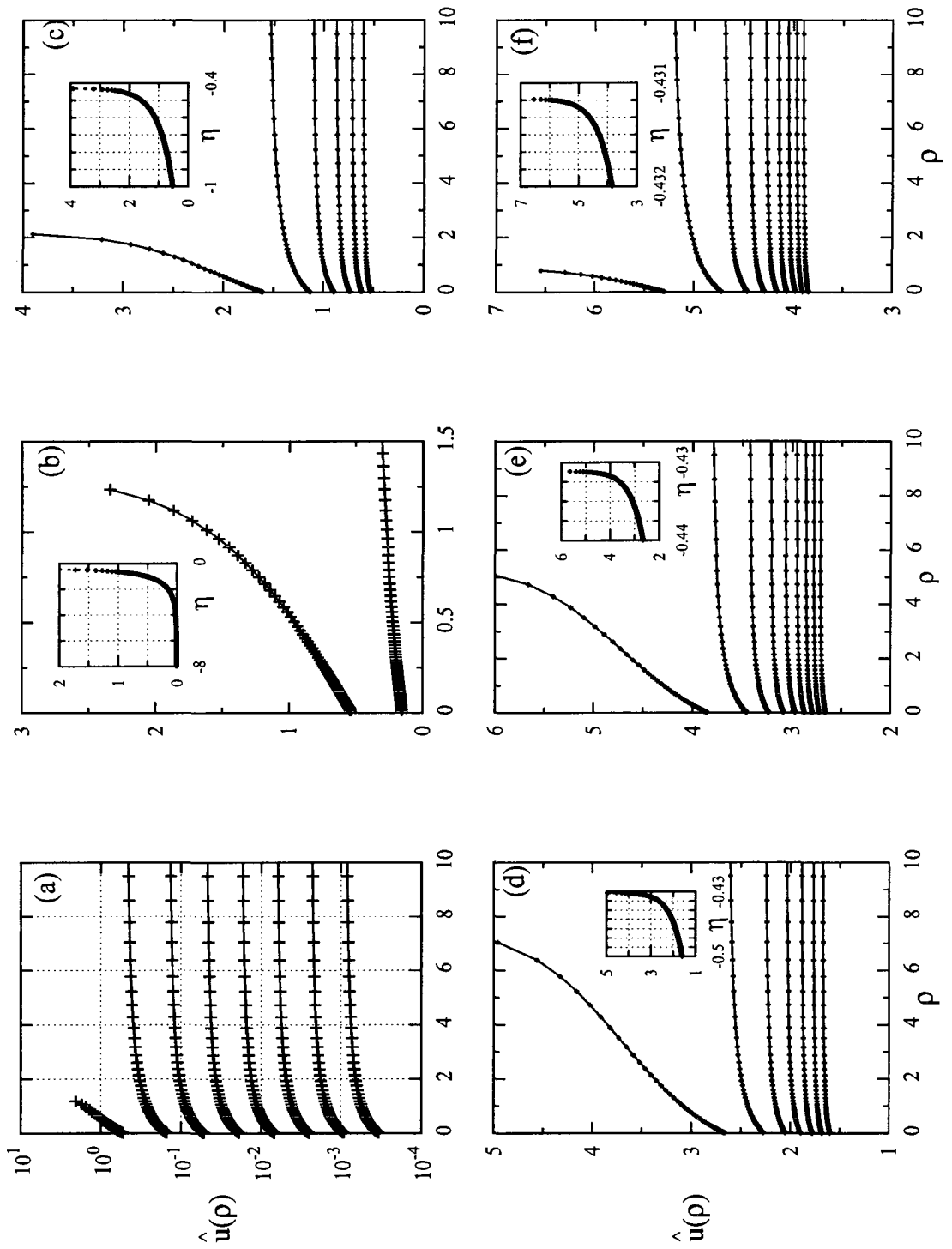


FIG. 2 Benchmark solution as function of fine-grid variable  $\rho$  for each coarse-grid interval. Insets show solution in original  $\eta$  variable. (a)  $\delta\eta = 1$ , (b)  $\delta\eta = 1$ , (c)  $\delta\eta = .1$ , (d)  $\delta\eta = .01$ , (e)  $\delta\eta = .001$ , (f)  $\delta\eta = .0001$ .

approximated by using the numerical integration routine DQAWS which appropriately handles the integrand's square root singularity at the upper limit. The integration process time marches the solution by first finding the value  $u_{i,j} = \hat{u}(\rho_j)$  when  $j = 1$  and then determining successively the solution when  $j = 2, 3, \dots, j_{max}$ . Values of  $\hat{u}(\rho)$  for all values of  $\rho$  are provided to the subroutine DQAWS using a cubic spline interpolation through  $u_{i+1,k}$  at the points  $\rho_k$  with  $-2 \leq k \leq j$ . The last two points from the previous interval,  $k = -2$  and  $k = -1$ , are put in terms of the variables on the new interval where  $\rho_{-2}$  and  $\rho_{-1}$  are negative. The point on the coarse grid is represented by  $k = 0$  where  $\rho_0 = 0$ . A nonlinear scalar equation of the form

$$u_{i+1,j} = \Phi(u_{i+1,j}) \quad (\text{III.3.4})$$

results, and the equation is solved for the unknown value  $u_{i+1,j} = u(\eta_{ij}) = \hat{u}(\rho_j)$  using a root finding method.

At this point, all of the quantities except for the solution on the coarse grid  $u_{i+1}$  are well defined. To define this quantity, the numerical solution on the fine grid must be extrapolated in the limit  $\rho \rightarrow \infty$ . Upon using the solution through the points  $\{\rho_{j-2}, \rho_{j-1}, \rho_j\}$  and the expansion

$$u \sim u_{i+1} - a \frac{1}{\rho} - b \frac{1}{\rho^2} + \dots, \quad (\text{III.3.5})$$

the approximation to the solution on the coarse grid  $u_{i+1}^j$  is found by solving the three-by-three system:

$$u_{i,j-2} = u_{i+1}^j - a \frac{1}{\rho_{j-2}} - b \frac{1}{\rho_{j-2}^2} + \dots \quad (\text{III.3.6})$$

$$u_{i,j-1} = u_{i+1}^j - a \frac{1}{\rho_{j-1}} - b \frac{1}{\rho_{j-1}^2} + \dots \quad (\text{III.3.7})$$

$$u_{i,j} = u_{i+1}^j - a \frac{1}{\rho_j} - b \frac{1}{\rho_j^2} + \dots \quad (\text{III.3.8})$$

Extrapolation is deemed to converge when the relative error between two successive approximations

$$\frac{|u_{i+1}^j - u_{i+1}^{j-1}|}{u_{i+1}^j} \quad (\text{III.3.9})$$

falls below a set tolerance level.

To start the integration, the discretization parameters that must be chosen are:  $\eta_0$ ,  $\delta\eta_i$ ,  $\rho_1$ ,  $\delta\rho$ , and  $j_{max}$ . Also, the relative and absolute error variables *ERRREL* and *ERRABS* for the subroutines D4QAG and D4QAWS must be specified. First, we present the converged solution using the values:  $\eta_0 = -8$ ,  $\delta\eta_i = 1$ ,  $\rho_1 = .01$ ,  $\delta\rho = .01$ ,  $j_{max} = 1000$ , *ERRREL* =  $10^{-7}$ , and *ERRABS* =  $10^{-14}$ . For consistency, the relative tolerance in the extrapolation that determines the value on the coarse grid is set to *ERRREL*.

Figure 2 shows the solution for each interval of the coarse grid. Figure 2(a) uses a logarithmic scale owing to the initial exponential behavior of the solution. As  $\rho$  increases from zero to infinity, the solutions are smooth and concave down for the integrations over the intervals corresponding to  $\eta = (-8, -1)$ . The solution has a different character for the integration corresponding to the last interval  $\eta = (-1, 0)$  which is seen in Figure 2(b). The solution curve becomes concave upwards on this interval representing a rapidly increasing solution in which a decrease in step size is needed for resolution. By halting the integration and decreasing the step size, time marching past a singularity (if one exists) is avoided. The inset shows that in the original  $\eta$  variable, the solution is smooth and seems to demonstrate singular behavior at some value of  $\eta$ . Since this singular behavior is on the interval  $\eta = (-1, 0)$ , the solution on this interval is recomputed using  $\delta\eta_i = .1$  while keeping the fine grid parameters the same. The change in  $\delta\eta_i$  increases the grid density by a factor of ten. Figure 2(c) shows that the solution corresponding to the interval  $\eta = (-.5, -.4)$  differs from the solutions corresponding to the sub-intervals on  $\eta = (-1, -.5)$  in the same way that the solution corresponding to the interval  $\eta = (-1, 0)$  differed from the solutions corresponding to the sub-intervals on  $\eta = (-8, -1)$ . Therefore, the last integration is discarded, and the solution over  $\eta = (-.5, -.4)$  is recomputed using  $\delta\eta_i = .01$  with the results shown in Figure 2(d). The same pattern is repeated on this finer interval. By changing to the  $\rho$  variable and properly adjusting the time steps, the solution near the singular point is accurately calculated without ever stepping past the point of singularity. Further refinements are shown in Figure 2(e) and Figure 2(f) on the interval  $\eta = (-.44, -.43)$  with  $\delta\eta_i = .001$  and on the interval  $\eta = (-.432, -.431)$  with  $\delta\eta_i = .0001$ , respectively.

The progression of the coarse grid is illustrated in the schematics, Figures 3(a)-(c). The integration time marches from the starting value  $\eta_0 = -8$  in increments of  $\delta\eta = 1$ . The solution is found to increase rapidly over the interval  $(\eta_7, \eta_8) = (-1, 0)$  (Figure 3(a)), and this last integration is discarded in favor of integration using a smaller  $\delta\eta$  as demonstrated in Figure 3(b). Again, the solution is found to increase rapidly over the interval  $(\eta_{12}, \eta_{13}) = (-.5, -.4)$ . The integration over this last interval is replaced by the integration

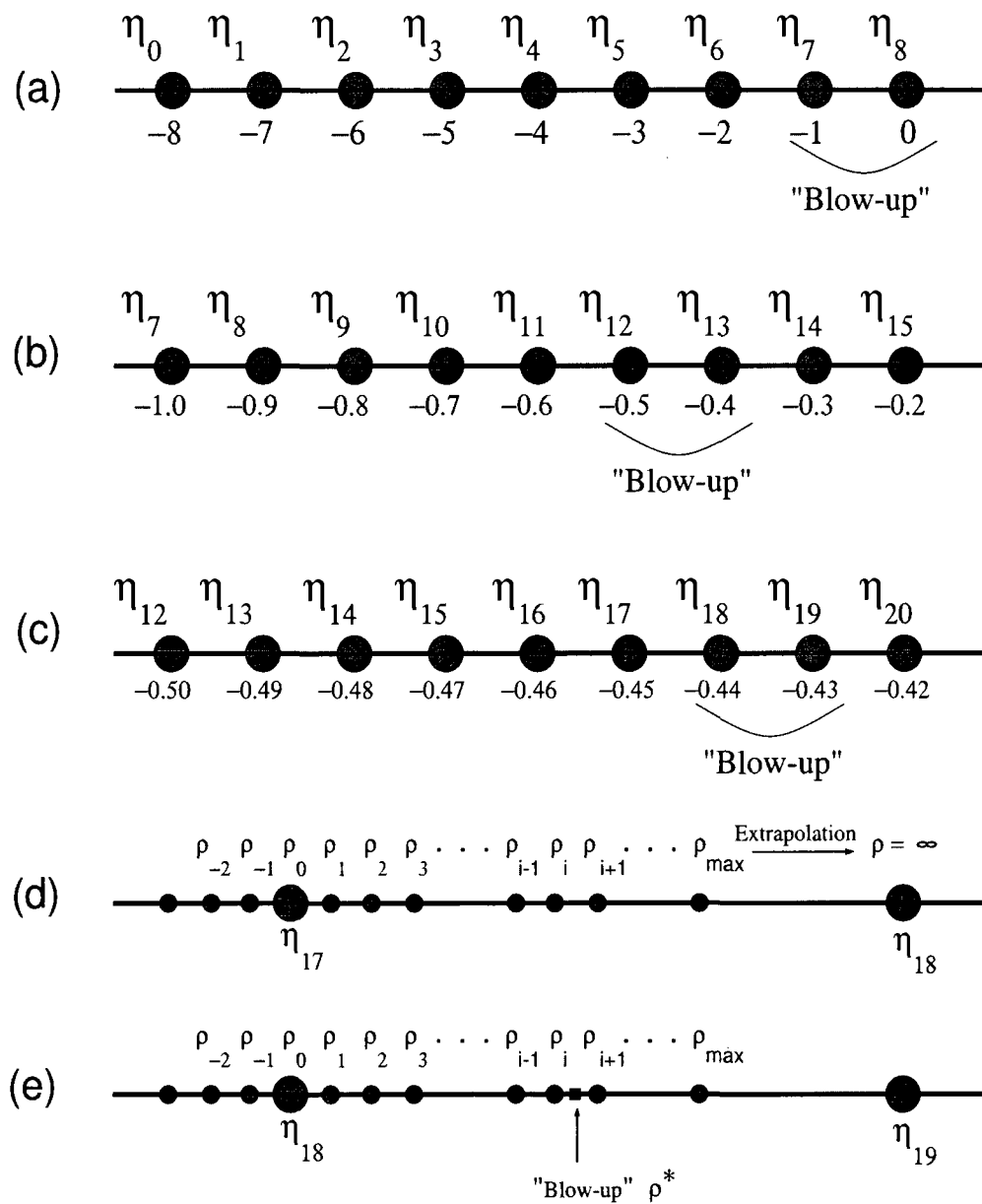


FIG. 3 Schematic showing fine and coarse grids for benchmark solution. (a-c) Coarse grids with  $\delta\eta = 1$ ,  $\delta\eta = .1$ , and  $\delta\eta = .01$ . (d) Fine-grid solution without blowup. (e) Fine-grid solution with blowup.



using  $\delta\eta = .01$  (Figure 3(c)). This process continues until the desired degree of accuracy is achieved or until reaching the limits of accuracy imposed by the various approximations and truncation errors. The schematics, Figures 3(d)-(e), illustrate the integration process over the fine grid. On coarse grid intervals that do not contain the blow-up point, the integration in the  $\rho$  variable continues until the extrapolation to  $\rho = \infty$  converges, Figure 3(d). On a coarse grid interval that contains the blow-up point, the integration continues until  $\rho$  nears  $\rho^*$  at which point a "blow-up criteria" (involving the second derivative with respect to  $\rho$ ) is met, Figure 3(e). Both fine grids show the points from the previous interval that are used in the cubic spline approximation when integrating in the  $\rho$  variable.

### III.3.1 Convergence and Accuracy Analysis of Numerical Routine

Nominally, the time-stepping routine has been successful. With minimal effort, the blow-up point has been determined to four digits of accuracy, and this value is consistent with the value determined using other methods. The next step is to determine the degree of accuracy possible with this approach. Four issues affecting the accuracy are addressed:

- How accurate is the numerical integration near the point of singularity?
- How accurate are the cubic-spline interpolations in both the  $\eta$  and  $\rho$  variables?
- How accurate is the determination of  $u_{\rho\rho}$  and  $u_{\rho\rho\rho}$  near the point of singularity?
- How does the extrapolation of the solution from the fine grid to the coarse grid affect the solution?

We start with evaluating the accuracy of the derivatives, as this analysis highlights important factors in determining the accuracy of the interpolation and integration.

#### III.3.1.1 Derivative Evaluation

When considered as a function of  $\rho$ , the solution on the interval which contains the singularity is markedly different than the solution on the intervals that do not contain the singularity. In particular,  $u_{\rho\rho} > 0$  for a significant region in the interval which contains the singularity, and developing a blowup criteria based on the value of the second derivative seems natural. Thus, determining the accuracy of the approximation to this important quantity is necessary. The first, second and third derivatives of  $u$  at the fine-grid point  $\rho_{n-2}$  are determined by using a five-point finite-difference approximation. The finite-difference

scheme is based on the Taylor-series approximation which is known to breakdown near the singular point. To examine the accuracy of the derivatives, the known asymptotic behavior of the integral equation solution near the point of singularity provides a test function. Thus, the logarithmic test function

$$U(\eta) = -\frac{1}{2} \ln(\bar{\eta}^* - \eta) - \bar{\eta}^* - \ln(2/\sqrt{\pi}) \quad (\text{III.3.10})$$

is converted to the  $\rho$  variable, and the exact derivatives are compared to the solutions of the four-by-four linear system of equations representing the finite-differences scheme using the values of  $u$  at the five points  $\rho_n, \rho_{n-1}, \rho_{n-2}, \rho_{n-3}$ , and  $\rho_{n-4}$ . The system is solved by using Gaussian elimination.

Figures 4(a)-(c) and Figures 5(a)-(c) show the relative errors of the derivative approximations for a generic interval  $\eta = (-1, -.9)$  and for each refinement of the coarse grid represented by smaller values of  $\delta\eta$  in the  $\eta$ -interval immediately before blow-up. The absolute errors of the second derivative approximations in the  $\eta$ -interval containing blow-up are shown in Figure 4(d) and Figure 5(d). Choosing  $\bar{\eta}^* = -.4311111111111111$  for these calculations produces nearly self-similar solutions since the solution near blow-up behaves as  $-.5 * \ln(\rho^* - \rho) + O(1)$  and since  $\rho^*$  is the same on each interval containing the blow-up point. The calculations presented in Figure 4 and Figure 5 represent different choices of the fine grid spacing  $\delta\rho$  and  $j_{max}$ .

The change to the  $\rho$  variable is designed so that Taylor-series approximations in the  $\rho$  variable are valid in each region without a singularity. The results for the generic interval  $\eta = (-1, -.9)$  indicate that the second derivative approximations in the  $\rho$  variable have relative errors in the range of  $10^{-9}$  when  $\rho$  is near zero and which increase with increasing  $\rho$  but never above  $10^{-4}$ . As  $\rho$  gets large, the solution asymptotes to a constant value and all derivatives become small in absolute value; therefore, the values of  $u$  at the five points differ by only a small amount. In addition, the absolute change in  $\rho$ ,  $\Delta\rho_i = \rho_i - \rho_{i-1} = \rho_{i-1} \delta\rho$ , is at its largest value. Thus, the loss of accuracy in the derivatives as  $\rho$  gets large is expected. Inaccuracies start to appear near  $\rho = 0$  for the other sub-intervals when  $\eta$  is near  $\bar{\eta}^*$ . These problems are partly attributable to the truncation error inherent in the difference  $\bar{\eta}^* - \eta$  when calculating the exact value of  $\ln(\bar{\eta}^* - \eta)$  as seen by the increase in relative errors when  $\delta\eta$  decreases making the values of  $\eta$  even closer to  $\bar{\eta}^*$ . Since the function is nearly self similar in the  $\rho$  variable, the presence of errors when calculating the values of  $U(\eta)$  is the only explanation for the increasing relative errors

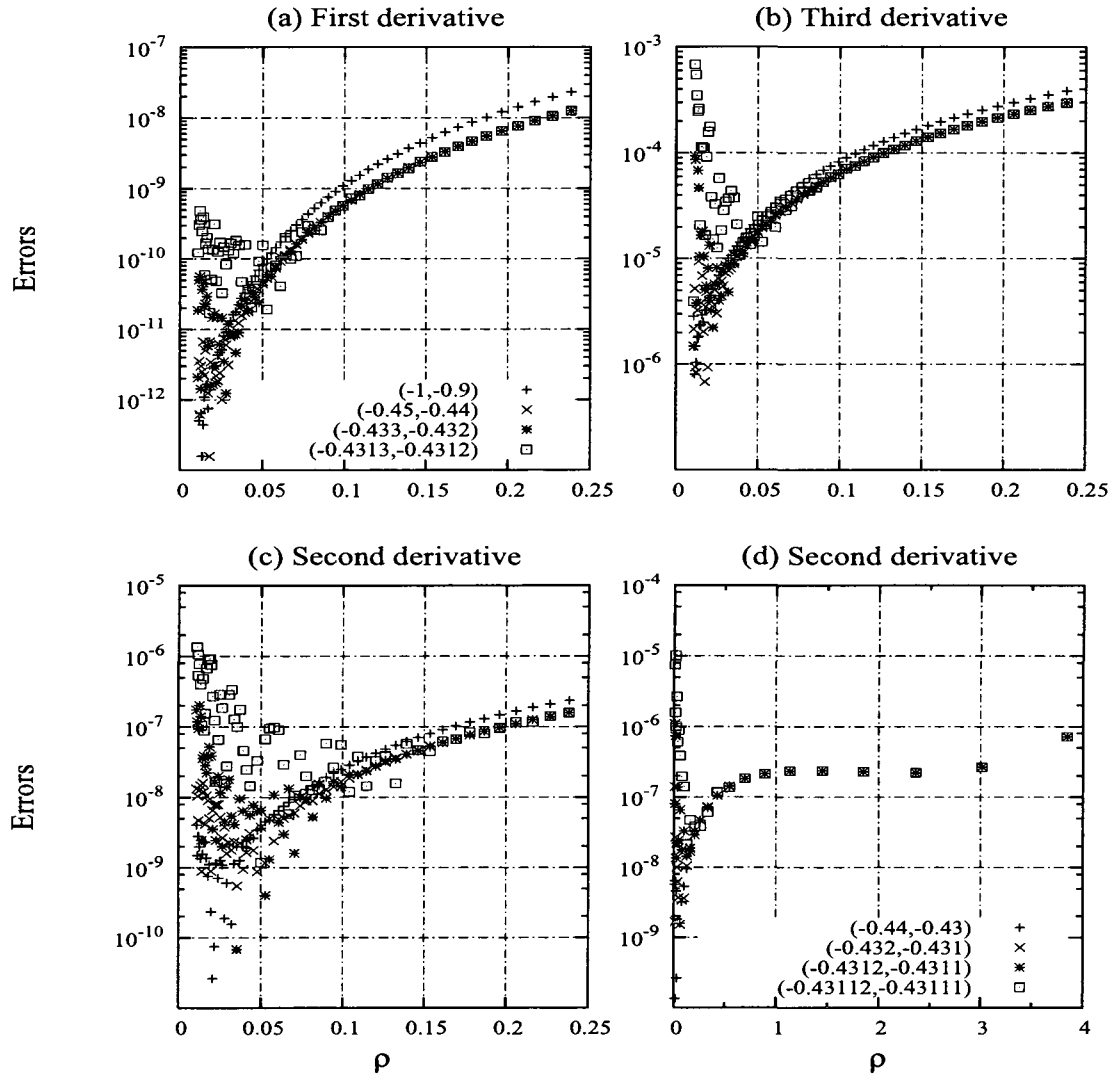


FIG. 4 Relative error in derivative approximations and absolute error near blowup for  $\delta\rho = .05$ ,  $j_{max} = 1000$ . (a)-(c) Relative error in derivative approximations,  $\delta\rho = .05$ ,  $j_{max} = 1000$ . (d) Absolute error near blowup.

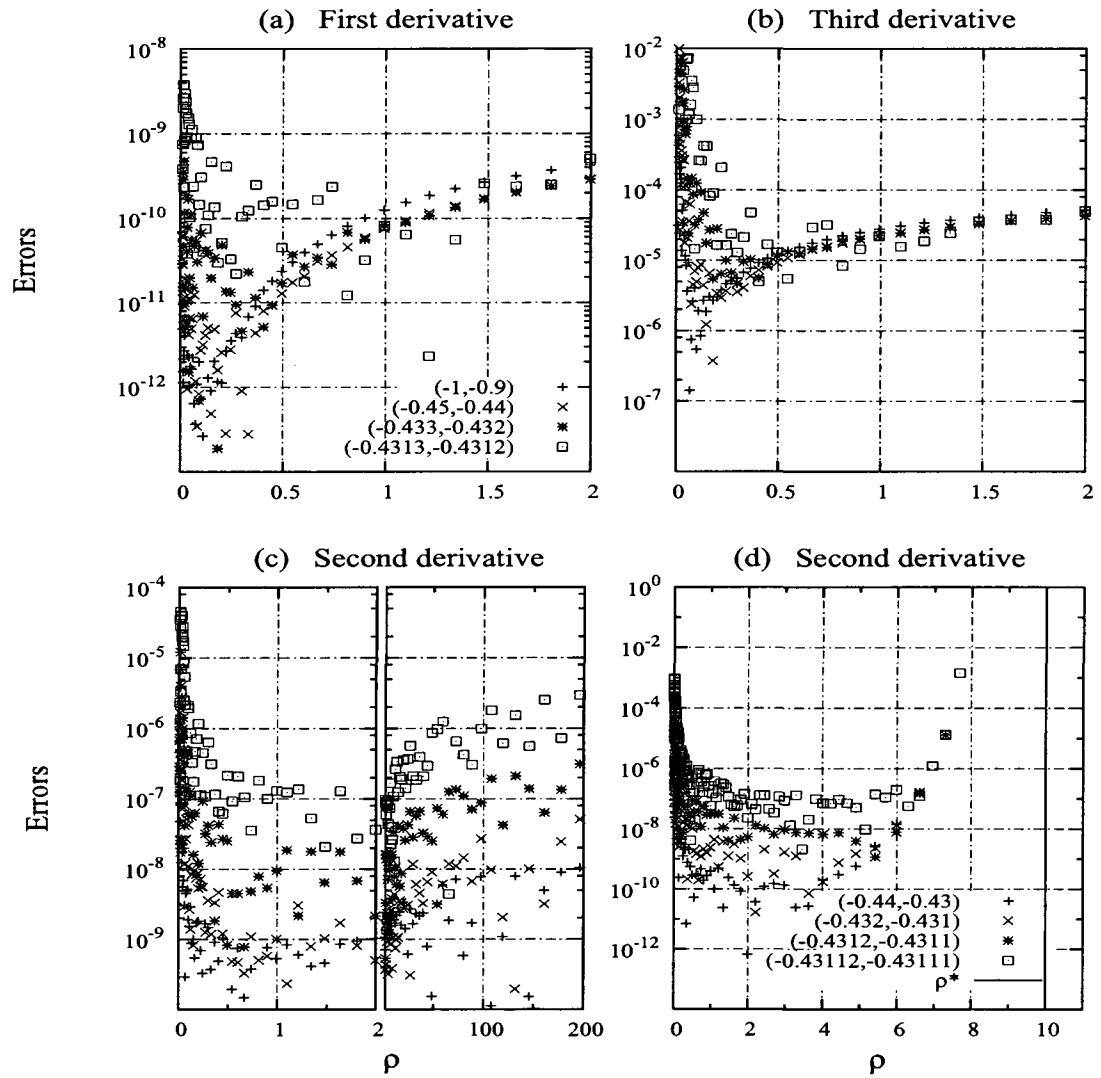


FIG. 5 Relative error in derivative approximations and absolute error near blowup for  $\delta\rho = .005$ ,  $j_{max} = 10000$ . (a)-(c) Relative error in derivative approximations,  $\delta\rho = .005$ ,  $j_{max} = 10000$ . (d) Absolute error near blowup.

in the derivatives. However, a second parameter also affects the size of relative errors. Compare the results presented in Figure 4 using  $\delta\rho = .05$  with the results presented in Figure 5 using  $\delta\rho = .005$ . Near  $\rho = 0$ , the absolute change in  $\rho$ ,  $\Delta\rho_i = \rho_i - \rho_{i-1} = \rho_{i-1}\delta\rho$ , is at its smallest value, and additional truncation errors in the differences calculated during Gaussian elimination increase the relative errors in the derivative approximations.

Of prime importance to the method employed in this manuscript is the calculation of the second derivative with respect to the  $\rho$  variable. This value is paramount in determining whether a singularity exists on a given  $\eta$  interval. Figure 4(d) and Figure 5(d) show the absolute error when calculating this important quantity on an interval containing a singularity. As  $\rho$  approaches  $\rho^*$ , the errors increase rapidly owing to the inaccuracy of the Taylor-series approximation in this region. However, the sign of the second derivative and its magnitude within a couple of digits of accuracy can still be determined for most values of  $\rho$ , and this is what the blowup criteria is based upon.

### III.3.1.2 Spline Fit

The numerical solution of the integral equation provides solution estimates at discrete points. The estimates differ from the true solution through previous use of numerical integration, interpolation, extrapolation and truncation. The first of the integration criteria (IC<sub>1</sub>) states: "the integral is numerically approximated by existing software that accounts for the Abel-type singularity and adapts to a rapidly changing function." This criterion is satisfied by choosing the numerical integration routines from QUADPACK [61]. However, these routines require the values of the solution at all points along the path of integration. Thus, an interpolation scheme must provide the missing solution values from the approximate solution values at the discrete points. The accuracy and robustness of the interpolation scheme must be assessed for the unique conditions pertaining to the solution of the integral equation.

For this study, the cubic-spline is chosen as the appropriate interpolation scheme and is calculated by using the FORTRAN subroutines SPLINE and SEVAL from *Computer Methods for Mathematical Computations*, by Forsythe, Malcolm, and Moler [23]. This particular version of the cubic spline is not the natural cubic spline in which the second derivative at the endpoints are set to zero, but rather matches the third derivative of the first cubic spline to the third derivative of the unique cubic polynomial passing through the first four points and matches the third derivative of the last cubic spline to the third derivative of the unique cubic polynomial passing through the last four points. Considering that the

second derivative of the solution approaches infinity near any singular point, this cubic spline should be a better representation of the solution in the region of the singularity than the natural cubic spline which would force the approximation to have a zero second derivative. The accuracy of the cubic spline interpolation is well known if applied to a smooth continuous function; however, the accuracy near a singular point depends on both the discretization scheme and the type of singularity. To test the accuracy of the interpolation scheme (independently of the numerical solution of the integral equation), the cubic spline is applied to the test function  $U(\eta)$  (defined in equation (III.3.10)) with the same singularity as the expected solution while using the same discretization near the point of singularity as used during the solution of the integral equation.

First, the spline is applied in the  $\eta$  variable on intervals not containing the singularity by evaluating the test function at every fifth fine grid point and at every coarse grid point over the interval  $[-2.0, \eta_i]$ . The endpoints,  $\eta_i$ , are the coarse grid points as in Figure 3 and equation (III.2.9). The maximum relative error and average relative error are calculated by selecting one-hundred evenly-spaced points in the test intervals  $[\eta_{i-1}, \eta_i]$  for  $i > 7$ . The results are presented in Table 2. For each level of  $\Delta\eta$ , the accuracy degrades as the interval with the singularity is approached, but the accuracy is recovered when the value of  $\Delta\eta$  is decreased. The relative accuracy over all the tested intervals is easily maintained as less than  $10^{-8}$  by decreasing the value of  $\delta\rho$ , and thereby, adding more points within the interval.

### III.3.1.3 Numerical Integration

In solving the integral equation, the method relies on using well developed software for achieving the actual quadrature. In this case, the adaptive routines D4QAG and D4QAWS from QUADPACK [61] have been chosen in order to handle the Abel-type singularity. However, it should be noted that these routines are applied to integrands in which the non-kernel part is itself singular, and the accuracy of this application needs to be examined. Therefore, the numerical quadrature of the well defined integral

$$I_{rest}(\eta) = \int_{\eta_0}^{\eta} \frac{1}{\sqrt{\pi(\eta - \xi)}} e^{U(\xi) + \xi} d\xi \quad (\text{III.3.11})$$

with

$$U(\eta) = -\frac{1}{2} \ln(\bar{\eta}^* - \eta) - \bar{\eta}^* - \ln(2/\sqrt{\pi}) \quad (\text{III.3.12})$$



is investigated. The coarse and fine grid structure developed for the solution of the integral equation is used to calculate the test integral which has the asymptotic solution

$$I_{test}(\eta) \sim -\frac{1}{2} \ln(\bar{\eta}^* - \eta) + O(1) \quad \text{as } \eta \rightarrow \bar{\eta}^*. \quad (\text{III.3.13})$$

The effects of using both direct calculation of the integrand and approximation of the integrand by cubic spline are investigated.

The results of calculating the test integral using direct evaluation of the integrand with the value  $\bar{\eta}^* = -.43111111111111$  are plotted versus  $u_{asy}(\eta) = -\ln(\bar{\eta}^* - \eta)/2$ . If the numerical results are correct, the resulting graph should be a straight line with a slope of unity in the limit  $u_{asy}(\eta) \rightarrow \infty$ . As seen in Figure 6(a), the chosen numerical routines sufficiently capture the singular nature of the result when using the coarse and fine grids proposed for the solution of the integral equation. The level of  $\Delta\eta$  for the coarse grid is indicated on the graph, and the points in between have been calculated using the  $\rho$  variable. The agreement of the test integral with the asymptotic form is quantitatively investigated in Figure 6(b) where the difference of the slope of the line in 6(a)

$$m = \frac{I_{test}(\eta_{i,j+1}) - I_{test}(\eta_{i,j})}{u_{asy}(\eta_{i,j+1}) - u_{asy}(\eta_{i,j})}$$

from unity is shown versus  $u_{asy}(\eta)$ . As expected, the difference of the slope from unity approaches zero as  $u_{asy}(\eta) \rightarrow \infty$ , at least, until the changes in the coarse grid  $\Delta\eta$  become too small. At this point, truncation errors in calculating the test integrand along with normal quadrature errors compromise the accuracy. As a further check on the calculations, computation of the test integral using the cubic spline interpolation rather than a direct evaluation of the test integrand was performed and no significant difference was found.

#### III.3.1.4 Extrapolation

As mentioned previously, the solution on the coarse grid is found by extrapolation using the asymptotic form

$$u \sim u_{i+1} - a\frac{1}{\rho} - b\frac{1}{\rho^2} + \dots \quad (\text{III.3.14})$$



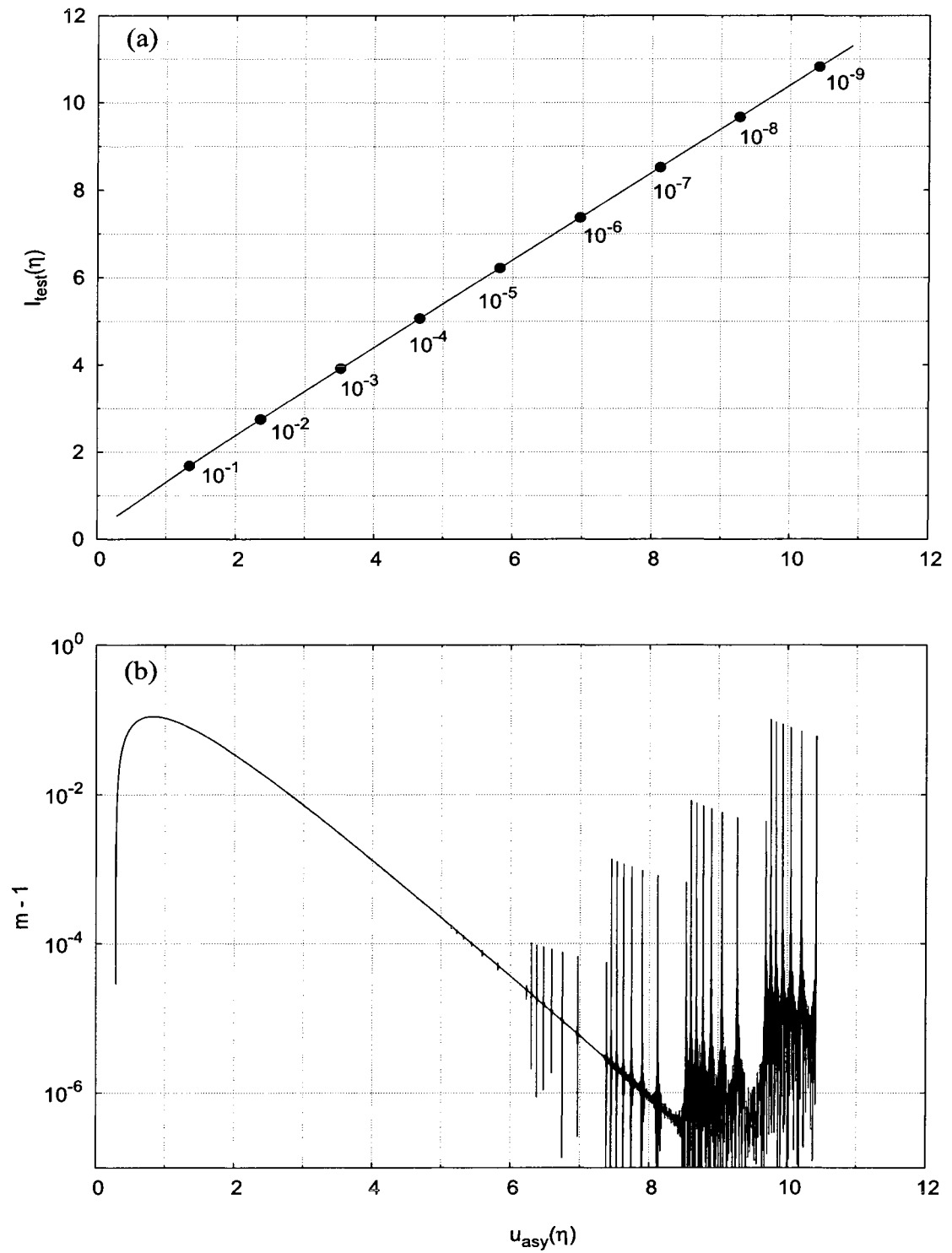


FIG. 6 Investigation of numerical integration routines. (a) Value of test integral versus asymptotic form. Values of  $\eta^* - \eta$  are indicated. (b) Variation of slope from unity.

The approximation to the solution on the coarse grid  $u_{i+1}^j$  is found by solving the three-by-three system:

$$u_{i,j-2} = u_{i+1}^j - a \frac{1}{\rho_{j-2}} - b \frac{1}{\rho_{j-2}^2} + \dots \quad (\text{III.3.15})$$

$$u_{i,j-1} = u_{i+1}^j - a \frac{1}{\rho_{j-1}} - b \frac{1}{\rho_{j-1}^2} + \dots \quad (\text{III.3.16})$$

$$u_{i,j} = u_{i+1}^j - a \frac{1}{\rho_j} - b \frac{1}{\rho_j^2} + \dots \quad (\text{III.3.17})$$

Extrapolation is deemed to converge when the relative error between two successive approximations

$$\frac{|u_{i+1}^j - u_{i+1}^{j-1}|}{u_{i+1}^j} \quad (\text{III.3.18})$$

falls below a set tolerance level.

Since it is possible for a "false" convergence to occur by happenstance, it is required that the relative error remains below the tolerance level for five successive values of the fine grid index  $j$ . Once the extrapolation criteria is satisfied, the integration over the interval  $(\eta_i, \eta_{i+1})$  is deemed complete (even if  $j < j_{max}$ ), and the integration continues on the next coarse grid interval.

The discretization parameters chosen for this part of the study are:  $\eta_0$ ,  $\delta\eta_i$ ,  $\rho_0$ ,  $\delta\rho$ , and  $j_{max}$ . Also, the relative and absolute error variables *ERRREL* and *ERRABS* for the subroutines D4QAG and D4QAWS must be specified. We present the converged solution using the values:  $\eta_0 = -8.0000001$ ,  $\delta\eta_i = .5$ ,  $\rho_1 = .01$ ,  $\delta\rho = .01$ , *ERRREL* =  $10^{-8}$ , and *ERRABS* =  $10^{-14}$ . Two values of the relative tolerance in the extrapolation,  $10^{-9}$  and  $10^{-7}$  along with two values for the maximum number of points on the fine grid,  $j_{max} = 1000$  and  $j_{max} = 1250$ , are investigated. On coarse grid intervals that do not terminate early due to extrapolation, the solution on the coarse grid point  $\eta_{i+1}$  is taken as the final extrapolated value  $u_{i+1}^{j_{max}}$  which occurs for the  $\rho$  value  $\rho_{max} = \rho_0(1 + \delta\rho)^{j_{max}}$ .

Tables 3, 4, 5 show the results of the calculations. With the value of  $10^{-9}$  for the relative tolerance in the extrapolation, the integration terminated early for the intervals  $(-8, -1)$  and went to the maximum for all intervals  $(-.5, \eta^*)$ . The only difference found between the solutions when  $j_{max} = 1000$  and  $j_{max} = 1250$  is that the solution terminated early by extrapolation on the interval  $(-1, -.5)$  when  $j_{max} = 1250$  but not when  $j_{max} = 1000$ . When  $j_{max} = 1000$ , the value of  $\eta^*$  was found to lie on the interval  $(-.431155610, -.431155605)$ ; when  $j_{max} = 1250$ , the value of  $\eta^*$  was found to lie on the

TABLE 3  
 Relative tolerance of the extrapolation  $10^{-9}$  with  $j_{max} = 1000$ .

$i$	$\eta_i$	$\eta_{i+1}$	$j$	$\rho_{max}$
1	-8.00000010	-7.50000010	916	90.0
2	-7.50000010	-7.00000010	916	90.0
3	-7.00000010	-6.50000010	917	90.9
4	-6.50000010	-6.00000010	916	90.0
5	-6.00000010	-5.50000010	917	90.9
6	-5.50000010	-5.00000010	915	89.1
7	-5.00000010	-4.50000010	905	80.6
8	-4.50000010	-4.00000010	919	92.7
9	-4.00000010	-3.50000010	921	94.6
10	-3.50000010	-3.00000010	909	83.9
11	-3.00000010	-2.50000010	928	101.4
12	-2.50000010	-2.00000010	939	113.1
13	-2.00000010	-1.50000010	959	138.0
14	-1.50000010	-1.00000010	991	189.7
15	-1.00000010	-0.50000010	1001	209.6
16	-0.50000010	-0.45000010	1001	209.6
17	-0.45000010	-0.44500010	1001	209.6
18	-0.44500010	-0.44000010	1001	209.6
19	-0.44000010	-0.43500010	1001	209.6
20	-0.43500010	-0.43450010	1001	209.6
⋮	⋮	⋮	⋮	⋮
50	-0.43115605	-0.43115600	1001	209.6
51	-0.43115600	-0.43115595	1001	209.6
52	-0.43115595	-0.43115590	1001	209.6
53	-0.43115590	-0.43115585	1001	209.6
54	-0.43115585	-0.43115580	1001	209.6
55	-0.43115580	-0.43115575	1001	209.6
56	-0.43115575	-0.43115570	1001	209.6
57	-0.43115570	-0.43115565	1001	209.6
58	-0.43115565	-0.43115565	1001	209.6
59	-0.43115565	-0.43115564	1001	209.6
60	-0.43115564	-0.43115564	1001	209.6
61	-0.43115564	-0.43115563	1001	209.6
62	-0.43115563	-0.43115563	1001	209.6
63	-0.43115563	-0.43115562	1001	209.6
64	-0.43115562	-0.43115562	1001	209.6
65	-0.43115562	-0.43115561	1001	209.6
66	-0.43115561	-0.43115561	1001	209.6

TABLE 4  
 Relative tolerance of the extrapolation  $10^{-9}$  with  $j_{max} = 1250$ .

$i$	$\eta_i$	$\eta_{i+1}$	$j$	$\rho_{max}$
1	-8.00000010	-7.50000010	916	90.0
2	-7.50000010	-7.00000010	916	90.0
3	-7.00000010	-6.50000010	917	90.9
4	-6.50000010	-6.00000010	916	90.0
5	-6.00000010	-5.50000010	917	90.9
6	-5.50000010	-5.00000010	915	89.1
7	-5.00000010	-4.50000010	905	80.6
8	-4.50000010	-4.00000010	919	92.7
9	-4.00000010	-3.50000010	921	94.6
10	-3.50000010	-3.00000010	909	83.9
11	-3.00000010	-2.50000010	928	101.4
12	-2.50000010	-2.00000010	939	113.1
13	-2.00000010	-1.50000010	959	138.0
14	-1.50000010	-1.00000010	991	189.7
15	-1.00000010	-0.50000010	1142	852.5
16	-0.50000010	-0.45000010	1251	2521.8
17	-0.45000010	-0.44500010	1251	2521.8
18	-0.44500010	-0.44000010	1251	2521.8
19	-0.44000010	-0.43500010	1251	2521.8
20	-0.43500010	-0.43450010	1251	2521.8
⋮	⋮	⋮	⋮	⋮
40	-0.43116510	-0.43116010	1251	2521.8
41	-0.43116010	-0.43115960	1251	2521.8
42	-0.43115960	-0.43115910	1251	2521.8
43	-0.43115910	-0.43115860	1251	2521.8
44	-0.43115860	-0.43115810	1251	2521.8
45	-0.43115810	-0.43115760	1251	2521.8
46	-0.43115760	-0.43115710	1251	2521.8
47	-0.43115710	-0.43115705	1251	2521.8
48	-0.43115705	-0.43115700	1251	2521.8
49	-0.43115700	-0.43115695	1251	2521.8
50	-0.43115695	-0.43115690	1251	2521.8
51	-0.43115690	-0.43115685	1251	2521.8
52	-0.43115685	-0.43115680	1251	2521.8

TABLE 5  
Relative tolerance of the extrapolation  $10^{-7}$  with  $j_{max} = 1250$ .

$i$	$\eta_i$	$\eta_{i+1}$	$j$	$\rho_{max}$
1	-8.00000010	-7.50000010	755	18.1
2	-7.50000010	-7.00000010	756	18.3
3	-7.00000010	-6.50000010	756	18.3
4	-6.50000010	-6.00000010	757	18.5
5	-6.00000010	-5.50000010	756	18.3
6	-5.50000010	-5.00000010	757	18.5
7	-5.00000010	-4.50000010	758	18.7
8	-4.50000010	-4.00000010	761	19.2
9	-4.00000010	-3.50000010	761	19.2
10	-3.50000010	-3.00000010	763	19.6
11	-3.00000010	-2.50000010	770	21.0
12	-2.50000010	-2.00000010	779	23.0
13	-2.00000010	-1.50000010	797	27.5
14	-1.50000010	-1.00000010	840	42.2
15	-1.00000010	-0.50000010	987	182.3
16	-0.50000010	-0.45000010	908	83.1
17	-0.45000010	-0.44500010	1251	2521.8
18	-0.44500010	-0.44000010	1251	2521.8
19	-0.44000010	-0.43500010	1251	2521.8
20	-0.43500010	-0.43450010	892	70.9
21	-0.43450010	-0.43400010	701	10.6
22	-0.43400010	-0.43350010	701	10.6
23	-0.43350010	-0.43300010	795	27.0
24	-0.43300010	-0.43250010	1251	2521.8
25	-0.43250010	-0.43200010	1251	2521.8
26	-0.43200010	-0.43195010	835	40.2

$i$	$\eta_i$	$\eta_{i+1}$	$j$	$\rho_{max}$
27	-0.43195010	-0.43190010	709	11.5
28	-0.43190010	-0.43185010	703	10.8
29	-0.43185010	-0.43180010	759	18.9
30	-0.43180010	-0.43175010	702	10.7
31	-0.43175010	-0.43170010	703	10.8
32	-0.43170010	-0.43165010	944	118.9
33	-0.43165010	-0.43160010	706	11.1
34	-0.43160010	-0.43155010	703	10.8
35	-0.43155010	-0.43150010	706	11.1
36	-0.43150010	-0.43145010	714	12.1
37	-0.43145010	-0.43140010	701	10.6
38	-0.43140010	-0.43135010	701	10.6
39	-0.43135010	-0.43130010	701	10.6
40	-0.43130010	-0.43125010	727	13.7
41	-0.43125010	-0.43120010	743	16.1
42	-0.43120010	-0.43115010	1251	2521.8
43	-0.43115010	-0.43115005	767	20.4
44	-0.43115005	-0.43115000	804	29.5
45	-0.43115000	-0.43114995	724	13.3
46	-0.43114995	-0.43114990	758	18.7
47	-0.43114990	-0.43114990	1032	285.3
48	-0.43114990	-0.43114989	889	68.8
49	-0.43114989	-0.43114989	906	81.4
50	-0.43114989	-0.43114988	961	140.8
51	-0.43114988	-0.43114988	1182	1269.2
52	-0.43114988	-0.43114987	1251	2521.8
53	-0.43114987	-0.43114987	1251	2521.8

interval  $(-0.43115685, -0.43115680)$ . Thus, a difference in the sixth significant digit exists. Using the value of  $10^{-7}$  for the relative tolerance in the extrapolation and  $j_{max} = 1250$ , the integration terminated early for the intervals  $(-8, -0.45)$  and on most intervals between  $(-0.45, \eta^*)$ . Furthermore, it was necessary to impose an additional condition that extrapolation cannot converge unless  $\rho > 10$  to prevent premature extrapolation. The value of  $\eta^*$  was found to lie on the interval  $(-0.431149870, -0.431149865)$ . This is a difference in the fifth significant digit as compared to the results using a relative tolerance of  $10^{-9}$ .

### III.3.2 Determining If the Solution is Singular on the Active Interval

When considered as a function of  $\rho$ , the solution on the interval which contains the singularity is markedly different than the solution on the intervals that do not contain the singularity. In particular,  $u_{\rho\rho} > 0$  for a significant region in the interval containing a singularity. A blowup criteria is developed using the derivatives of  $u$  at the point  $\rho_{n-2}$ . If  $u_{\rho\rho} > u_{\rho\rho_{crit}}$ ,  $u_{\rho\rho\rho} > 0$ , and  $u_{\rho} > u_{\rho_{crit}}$ , then the blow-up point is assumed to exist on the current interval. If this switch is tripped, the solution on the current interval is recalculated using a smaller value of  $\delta\eta_i$  and proceeds as before until the switch is tripped on the new (smaller) interval indicating the singularity is found. The solution on this last interval is recalculated by again reducing the value of  $\delta\eta_i$ . Thus, the accuracy of determining  $\eta^*$  is improved recursively. The last criteria is necessary to prevent premature tripping of the switch determining blow-up. As seen in the previous section, errors in the second and third derivatives first appear near  $\rho = 0$  whenever errors appear in the  $u$  variable. The fluctuations in the second and third derivatives owing to these errors can easily trip the switch even when the singularity is not in the current computational interval. By requiring  $u_{\rho}$  to be significantly large also, the switch is tripped only near the singularity. Using the value  $u_{\rho\rho_{crit}} = 20$  and  $u_{\rho_{crit}} = 1$  was sufficient for the benchmark problem when  $\delta\rho$  is small enough to capture the developing singularity.

### III.4 Solution of Second Benchmark Problem

The second benchmark problem is derived by considering the effect of replacing the usual external heating conditions with marginal heating conditions in the ignition problem. The governing integral equation as derived in Lasseigne and Olmstead [50] is

$$u(\eta) = \gamma \int_{-\infty}^{\eta} \frac{1}{\sqrt{\pi(\eta - \xi)}} e^{u(\xi) - \xi^2} d\xi. \quad (\text{III.4.1})$$

Lasseigne and Olmstead [50] proved that a bounded (i.e., non-blowup) solution exists if the value of the parameter  $\gamma$  satisfies  $\gamma < .303$ ; and they proved that a blowup solution exist if the parameter  $\gamma$  satisfies  $\gamma > .825$ . Thus, it is important to be able to numerically integrate the governing equation in a way that takes into account both possibilities, and providing this ability is the purpose of the scheme proposed and investigated in this thesis.

The integral was divided as

$$\gamma \int_{-\infty}^{\eta} \frac{1}{\sqrt{\pi(\eta - \xi)}} e^{u(\xi) - \xi^2} d\xi = \tag{III.4.2}$$

$$\gamma \int_{-\infty}^{\eta_0} \frac{1}{\sqrt{\pi(\eta - \xi)}} e^{-\xi^2} d\xi + \gamma \int_{\eta_0}^{\eta} \frac{1}{\sqrt{\pi(\eta - \xi)}} e^{u(\xi) - \xi^2} d\xi,$$

where  $\eta_0$  is a sufficiently large negative number so that the asymptotic form of  $u(\eta) \sim e^{-\eta^2}$  found in Lasseigne and Olmstead [50] was applicable. For  $\eta$  slightly greater than  $\eta_0$  and still a large negative number, the solution determined through numerical integration agreed with the asymptotic solution.

The following parameters were chosen for the integration:  $\eta_0$ ,  $\delta\eta_i$ ,  $\rho_1$ ,  $\delta\rho$ , and  $j_{max}$ . Also, the relative and absolute error variables *ERRREL* and *ERRABS* for the subroutines DQAG and DQAWS must be specified. First, we present the converged solution using the values:  $\eta_0 = -8$ ,  $\delta\eta_i = 1$ ,  $\rho_1 = .01$ ,  $\delta\rho = .01$ ,  $j_{max} = 1000$ , *ERRREL* =  $10^{-8}$ , and *ERRABS* =  $10^{-14}$ . The initial integral is calculated by using QUADPACK's [61] D4QAGI routine to integrate over infinite intervals not containing singularities.

The solution for  $\gamma \in (0, 3.0)$  by  $\Delta\gamma = .5$  is shown in Figure 7(a). Obviously,  $u(\eta) = 0$  when  $\gamma = 0$ , but blowup is found for all other investigated values of  $\gamma$  in this range. The blowup time  $\eta^*(\gamma)$  increased rapidly between  $\gamma = 1$  and  $\gamma = .5$ ; thus, the next investigation considered  $\gamma \in (0, 1.0)$  by  $\Delta\gamma = .1$  which is shown in Figure 7(b). These curves clearly show that the critical value of  $\gamma$  lies on the interval  $(.4, .5)$ . In order to determine the critical value  $\gamma_c$ , as well as, the behavior  $\eta^*(\gamma)$  as  $\gamma \rightarrow \gamma_c^+$ , the investigation continues by starting from  $\gamma = .5$  and using  $\Delta\gamma = -.01$ . The results are shown in Figure 8(a), and the value of  $\gamma_c$  is determined to lie between  $(.46, .47)$ . This investigation is repeated using  $\Delta\gamma = -.001$ ,  $\Delta\gamma = -.0001$ , and  $\Delta\gamma = -.00001$ . Some of the results for  $\Delta\gamma = -.001$  and  $\Delta\gamma = -.0001$  are shown in Figure 8(a), and the value of  $\gamma_c$  is determined to lie between  $(.4631, .4630)$ . The results for  $\Delta\gamma = -.00001$ . are seen in Figure 8(b).

Figure 9(a-b) and Figure 10 show closeups of the results all the way to  $\Delta\gamma = -10^{-10}$ ,

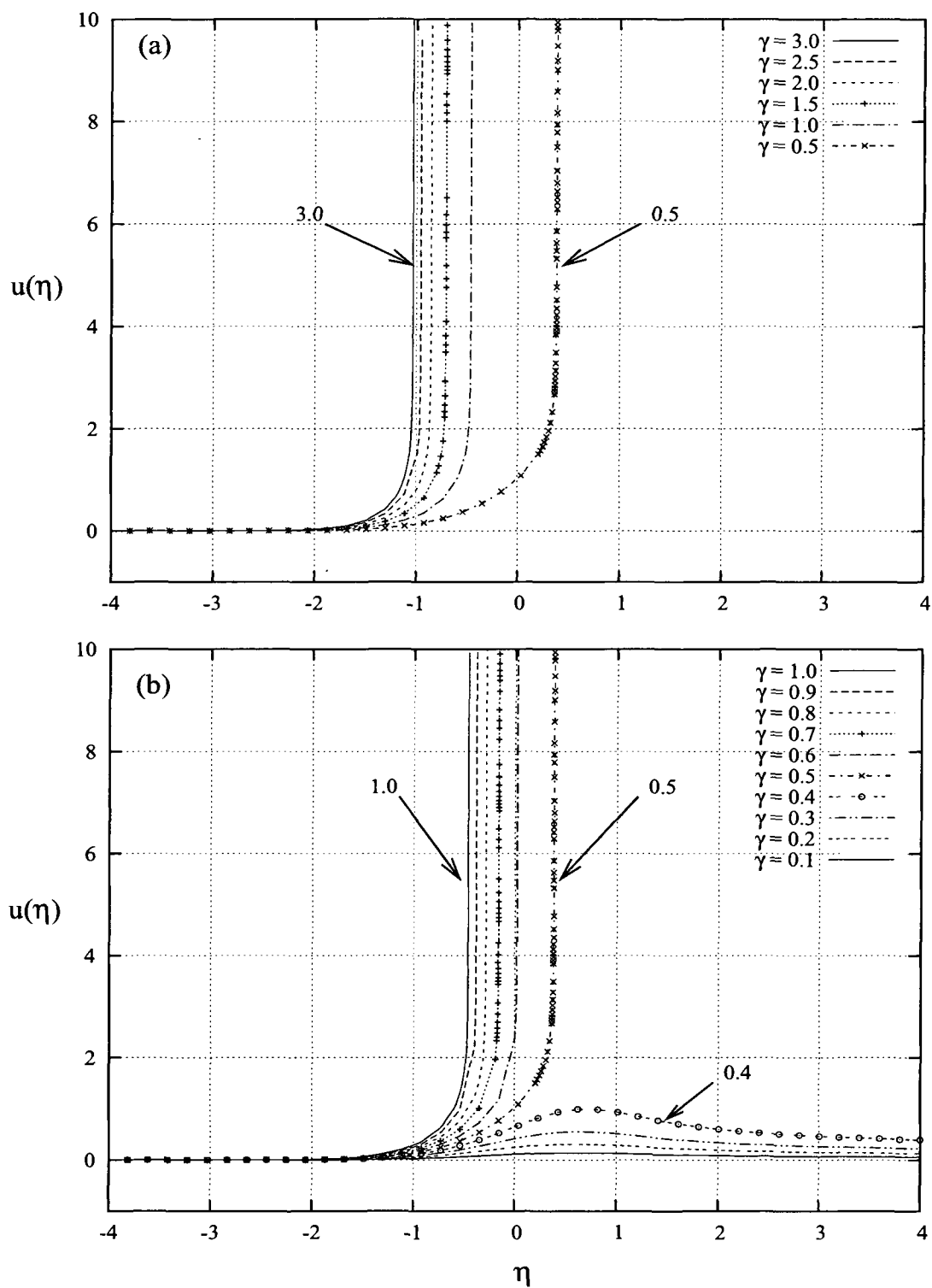


FIG. 7 Second benchmark solution as a function of  $\eta$  depending on  $\gamma$ . (a)  $\gamma \in (0, 3.0)$  by  $\Delta\gamma = -0.5$ , (b)  $\gamma \in (0, 1.0)$  by  $\Delta\gamma = -0.1$ .



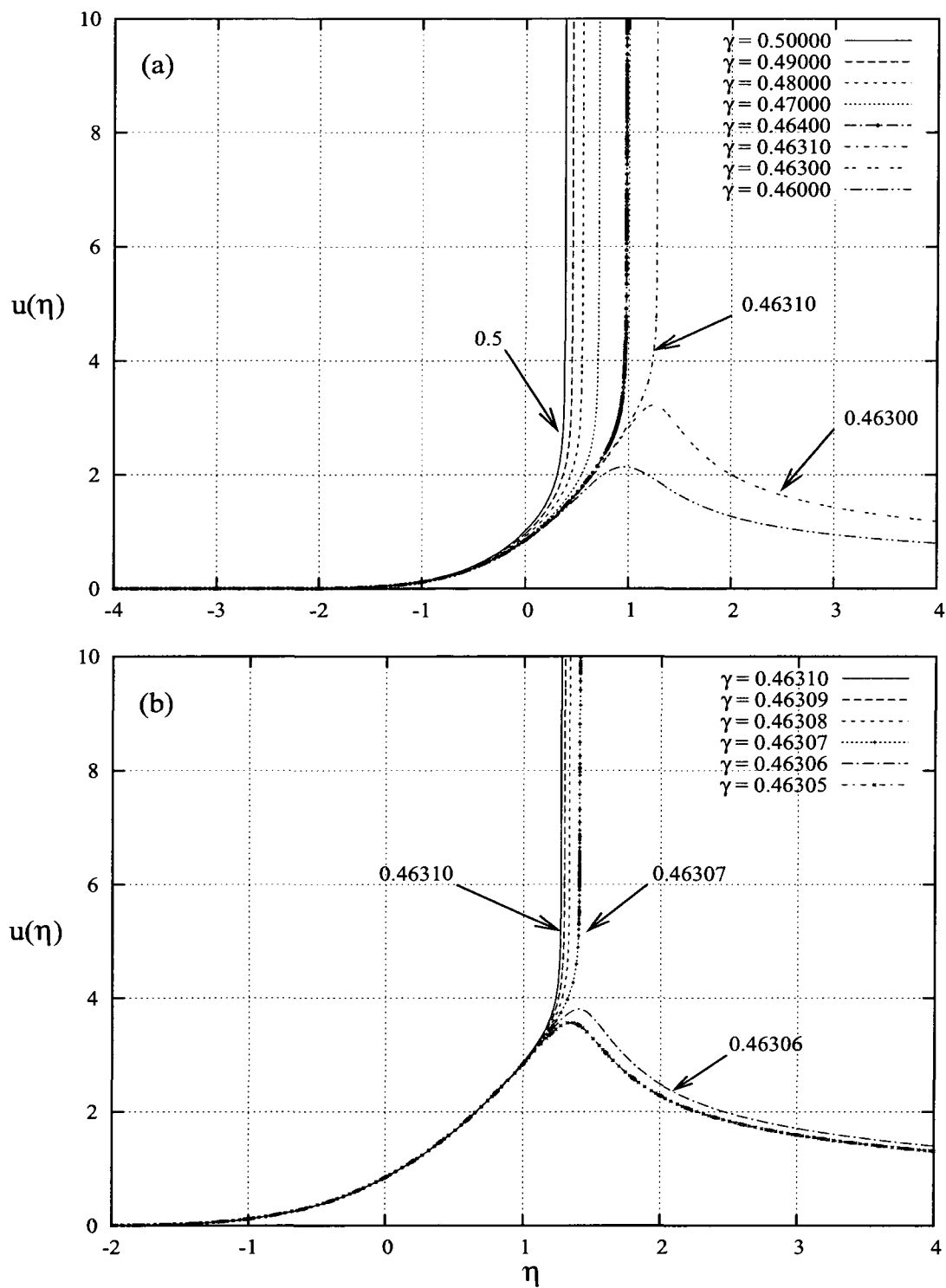


FIG. 8 Second benchmark solution as a function of  $\eta$  depending on  $\gamma$ . (a)  $\gamma \in (0.46, 0.5)$  by  $\Delta\gamma = -0.01$  and  $\Delta\gamma = -0.001$ , (b)  $\gamma \in (0.4631, 0.46305)$  by  $\Delta\gamma = -0.0001$ .

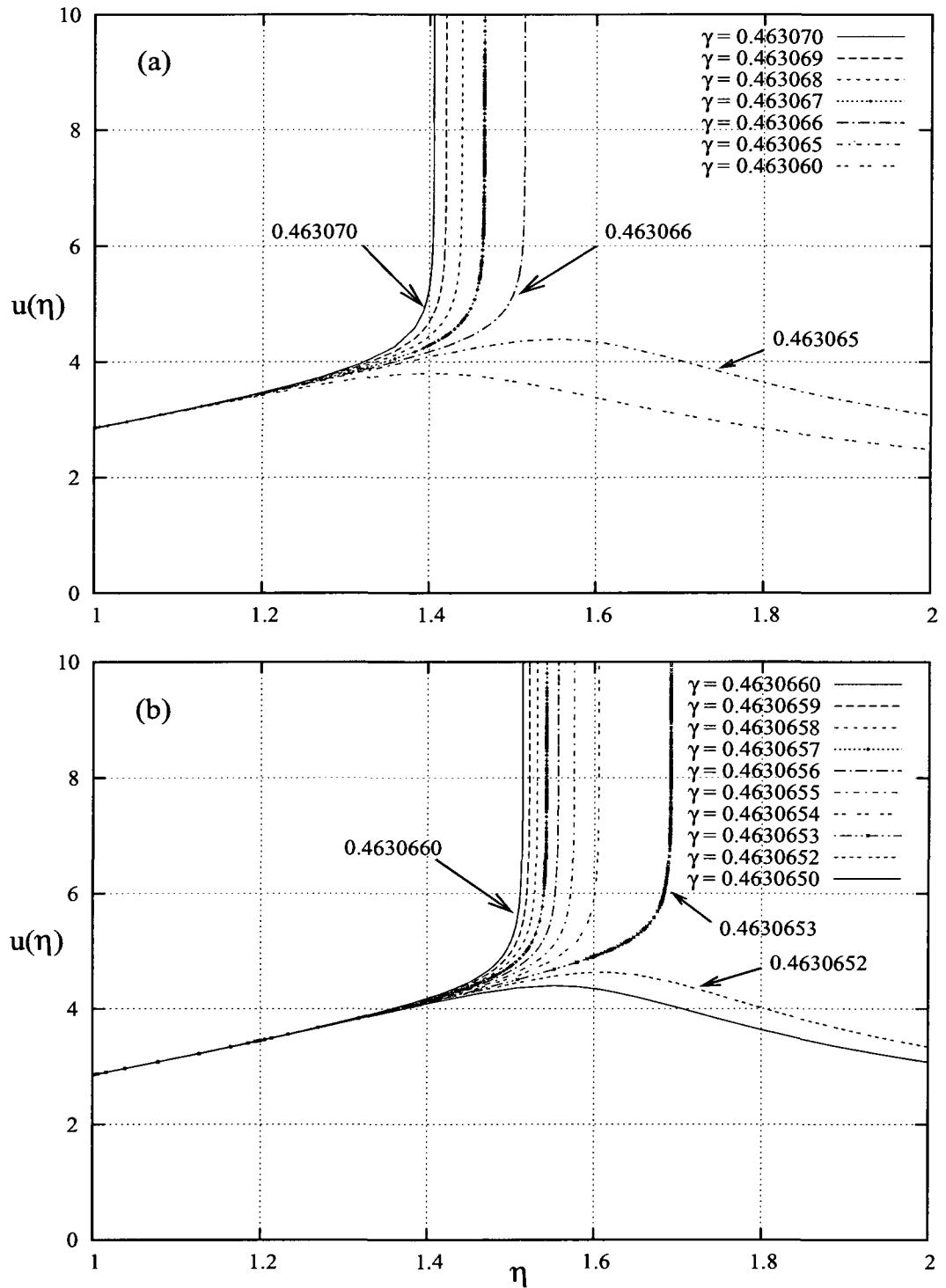


FIG. 9 Second benchmark solution as a function of  $\eta$  depending on  $\gamma$ . (a)  $\gamma \in (0.46307, 0.46306)$  by  $\Delta\gamma = -0.00001$ , (b)  $\gamma \in (0.463066, 0.463065)$  by  $\Delta\gamma = -0.000001$ .

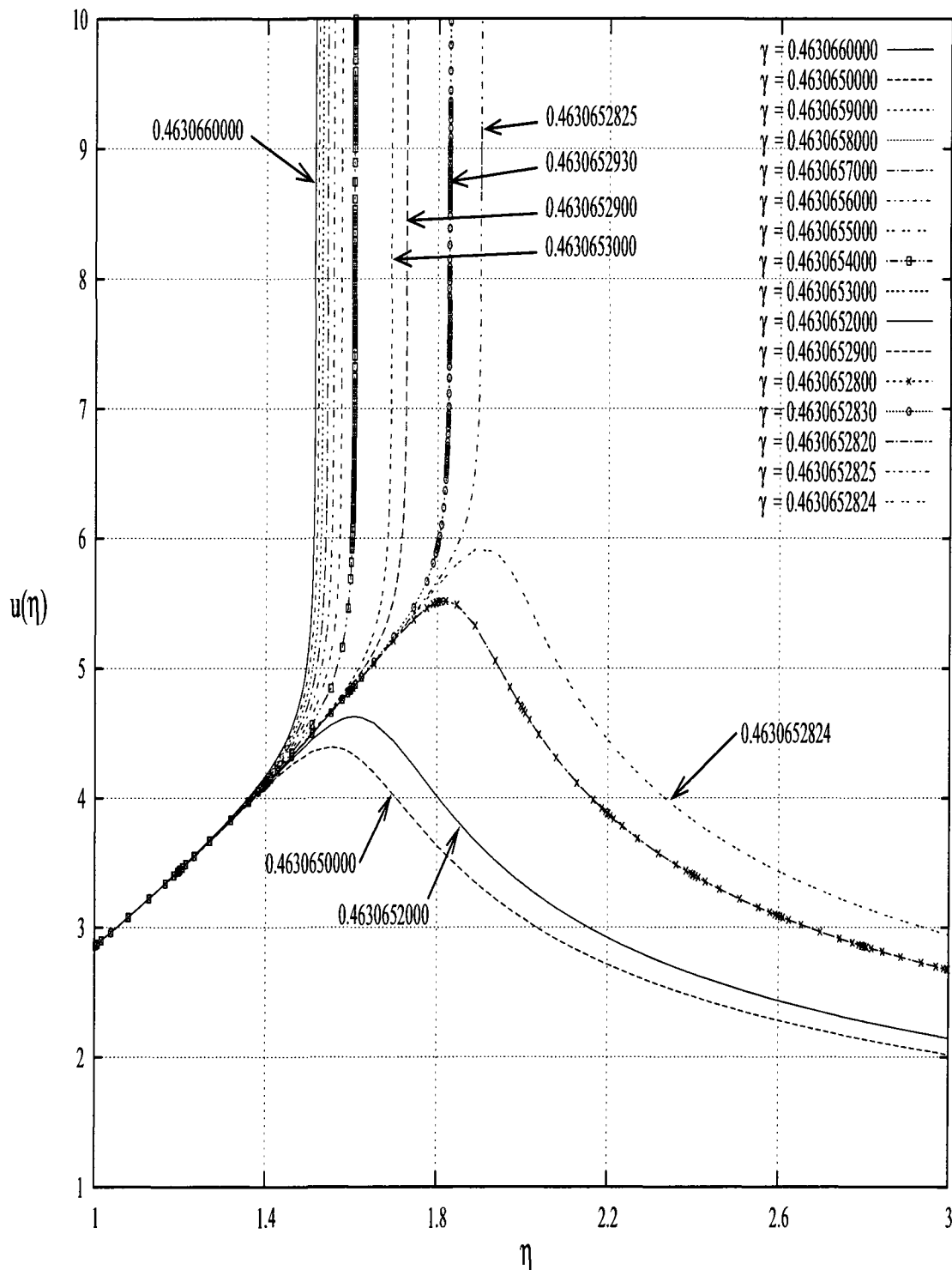


FIG. 10 Second benchmark solution as a function of  $\eta$  depending on  $\gamma$ .  $\gamma \in (0.463065, 0.4630652824)$  by  $\Delta\gamma = -0.000001$ ,  $\Delta\gamma = -0.0000001$  and  $\Delta\gamma = -0.00000001$ .

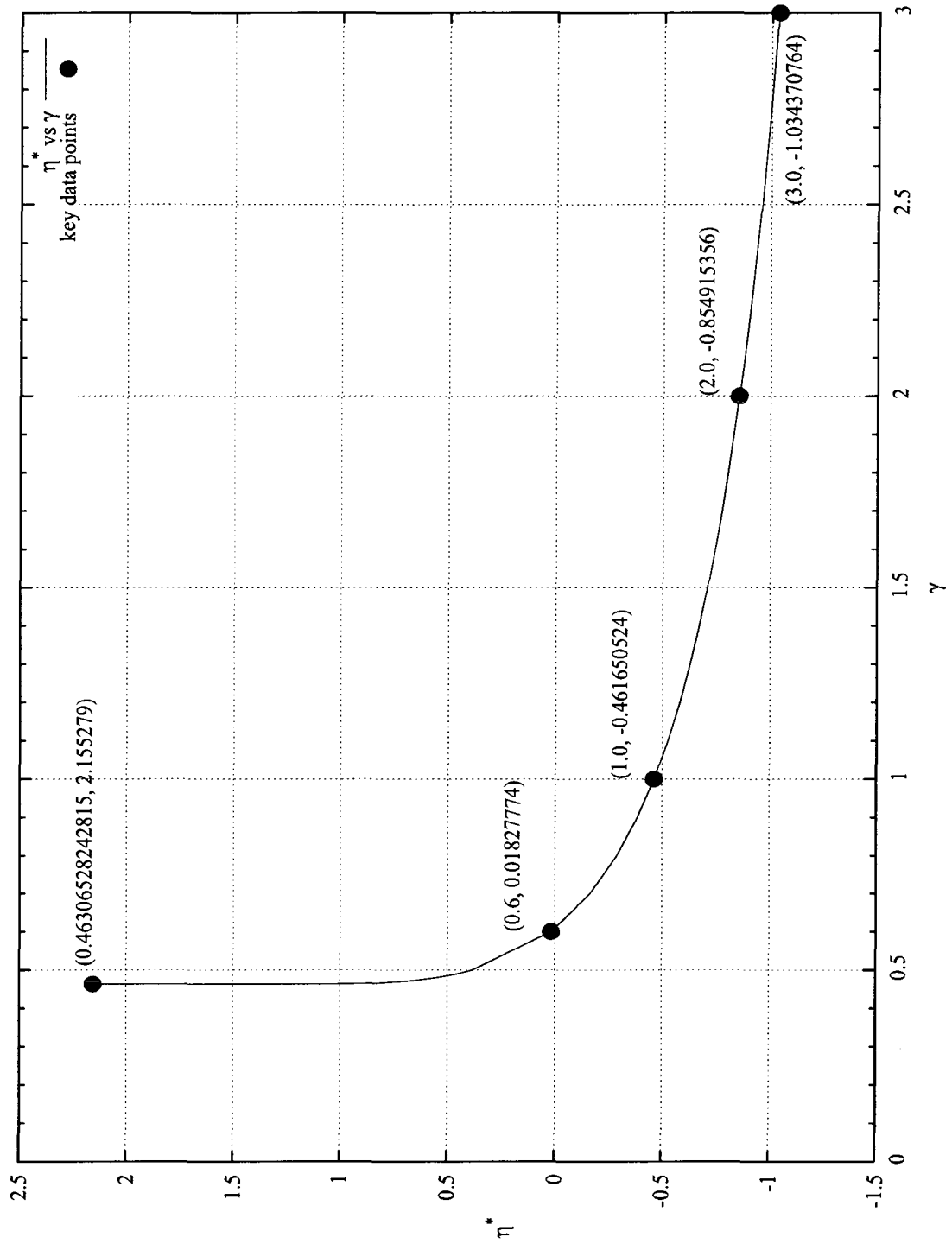


FIG. 11 Plot of the blow-up time  $\eta^*$  vs the parameter  $\gamma$ .

and the resulting curve for  $\eta^*(\gamma)$  is given in Figure 11. Clearly,  $\eta^*(\gamma) \rightarrow \infty$  as  $\gamma \rightarrow \gamma_c^+$  which is determined to lie on the interval  $(.4630652824, .4630652825)$ ; however, this growth appears to be very slow. Thus, it is surmised that the rate of growth is logarithmic, and an investigation to follow shows this to be so. In all cases, whether or not the solution attains blowup is determined through the criteria previously prescribed which did not need to be adjusted even for the extremely small values of  $\Delta\gamma$ . For these calculations, the extrapolation feature was not used since this would introduce inconsistencies in the approximate solutions and only allow determination of  $\gamma_c$  to four or five decimal places. Of course, the results determined above apply to the numerical approximation scheme at the current numerical precision and not necessarily to the solution of the integral equation. The above analysis can be continued, and the approximate value of  $\gamma_c$  determined to more than nine decimal places; however, this value will not agree with the real value of  $\gamma_c$  to that many decimal places unless the numerical precision of the integration and cubic spline schemes are greatly increased.

Upon examining the solutions, it is surmised that  $\eta^*(\gamma)$ , determined from the approximation scheme, satisfies

$$\eta^*(\gamma) \sim A \ln(\gamma - \gamma_c) \quad (\text{III.4.3})$$

as  $\gamma \rightarrow \gamma_c^+$ . This conjecture is examined by forming a table of the values  $\eta^*(\gamma_j)$  where  $\gamma_c < \gamma_{j+1} < \gamma_j$ . The differences

$$\Delta_j = \frac{\eta^*(\gamma_{j+1}) - \eta^*(\gamma_j)}{\ln(\gamma_{j+1} - \gamma_c) - \ln(\gamma_j - \gamma_c)} \quad (\text{III.4.4})$$

should converge to  $A$  as  $\lim_{j \rightarrow \infty} \gamma_j \rightarrow \gamma_c$ , if the value of  $\gamma_c$  is known to infinite precision. Since  $\gamma_c$  remains unknown, a number of approximate values to  $\gamma_c$ , say  $\gamma_c^k$ , are chosen and the differences  $\Delta_j^k$  are plotted versus  $-\ln(\gamma_j - \gamma_c^k)$ . Figure 12 shows the results of this investigation.

### III.5 Solution of Third Benchmark Problem

The third benchmark problem is derived by considering the effect of reactant consumption on the ignition problem. The governing integral equation as derived in Lasseigne and Olmstead [49] is

$$u(\eta) = \int_{-\infty}^{\eta} \frac{1}{\sqrt{\pi(\eta - \xi)}} e^{u(\xi) + \xi} F(\lambda v(\xi)) d\xi \quad (\text{III.5.1})$$

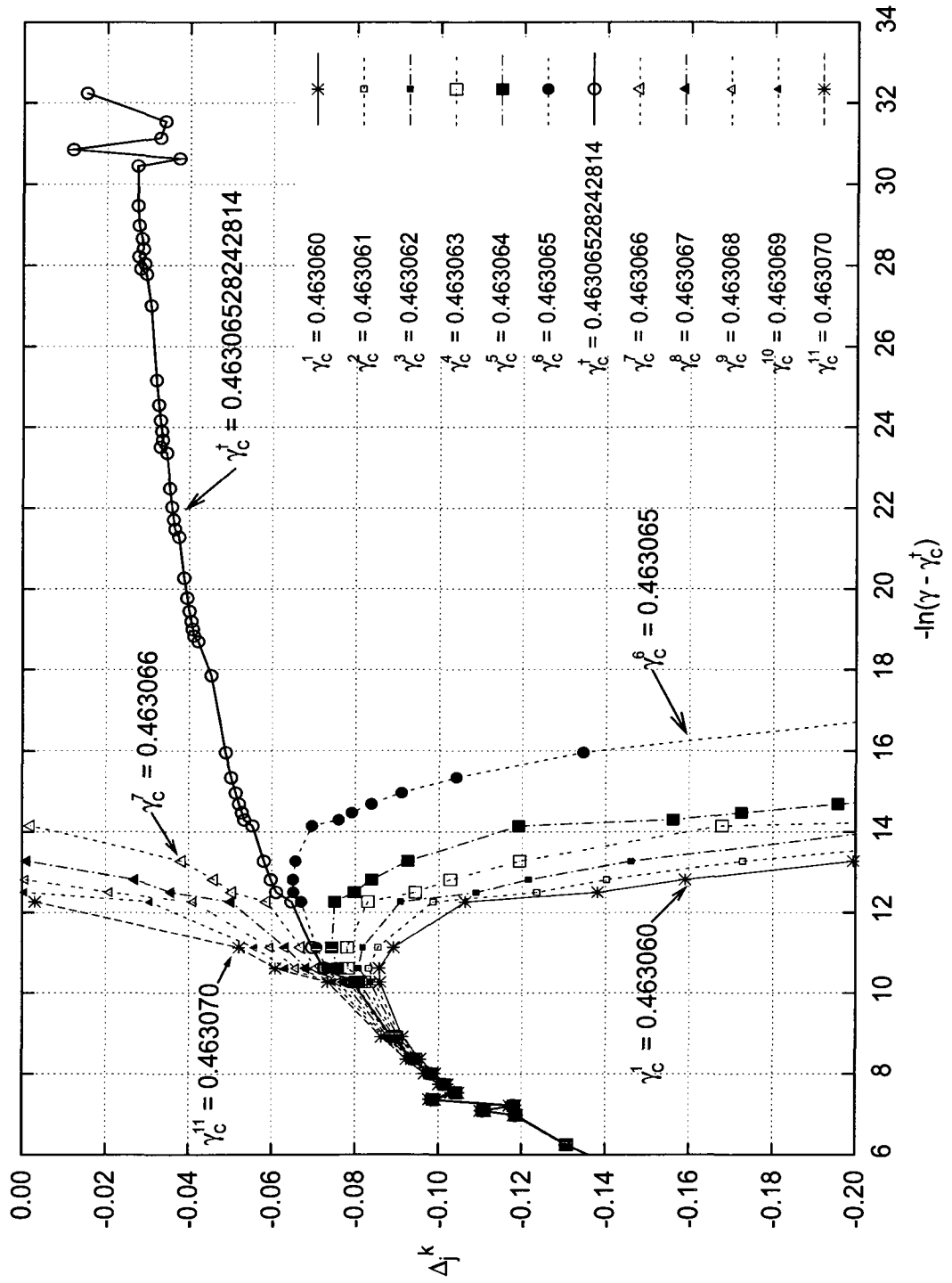


FIG. 12 Investigation scheme fit to  $\eta^*(\gamma) \sim A \ln(\gamma - \gamma_c)$ . Plot of the  $\Delta_j^k$  vs  $-\ln(\gamma_j - \gamma_c^\dagger)$ .

with

$$F(x) = \frac{1 - e^{-x}}{x},$$

$$v(\xi) = \int_{-\infty}^{\xi} e^{u(\xi') + \xi'} d\xi'.$$

This integral equation reduces to the first benchmark case as  $\lambda \rightarrow 0$ . It was shown by analytical and numerical methods that a solution to this integral equation exists for all values of  $\eta$  if  $\lambda > \lambda_c$  and that a blowup solution to the equation exists if  $\lambda < \lambda_c$ . Upon using an *ad hoc* numerical method based on low-order finite differences, the critical value was determined as  $\lambda_c \approx 1.089$ .

TABLE 6  
The blowup value  $\eta^*$  vs  $\lambda < \lambda_c$ .

$\lambda$	$\eta^*$
0.0	-0.4311
0.1	-0.3943
0.5	-0.2099
1.0	0.2980
1.08	0.6627
1.085	0.7500

Here, we apply the proposed routine to determine the critical value of  $\lambda$  by numerically integrating equation III.5.1. The following parameters were chosen for the integration:  $\eta_0$ ,  $\delta\eta_i$ ,  $\rho_1$ ,  $\delta\rho$ , and  $j_{max}$ . Also, the relative and absolute error variables *ERRREL* and *ERRABS* for the subroutines DQAG and DQAWS are specified. The converged solution using the values:  $\eta_0 = -10$ ,  $\delta\eta_i = 1$ ,  $\rho_1 = .01$ ,  $\delta\rho = .01$ ,  $j_{max} = 1250$ , *ERRREL* =  $10^{-8}$ , and *ERRABS* =  $10^{-14}$ . The results are presented in a series of graphs below. Since there was some discrepancy between the previously published values of the ignition time  $\eta^*$  for certain values of  $\lambda$ , we verified the current results by once again solving the inverse problem using a temperature marching scheme, but this time, the integration is performed using spline approximations and the QUADPACK quadrature schemes. The new results are listed in Table 6. As to be discussed, the critical value of  $\lambda$  is determined to lie on the interval  $\lambda_c \in (1.0882232, 1.0882233)$  when using the indicated parameter values in

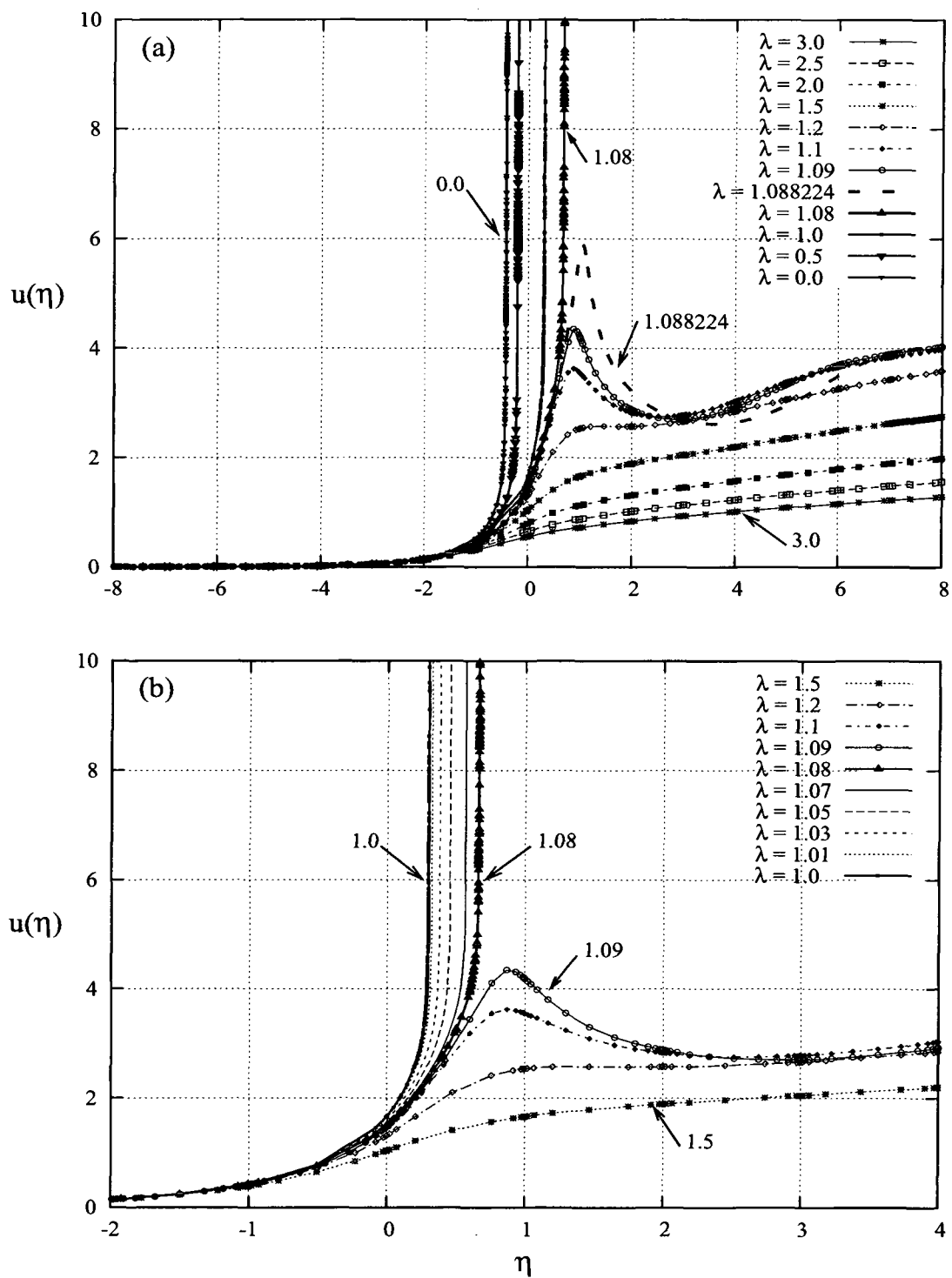


FIG. 13 Third benchmark solution as a function of  $\eta$  depending on  $\lambda$ . (a)  $\lambda \in (0, 3.0)$ , (b)  $\lambda \in (1.0, 1.5)$ .



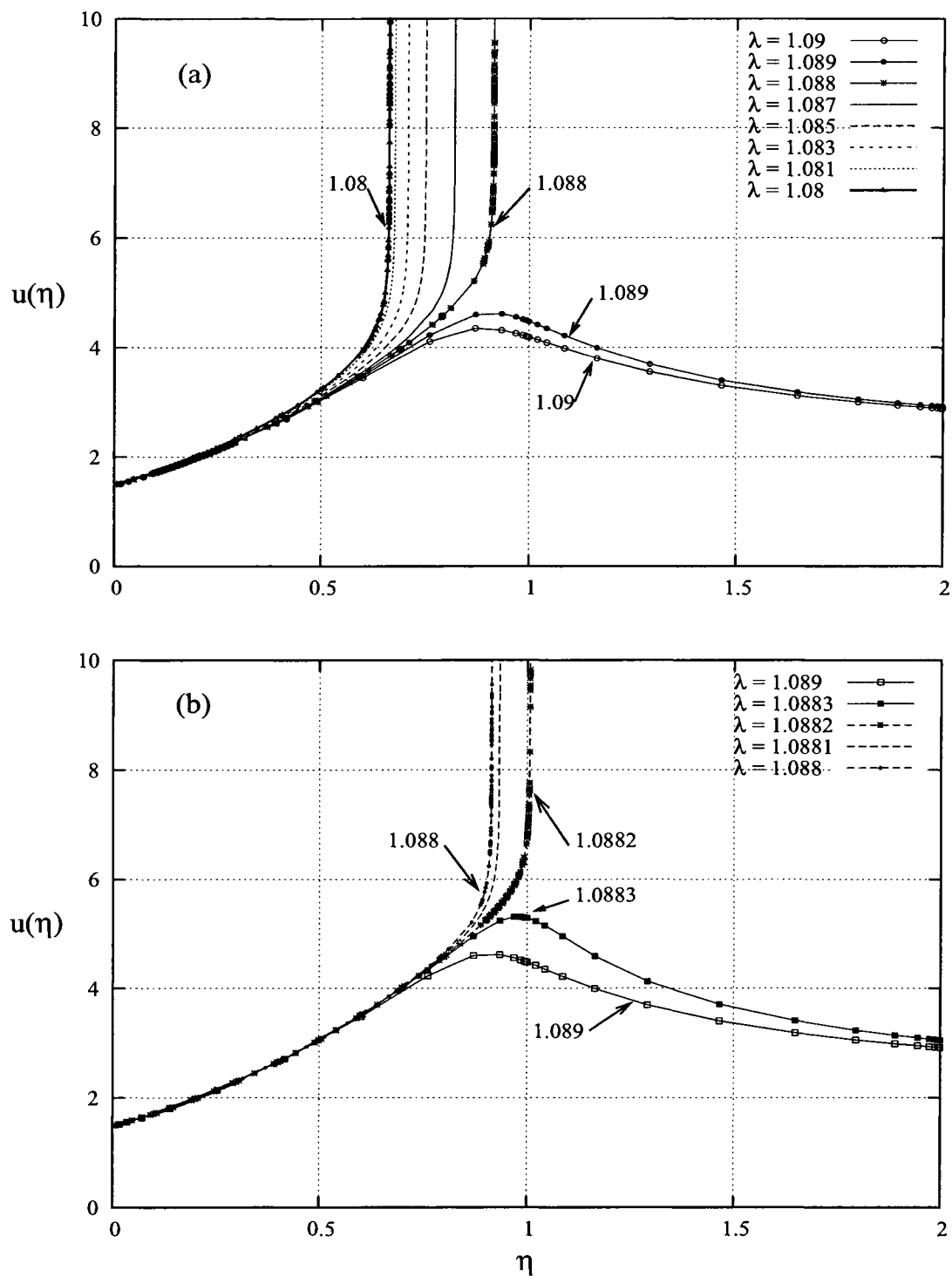


FIG. 14 Third benchmark solution as a function of  $\eta$  depending on  $\lambda$ . (a)  $\lambda \in (1.08, 1.09)$ , (b)  $\lambda \in (1.088, 1.089)$ .

the scheme. It is conceivable that a slight change in the critical value could occur upon using higher numerical precision. We also test the assumption that  $\eta^*(\lambda) \propto -\ln(\lambda_c - \lambda)$  as  $\lambda \rightarrow \lambda_c^-$ .

The results of integrating equation III.5.1 using the values

$$\lambda \in \{0, 0.5, 1.0, 1.08, 1.088224, 1.09, 1.1, 1.2, 1.5, 2.0, 2.5, 3.0\}$$

are shown in Figure 13(a). Consistent with previous work, blowup solutions exist when  $\lambda \leq 1.08$  and non-blowup solutions exist when  $\lambda \geq 1.09$ . The non-blowup solutions are seen to grow proportional to  $\sqrt{\eta}$  as  $\eta \rightarrow \infty$  and the proportionality constant is inversely related to  $\lambda$  as predicted analytically. For reference, the solution with  $\lambda = 1.088224$  is shown on this graph to demonstrate that a non-blowup solution with  $\lambda$  very near  $\lambda_c$  closely follows the blowup solutions before the temperature declines rapidly. This solution also demonstrates growth proportional to  $\sqrt{\eta}$  as  $\eta \rightarrow \infty$ . It should be noted that  $u(\eta; \lambda_2)$  is not always greater than  $u(\eta; \lambda_1)$  when  $\lambda_2 < \lambda_1$  for all  $\eta$ . Furthermore, the solutions are not monotone in  $\eta$  for  $\lambda$  between  $\lambda_c$  and the value  $\lambda \approx 1.2$ . Determining these solutions requires a time-marching scheme and not a temperature marching scheme. A close up view using

$$\lambda \in \{1.0, 1.01, 1.03, 1.05, 1.07, 1.08, 1.09, 1.1, 1.2, 1.5\}$$

is shown in Figure 13(b). Of particular note is the almost complete overlap of the solutions on the interval  $\eta \in (-2, -1)$ . The solutions presented in the next series of graphs emerge from the small region lying between the solutions for  $\lambda = 1.08$  and  $\lambda = 1.09$ .

Figure 14(a) shows the solution for

$$\lambda \in \{1.08, 1.081, 1.083, 1.085, 1.087, 1.088, 1.089, 1.09\}.$$

Clearly, the critical value is seen to lie on  $\lambda_c \in (1.088, 1.089)$ . Figure 14(b) shows the solution for

$$\lambda \in \{1.088, 1.0881, 1.0882, 1.0883, 1.089\},$$

and the critical value is seen to lie on  $\lambda_c \in (1.0882, 1.0883)$ . Note that the solutions for  $\eta \in (\eta_0, 0.5)$  are almost identical for these last values of  $\lambda$ . Figure 15 shows the solutions for values of  $\lambda$  on the interval  $(1.0882, 1.0883)$ . As a function of  $\lambda$ , the solutions progress in a monotone manner until the values of lambda are narrowed to the interval  $(1.088223, 1.088224)$ . With further refinement of the parameter  $\lambda$  (starred values in the

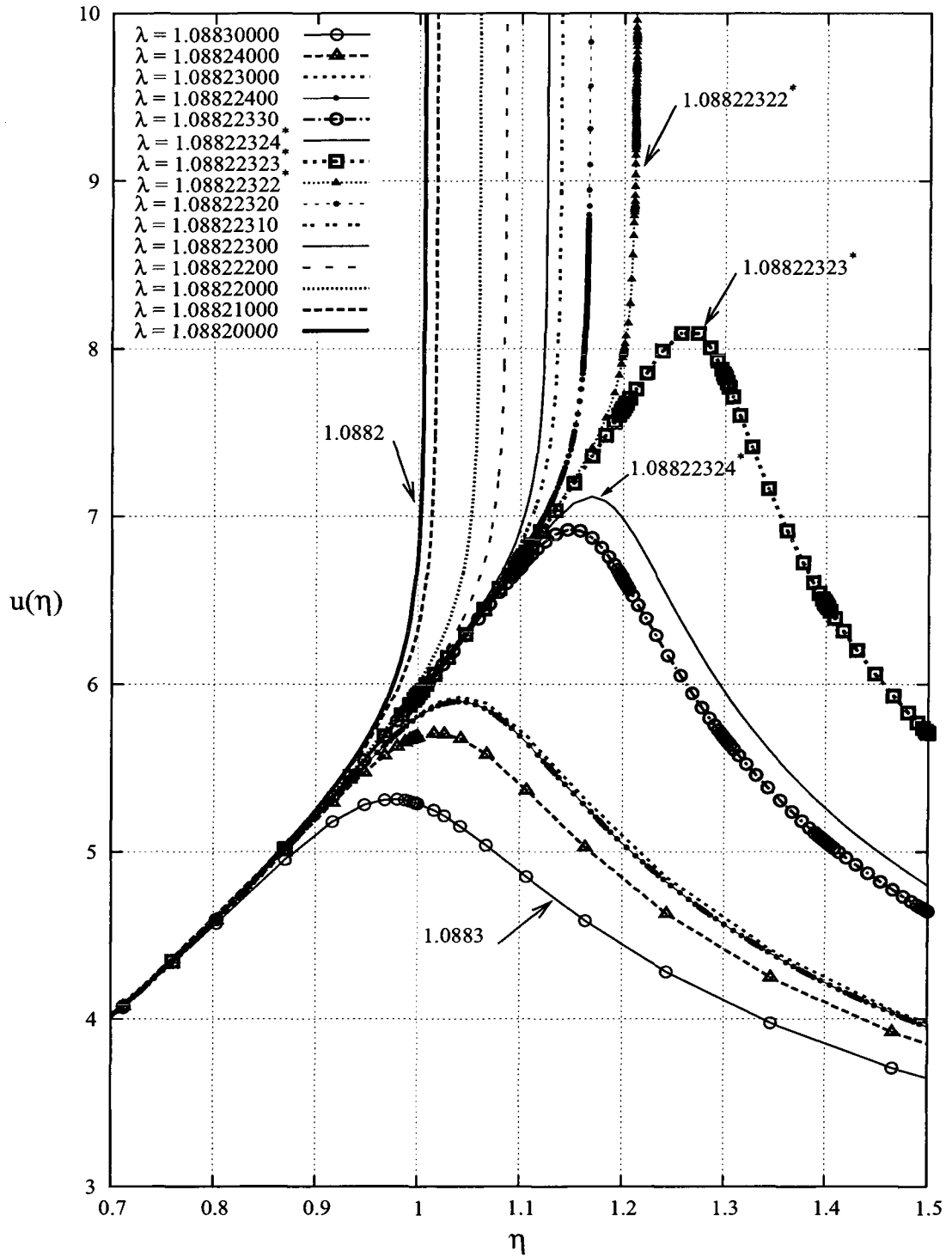


FIG. 15 Third benchmark solution as a function of  $\eta$  depending on  $\lambda$  for  $\lambda \in (1.0883, 1.08822322)$ .

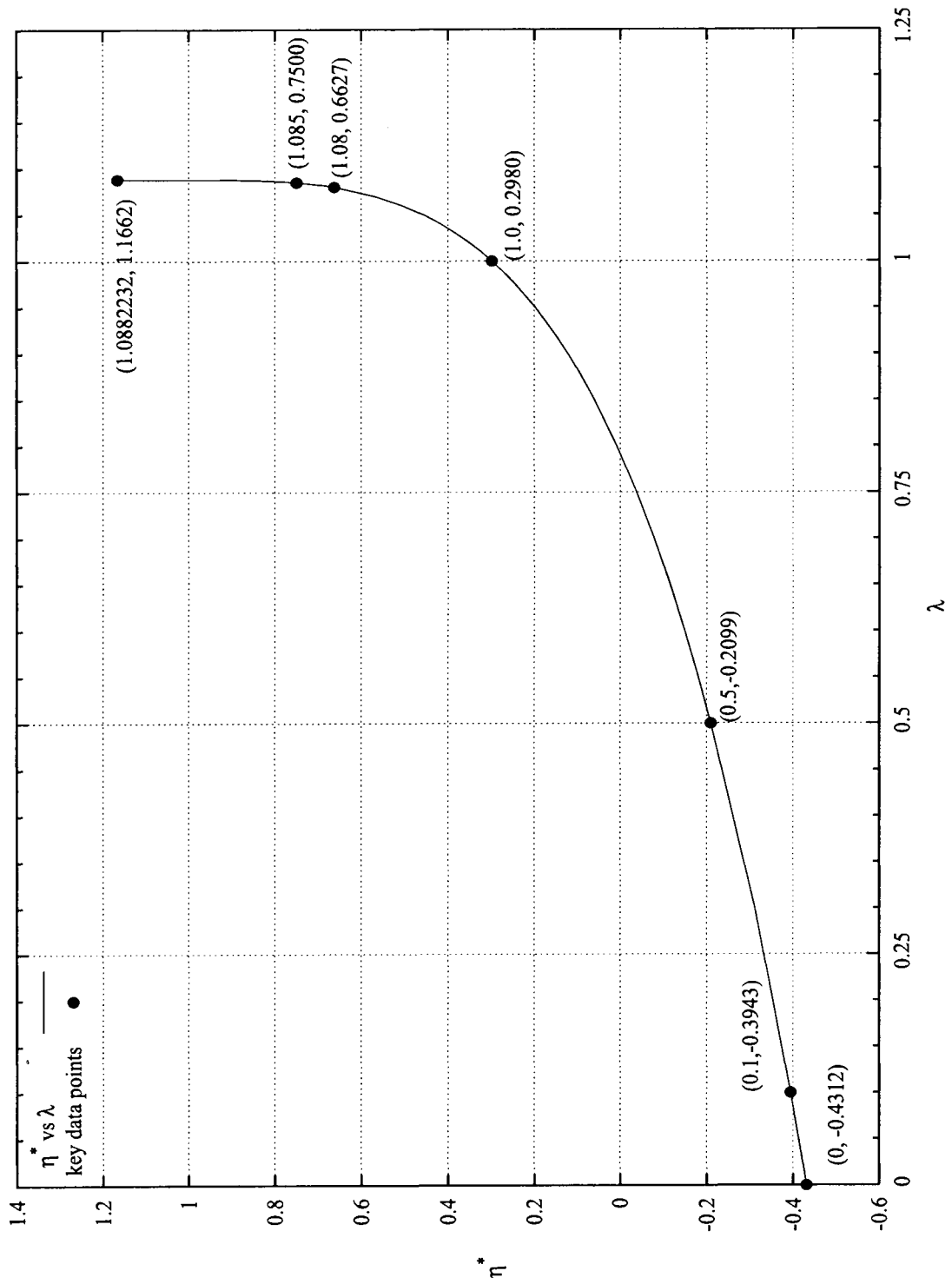


FIG. 16 Plot of the blow-up time  $\eta^*$  vs the parameter  $\lambda$ .

figure), the solutions are not necessarily dependent on  $\lambda$  in a monotone manner. It is suspected that the limit of numerical precision has been reached. The resulting curve for  $\eta^*(\lambda)$  is given in Figure 16.

Upon examining the solutions, it is surmised that  $\eta^*(\lambda)$ , determined from the approximation scheme, satisfies

$$\eta^*(\lambda) \sim A \ln(\lambda_c - \lambda) \quad (\text{III.5.2})$$

as  $\lambda \rightarrow \lambda_c^-$ . This conjecture is examined by forming a table of the values  $\eta^*(\lambda_j)$  where  $\lambda_j < \lambda_{j+1} < \lambda_c$ . The differences

$$\Delta_j = \frac{\eta^*(\lambda_{j+1}) - \eta^*(\lambda_j)}{\ln(\lambda_c - \lambda_{j+1}) - \ln(\lambda_c - \lambda_j)} \quad (\text{III.5.3})$$

should converge to  $A$  as  $\lim_{j \rightarrow \infty} \lambda_j \rightarrow \lambda_c$ , if the value of  $\lambda_c$  is known to infinite precision. Since  $\lambda_c$  remains unknown, a number of approximate values to  $\lambda_c$ , say  $\lambda_c^k$ , are chosen and the differences  $\Delta_j^k$  are plotted versus  $-\ln(\lambda_j - \lambda_c^k)$ . Figure 17 shows the results of this investigation.

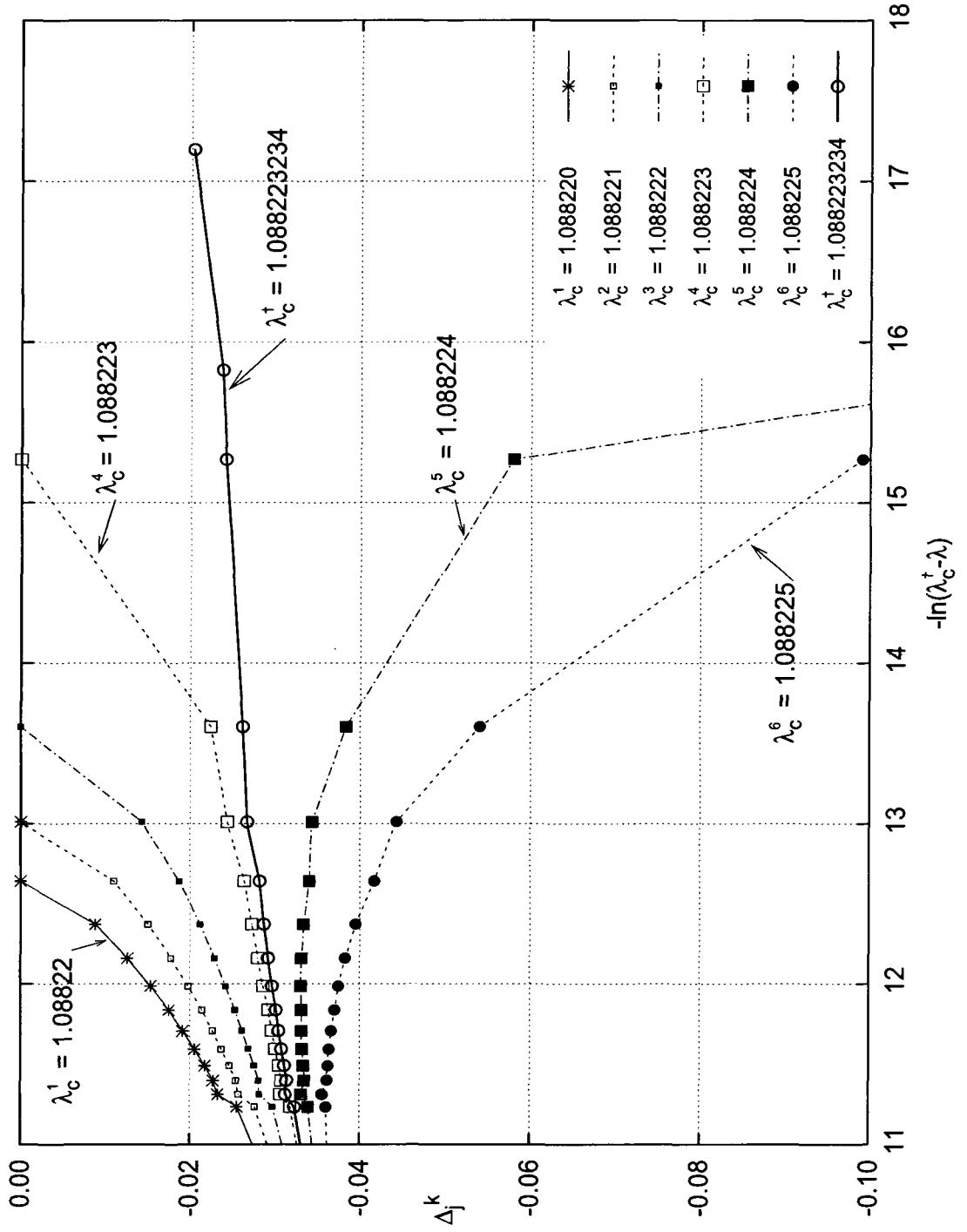


FIG. 17 Investigation scheme fit to  $\eta^*(\lambda) \sim A \ln(\lambda_c - \lambda)$ . Plot of the  $\Delta_j^k$  vs  $-\ln(\lambda_c^\dagger - \lambda_j)$ .

## CHAPTER IV

### ORDINARY DIFFERENTIAL EQUATIONS

#### IV.1 Introduction

The method of solution from Chapter III is applied to test ordinary differential equations (ODE's) with known blow-up solutions or regions of rapid change. The method allows the investigator to easily distinguish between a singular solution and a non-singular solution, thus, avoiding the *ad hoc* approach used in the past. Furthermore, the solution develops in the natural variables where the temperature is the dependent variable and time is the independent variable. Upon determining that a singular solution or a region of extreme stiffness exists, the time step is adjusted appropriately to maintain accuracy. Another virtue of the present technique is the use of well-developed software. In this case, a standard Runge-Kutta method is used to integrate the given ODE. When applying a Runge-Kutta method in the regular time variable, an interval of integration must be specified. If this interval contains a singularity or region of extreme stiffness, the integration will fail. Thus, the current solution algorithm is used to solve all of the ODE's given in Table 7 by avoiding attempts to integrate over a region containing the singularity. Any necessary modifications for a particular equation is discussed in the text.

TABLE 7  
*Ordinary differential equations solved.*

Description	Equation
<i>p</i> th order growth	$\frac{du}{dt} = Au^p, \quad u(t_0) = u_0, \quad t \geq 0, \quad p > 0, \quad p \neq 1, \quad A > 0$
Exponential growth	$\frac{du}{dt} = A \exp(u), \quad u(t_0) = u_0, \quad t \geq 0, \quad A > 0$
Kassoy's thermal explosion	$\frac{dT}{dt} = \frac{\varepsilon}{\beta} (1 + \beta - T) \exp\left(\frac{T-1}{\varepsilon T}\right), \quad T(0) = 1$

## IV.2 Runge-Kutta

The Runge-Kutta method is a method of numerically integrating ordinary differential equations by using a trial step in the interval to cancel out lower-order error terms. The method requires evaluating the function several times, eliminating the need to compute higher derivatives. The fourth-order Runge-Kutta (RK4) method is the most popular and is a good choice for practical use since it is accurate, stable and easy to program. Higher order Runge-Kutta methods, with higher computational costs, are not required since the fourth-order method can be made more accurate by either using a smaller step size globally or adapting the step size to the solution characteristics.

The fourth-order Runge-Kutta method, when used to solve initial value problems, samples the slope at intermediate points as well as the end points to find a good average of the slope across the interval. The RK4 formula used here to compute the next solution is:

$$y_{i+1} = y_i + h \frac{K_1 + 2K_2 + 2K_3 + K_4}{6} \quad (\text{IV.2.1})$$

where

$$K_1 = f(t_0, y_0) \quad (\text{IV.2.2})$$

$$K_2 = f\left(t_0 + \frac{1}{2}h, y_0 + \frac{1}{2}hK_1\right) \quad (\text{IV.2.3})$$

$$K_3 = f\left(t_0 + \frac{1}{2}h, y_0 + \frac{1}{2}hK_2\right) \quad (\text{IV.2.4})$$

$$K_4 = f(t_0 + h, y_0 + hK_3). \quad (\text{IV.2.5})$$

One way to check the accuracy of the solution to an initial value problem is to solve the problem twice, once with step size  $h$  and a second time with step size  $h/2$  and then compare the answers. If the solutions agree, they are deemed accurate. If differences in the approximate solutions are too large, the smaller step size solution is adopted and checked by solving again with an even smaller step size. This is inefficient if the solution is only problematic in a small region of the domain. In such a case, an adaptive method is desirable.

The Runge-Kutta-Fehlberg (RKF45) method is an adaptive Runge-Kutta method that uses two separate calculations, one of  $O(h^4)$  and the other  $O(h^5)$ , to determine if the step size is sufficiently small and allows for the appropriate modification of the step size to the optimal step size. The Runge-Kutta-Fehlberg method adds flexibility to the standard



Runge-Kutta method.

The Runge-Kutta-Fehlberg method samples the slopes with linear combinations of the of the previous slopes.

$$K_1 = f(t_0, y_0) \quad (\text{IV.2.6})$$

$$K_2 = f\left(t_0 + \frac{1}{4}h, y_0 + \frac{1}{4}hK_1\right) \quad (\text{IV.2.7})$$

$$K_3 = f\left(t_0 + \frac{3}{8}h, y_0 + \frac{3}{8}h\widehat{K}_2\right) \quad (\text{IV.2.8})$$

$$K_4 = f\left(t_0 + \frac{12}{13}h, y_0 + \frac{12}{13}h\widehat{K}_3\right) \quad (\text{IV.2.9})$$

$$K_5 = f\left(t_0 + h, y_0 + h\widehat{K}_4\right) \quad (\text{IV.2.10})$$

$$K_6 = f\left(t_0 + \frac{1}{2}h, y_0 + \frac{1}{2}h\widehat{K}_5\right) \quad (\text{IV.2.11})$$

where

$$\widehat{K}_2 = \frac{1}{4}K_1 + \frac{3}{4}K_2 \quad (\text{IV.2.12})$$

$$\widehat{K}_3 = \frac{161}{169}K_1 - \frac{600}{169}K_2 + \frac{608}{169}K_3 \quad (\text{IV.2.13})$$

$$\widehat{K}_4 = \frac{8341}{4104}K_1 - \frac{32832}{4104}K_2 + \frac{29440}{4104}K_3 - \frac{845}{4104}K_4 \quad (\text{IV.2.14})$$

$$\begin{aligned} \widehat{K}_5 = & -\frac{6080}{10260}K_1 + \frac{41040}{10260}K_2 - \frac{28352}{10260}K_3 \\ & + \frac{9295}{10260}K_4 - \frac{5643}{10260}K_5. \end{aligned} \quad (\text{IV.2.15})$$

Then two approximations to the solution are made: a) by using a Runge-Kutta method of order four:

$$y_{i+1} = y_i + h \frac{2375K_1 + 11264K_3 + 10985K_4 - 4104K_5}{20520}; \quad (\text{IV.2.16})$$

and b) by using a Runge-Kutta method of order five:

$$z_{i+1} = z_i + h \frac{33440K_1 + 146432K_3 + 142805K_4 - 50787K_5 + 10260K_6}{282150}. \quad (\text{IV.2.17})$$

Lastly, the step size is adjusted dynamically,  $h \rightarrow sh$ , where the scalar  $s$  is

$$s = \left( \frac{\varepsilon h}{2|z_{i+1} - y_{i+1}|} \right)^{\frac{1}{4}} \quad (\text{IV.2.18})$$

and  $\varepsilon$  is the user specified error control tolerance [63, 21]. The RKF45 FORTRAN code adjusts the step size by the following rule

$$h = \begin{cases} 0.5h & s < 0.1, \\ sh & 0.1 < s < 4, \\ 4h & s > 4. \end{cases} \quad (\text{IV.2.19})$$

If the step size is smaller than  $10^{-13}$  the routine stops. Even adaptive Runge-Kutta methods are not sufficient to solve blow-up problems.

### IV.3 Initial Value Problem Examples

#### IV.3.1 Blow-up Conditions

Some nonlinear ODE's exhibit solutions with blow-up behavior. A few examples with known solutions are *Bernoulli*, exponential growth and *p*th-order growth equations. The *Bernoulli* type reaction-diffusion differential equation

$$y'(t) = \lambda y(t) + Ay^p(t), \quad t > 0, \quad \lambda \leq 0, \quad y(0) = y_0 > 0, \quad A > 0 \quad (\text{IV.3.1})$$

reduces to the *p*th-order growth equation when  $\lambda = 0$ . The *p*th-order growth equation has the solution

$$y(t) = \begin{cases} \left( \frac{\beta}{t^* - At} \right)^\beta, & \beta = \frac{1}{p-1} \quad p > 1, \\ \frac{1}{\left( A(1-p)t + y_0^{1-p} \right)^{\frac{1}{1-p}}} & p < 1. \end{cases} \quad (\text{IV.3.2})$$

When  $p > 1$ , the solution approaches infinity as  $t$  approaches  $t^*$  where  $t^*$  is the blow-up time given by

$$t^* = \frac{y_0^{1-p}}{A(p-1)}. \quad (\text{IV.3.3})$$

Blow-up does not occur when  $0 < p < 1$ , and the solution exists for all time. Likewise,

the solution to the initial value problem (IV.3.1) of the *Bernoulli* type reaction-diffusion differential equation when  $\lambda < 0$  and  $p > 1$  is

$$y(t) = \left( \frac{\lambda}{(\lambda y_0^{1-p} + 1) \exp[(1-p)\lambda t] + 1} \right)^{\frac{1}{p-1}} \quad (\text{IV.3.4})$$

which is singular with blow-up time

$$t^* = \frac{1}{(1-p)\lambda} \ln \left( \frac{1}{\lambda y_0^{1-p} + 1} \right). \quad (\text{IV.3.5})$$

In addition to the *Bernoulli* type reaction-diffusion differential equation, the generalized growth equation given by

$$\frac{du}{dt} = f(u), \quad t \geq 0, \quad u(0) = u_0 \geq 0, \quad (\text{IV.3.6})$$

for any positive and continuous function  $f$ , also has a known solution given by

$$\int_{u_0}^u \frac{d\hat{u}}{f(\hat{u})} = t. \quad (\text{IV.3.7})$$

Blow-up occurs if the function  $f$  fulfills the *Osgood's condition* [57],

$$\int_{u_0}^{\infty} \frac{ds}{f(s)} < \infty, \quad (\text{IV.3.8})$$

a necessary and sufficient condition formulated around 1898 for positive initial data. If  $f(u) = \exp(u)$  in (IV.3.6), the solution is

$$u(t) = -\ln|t^* - t|, \quad (\text{IV.3.9})$$

where  $t^* = \exp(u_0)$  is the blow-up time. The solution grows logarithmically as  $t \rightarrow t^*$ . This logarithmic blow-up behavior is especially challenging to capture numerically.

The *p*th-order growth equation has an algebraic singularity while the exponential growth equation has a logarithmic singularity. The current algorithm is shown below to readily handle these two cases. Perhaps more challenging is to capture the solution to Kasoy's thermal explosion problem where even computing values for the analytic solution is problematic owing to the extreme stiffness of the solution. The solution to this problem will be discussed in greater detail.

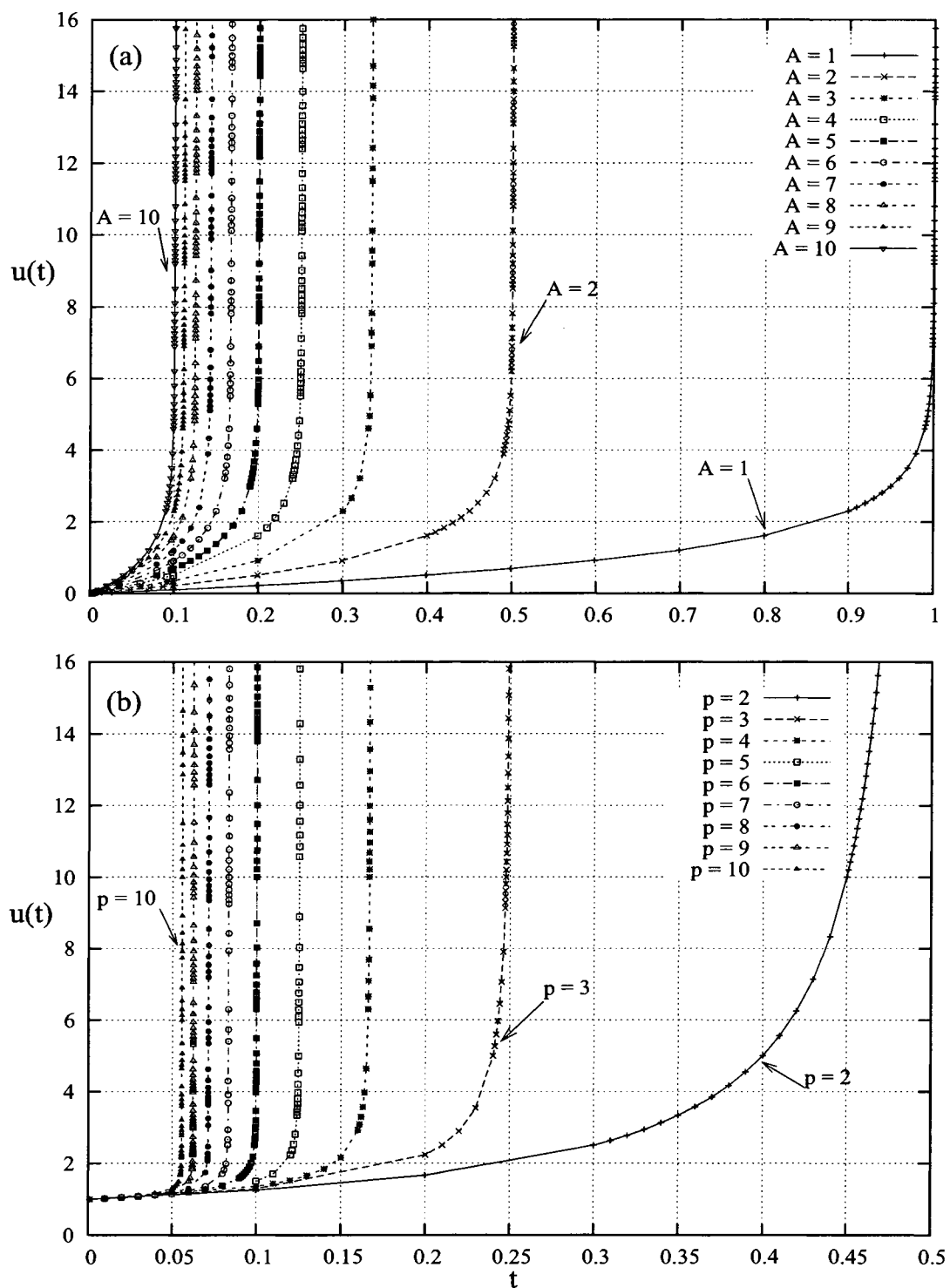


FIG. 18 Self-similar solutions to the Exponential and  $p$ th-order growth equations. (a) exponential growth solution. (b)  $p$ th-order growth solution.

#### IV.4 Solution to the Exponential Growth Equation

The exponential growth equation,

$$\frac{du}{dt} = A \exp(u), \quad u(t_0) = u_0, \quad t \geq 0, \quad A > 0, \quad (\text{IV.4.1})$$

has the exact solution  $u(t) = -\ln(\exp(-u_0) - A(t - t_0))$  and is singular at  $t^* = t_0 + \exp(-u_0)/A$ . The numerically computed solution is shown in Figure 18(a) for  $t_0 = 0$ ,  $u_0 = 0$ , and various values of  $A$ . Clearly, the routine captures the strong singularity in the solution at  $t^* = 1/A$ . Furthermore, the solution evolved such that no attempt was made to integrate past the point of singularity.

#### IV.5 Solution to the $p$ th-order Growth Equation

The  $p$ th order growth,

$$\frac{du}{dt} = Au^p, \quad u(t_0) = u_0, \quad t \geq 0, \quad p > 0, \quad p \neq 1, \quad A > 0, \quad (\text{IV.5.1})$$

has the exact solution  $u(t) = \left( A(1-p)(t - t_0) + u_0^{1-p} \right)^{1/1-p}$  and the solution is singular when  $p > 1$  and  $t^* = t_0 - u_0^{1-p}/(A(1-p))$ .

The numerically computed solution is shown in Figure 18(b) for  $t_0 = 0$ ,  $u_0 = 1$ ,  $A = 2$ , and various values of  $p \geq 2$ . Clearly, the routine captures the singularity in the solution at  $t^* = 1/(2(p-1))$  for these values; however, the strength of the singularity weakens as  $p$  decreases to unity. The issue of a weakening singularity was further investigated. It was found that even for  $p = 1.7$ , which is not very close to the critical value of  $p_c = 1$ , an excessive number of calculational points are required to resolve the rapidly growing solution in the regions *away* from the singular point. Furthermore, the criteria used to determine if a singular solution resides on a particular coarse grid is often tripped prematurely owing to the excessively large solution and large values of the solution derivatives. With some modification, the criteria could possibly be adapted to capture these weak singularities.

#### IV.6 Solution to Kassoy's Thermal Explosion Problem

The third test problem is a nonlinear spatially homogeneous thermal explosion based on the work of Kassoy [39] given in Kapila [37]. The physical situation considers a well-stirred insulated container in which a one-step irreversible exothermic reaction  $A \rightarrow B$  governed by Arrhenius kinetics occurs. The equations are

$$\frac{dY}{d\hat{t}} = -AY \exp\left(\frac{-E}{R\hat{T}}\right) \quad (\text{IV.6.1})$$

$$\frac{d\hat{T}}{d\hat{t}} = \frac{Q}{c}AY \exp\left(\frac{-E}{R\hat{T}}\right), \quad (\text{IV.6.2})$$

with the initial conditions:

$$Y(0) = Y_0, \quad \hat{T}(0) = T_0. \quad (\text{IV.6.3})$$

The independent variable is time and the dependent variables are  $Y$ , the mass fraction of reactant, and temperature  $\hat{T}$ . There are five positive constants: the specific heat  $c$ , the heat of reaction  $Q$ , a pre-exponential factor  $A$ , the activation energy  $E$  and the universal gas constant  $R$ .

Manipulating equations (IV.6.1) and (IV.6.2) shows that  $\hat{T} + QY/c$  is a constant calculable from the initial conditions,  $\hat{T} + QY/c = T_0 + QY_0/c$ . The mass fraction of reactant is eliminated from consideration, and the temperature only equation is

$$\frac{d\hat{T}}{d\hat{t}} = A \left( T_0 + \frac{Q}{c}Y_0 - \hat{T} \right) \exp\left(\frac{-E}{R\hat{T}}\right), \quad \hat{T}(0) = T_0. \quad (\text{IV.6.4})$$

The equation is made dimensionless by defining  $T = \hat{T}/T_0$  and  $t = \hat{t}/t_0$ . The characteristic time is chosen to be

$$t_0 = \frac{cT_0^2R}{AQY_0E} \exp\left(\frac{E}{RT_0}\right) \quad (\text{IV.6.5})$$

which gives

$$\frac{dT}{dt} = \frac{\varepsilon}{\beta} (1 + \beta - T) \exp\left(\frac{T-1}{\varepsilon T}\right), \quad T(0) = 1. \quad (\text{IV.6.6})$$

The *heat release parameter* is denoted as  $\beta = QY_0/(cT_0)$ , and the reciprocal of the *dimensionless activation energy* is denoted by  $\varepsilon = RT_0/E$ .

### IV.6.1 Unique Solution of Initial Value Problem

The initial value problem, equation (IV.6.6), has an unique solution [59, 37] that is monotonically increasing from 1 to  $1 + \beta$  as  $t \rightarrow \infty$ . The solution is given by the implicit relation:

$$t = t_e + t_T \quad (\text{IV.6.7})$$

where

$$t_T = \frac{\beta}{\varepsilon} \left[ \exp\left(-\frac{1}{\varepsilon}\right) \text{Ei}\left(\frac{1}{\varepsilon T}\right) - \exp\left\{-\frac{\beta}{\varepsilon(1+\beta)}\right\} \text{Ei}\left\{\frac{1+\beta-T}{\varepsilon T(1+\beta)}\right\} \right] \quad (\text{IV.6.8})$$

$$t_e = -\frac{\beta}{\varepsilon} \left[ \exp\left(-\frac{1}{\varepsilon}\right) \text{Ei}\left(\frac{1}{\varepsilon}\right) - \exp\left\{-\frac{\beta}{\varepsilon(1+\beta)}\right\} \text{Ei}\left\{\frac{\beta}{\varepsilon(1+\beta)}\right\} \right], \quad (\text{IV.6.9})$$

with the exponential integral function defined as the Cauchy principle value integral

$$\text{Ei}(x) = P.V. \int_{-\infty}^x \frac{e^y}{y} dy. \quad (\text{IV.6.10})$$

The exact solution is often disregarded in combustion reactions involving small  $\varepsilon$  because the solution's behavior is not clearly understood owing to the difficulty of numerically computing the exponential and the exponential integral for large arguments. To alleviate this difficulty, Kassoy [39] constructed an asymptotic approximation to the solution for fixed  $\beta$  and small positive  $\varepsilon$ . It is determined that the time subsequent to the major part of the explosion is given by

$$t^* = 1 + \left(2 + \frac{1}{\beta}\right) \varepsilon + O(\varepsilon^2). \quad (\text{IV.6.11})$$

The numerical solution, presented below, explores the validity of this expansion.

### IV.6.2 The Numerical Solution for the Initial Value Problem

In this problem, it is known that the solution is bounded by  $1 + \beta$  for all time. Thus, a singularity does not exist. However, it is also known that the solution contains regions of extreme stiffness in the limit as  $\varepsilon \rightarrow 0$ . The stiffness is so great that standard adaptive time-step routines fail. Thus, we adapt our proposed routine to handle this integration.

Figure 19(a) shows the solutions with  $\beta = 2$  and  $\varepsilon = \{2, 1, .5, .2, .1\}$  on the interval  $t \in (0, 5)$ . On this time interval, it appears that the solution for  $\varepsilon = .1$  is developing regions

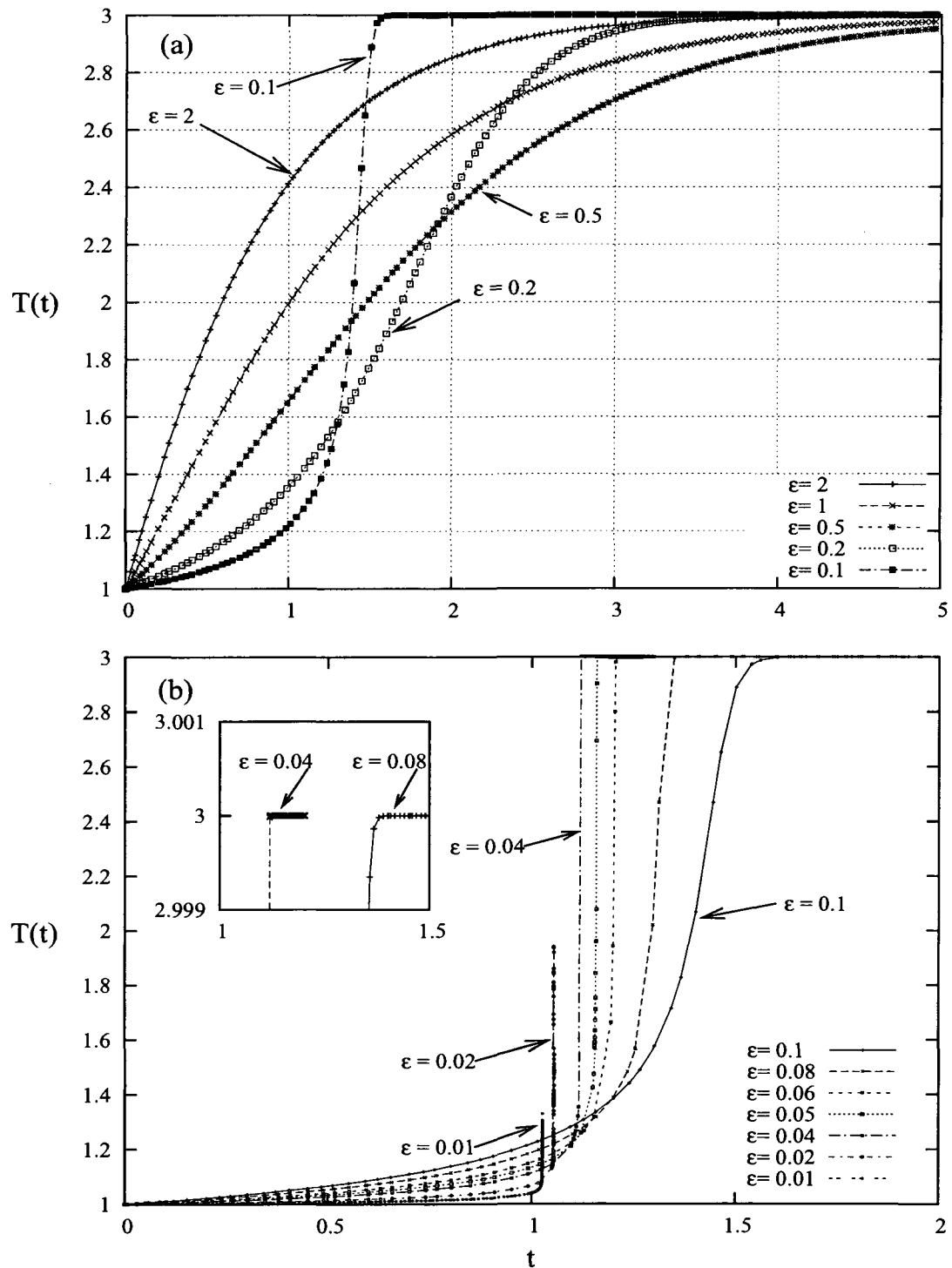


FIG. 19 Solutions of Kassoy problem. (a) Solutions with  $\beta = 2$  and  $\epsilon = \{2, 1, .5, .2, .1\}$  on the interval  $t \in (0, 5)$ . (b) Solutions with  $\beta = 2$  and  $\epsilon = \{.1, .08, .06, .05, .04, .02, .01\}$  on the interval  $t \in (0, 2)$ . The insert shows the approach to the final value  $1 + \beta$  for  $\epsilon = .08$  and  $\epsilon = .04$ . The turn is sharper for small  $\epsilon$ .



of stiffness, especially as the temperature nears the limiting value of  $1 + \beta$ . Figure 19(b) shows the solutions with  $\beta = 2$  and  $\varepsilon = \{.1, .08, .06, .05, .04\}$  on the interval  $t \in (0, 2)$ . On this time interval, the solution for  $\varepsilon = .1$  does not appear to be stiff; however, the solution for  $\varepsilon = .08$  is developing a region of extreme stiffness as the temperature nears the limiting value of  $1 + \beta$ . For the values  $\varepsilon = \{.06, .05, .04\}$ , the solutions show an "almost" singular behavior at finite time, but the solutions reach a value near  $1 + \beta$  where it ceases to grow. The approach to the final value  $1 + \beta$  is seen in the figure insert for  $\varepsilon = .08$  and  $\varepsilon = .04$ . Clearly, the turn becomes sharper as  $\varepsilon$  decreases.

A measure of the stiffness of the solution is the number of refinements of the coarse grid used to capture the structure, and this information is provided in Table 8. Clearly, this number increases as  $\varepsilon \rightarrow 0$  with "extreme stiffness" starting around the value  $\varepsilon = .04$ .

TABLE 8  
*Number of coarse grid refinements vs  $\varepsilon$ .*

$\varepsilon$	number of refinements
0.08	0
0.06	2
0.05	2
0.04	4
0.02	8

Once the solution nears the final value of  $1 + \beta$ , the refinement in the  $\eta$ -grid is not necessary because the solution has lost its stiffness. Thus, we must allow the grid to unrefine or backup in scale. Once refinement of the coarse grid has been initiated, the number of coarse grid steps at each level is counted. If twenty coarse grid steps are executed on any one level, then it is assumed that the integration has passed the region of stiffness. At this point, the coarse grid scale is increased by a factor of ten. This unrefinement of the grid continues until the original time step is reached.

Figure 19(b) also shows the solutions with  $\beta = 2$  and  $\varepsilon = \{.02, .01\}$  on the interval  $t \in (0, 2)$ . One quickly notes that the solution does not continue to its final value of  $1 + \beta$ . For these values of  $\varepsilon$ , the maximum number of refinements is reached as the program attempts to resolve the stiffness in the solution. This maximum number of refinements allowed is based on the numerical precision of the computation; in theory, the maximum number of refinements can be increased by recalculating the solution with greater numerical precision

(say, 128 bit precision rather than 64 bit precision). With greater precision, one expects the solutions for these values of  $\varepsilon$  to have the same properties as the solutions with  $\varepsilon = \{.06, .05, .04\}$ .

Figure 20(a) shows the solutions with  $\beta = 2$  and  $\varepsilon = \{.01, .005, .001\}$  on the interval  $t \in (0, 1.2)$ , and Figure 20(b) shows a close-up of the same solutions on the interval  $t \in (.9, 1.1)$ . Even with the extreme stiffness of the solution, our proposed routine is able to capture the near singularity. Table 9 shows the "blow-up" time as a function of  $\varepsilon$ . From this table, it is clear that we have verified the accuracy of the asymptotic solution (IV.6.11).

TABLE 9  
The "blow-up" time vs  $\varepsilon$ .

$\varepsilon$	$t^*$
0.06	1.4201029887
0.05	1.1889999977
0.04	1.1217996477
0.03	1.0996219149
0.02	1.0542505281
0.01	1.0260021947
0.005	1.0127965757
0.001	1.0025253124
0.0005	1.0012540173
0.0001	1.0002512893

### IV.6.3 Comparison of the Numerical Solution and the Analytic Solution

As mentioned previously, the calculation of the analytic solution presents many numerical difficulties, especially in the limit  $\varepsilon \rightarrow 0$ . Thus, we first investigate the differences between the calculated solution and the numerically evaluated analytic solution for the moderately small value  $\varepsilon = .1$ . This investigation determines that the weakest point of the proposed algorithm is the extrapolation used to terminate the integration at the end of each fine grid calculation.

The analytic solution (IV.6.7) is an implicit relation. Thus, a value of  $t$  is found for each given  $u$ . Figure 21 shows the relative difference in the time variables calculated in the following manner:

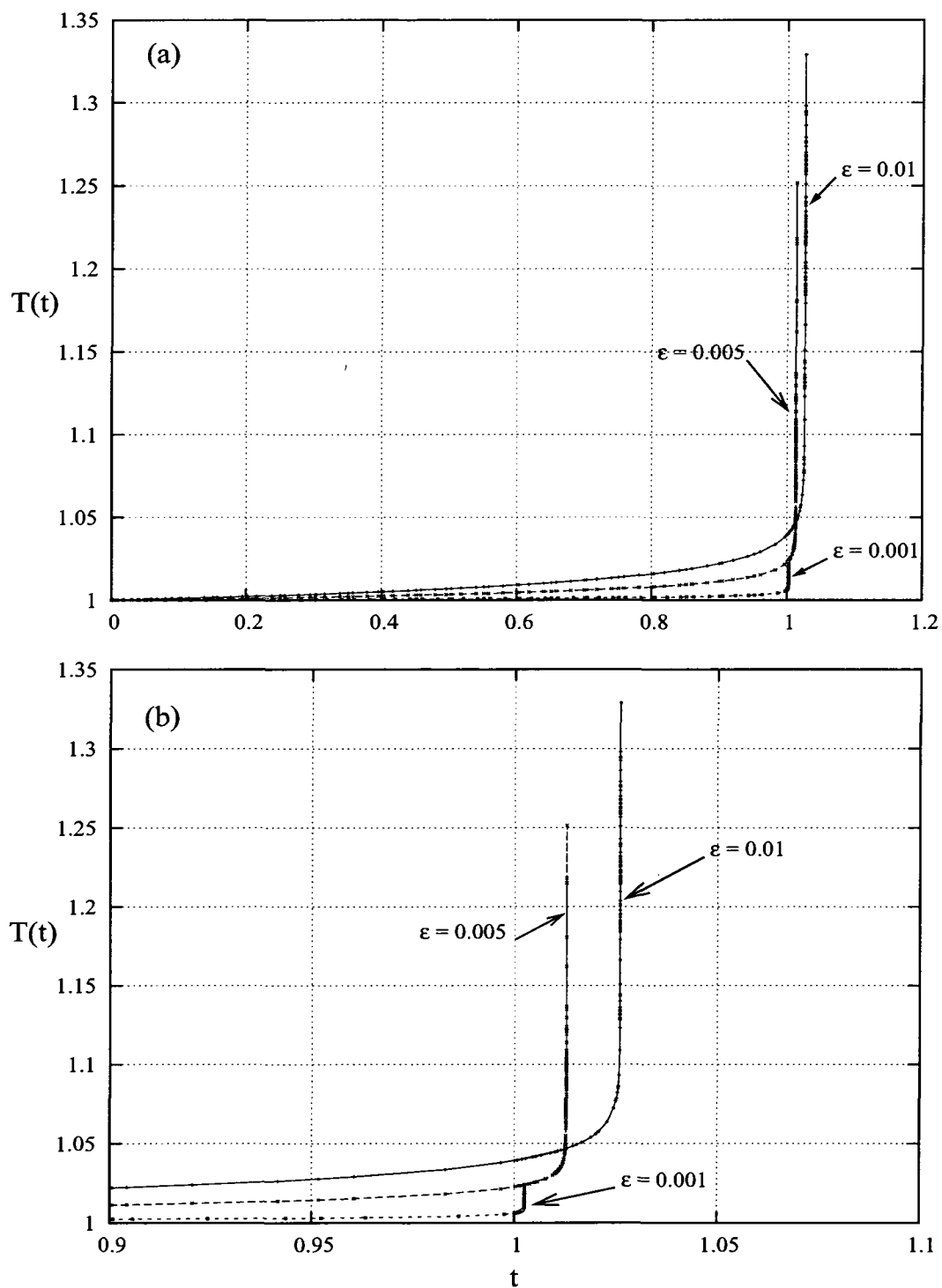


FIG. 20 Solutions of Kasso problem. (a) Solutions with  $\beta = 2$  and  $\epsilon = \{.01, .005, .001\}$  on the interval  $t \in (0, 1.2)$ . (b) Close-up the solutions on the interval  $t \in (.9, 1.1)$ .

- The fine grid solution  $u_{ij}$  is determined for the time variable  $t_{ij} = t_{i+1} - \delta t_i / (1 + \rho_j)$ ,
- The time variable predicted by the numerical evaluation of equation (IV.6.7) for the  $u$  value  $u_{ij}$  is calculated and designated as  $t_{ij}^A$ ,
- The relative difference  $\Delta t_{rel} = (t_{ij}^A - t_{ij}) / t_{ij}$  is determined.

For reference, the solution as a function of time is displayed in Figure 21(c). Figure 21(a) shows the calculated relative difference subject to  $\delta t_i = .1$ , the initial coarse grid spacing,  $\rho_0 = .01$ ,  $\Delta\rho = .01$ , and  $\rho_{max} = \rho_0(1 + \Delta\rho)^{j_{max}}$  with  $j_{max} = 1000$  or  $j_{max} = 2000$ . In proposing the current algorithm, it was assumed that the integration on the fine grid could be terminated by extrapolating to the coarse grid value of  $u = u_{i+1}$  in the limit  $\rho \rightarrow \infty$  (see equation (III.3.5)). In calculating the solution using this early extrapolation, the value of the relative difference is seen to jump at the end of the first coarse grid, and then the relative difference remains steady. Allowing the fine grid integration to proceed until the value  $\rho_{max}$  is achieved reduces the relative difference significantly, and the larger  $\rho_{max}$  produces a smaller relative difference. The calculation of Figure 21(a) is repeated using an initial coarse grid  $\delta t_i = .01$ , and the results are shown in Figure 21(b). As expected, using smaller initial step sizes reduces the relative differences, but highlights the transition between the coarse grids produces the greatest numerical errors. This effect is perhaps greater for an ordinary differential equation as opposed to an integral equation where the effects of these minor errors are "smoothed over" by the integration.

One might be concerned with the great increase in the relative differences in the times that occurs once  $t > 1.5$ ; however, by examining the solution itself, see Figure 21(c), one notices that the solution is extremely close to its maximum value  $u = 1 + \beta$ . Under this circumstance, the difficulty in numerically evaluating the analytic solution (IV.6.7) is greatest. Therefore, we assume the growing differences are attributable to this problem and not the direct numerical evaluation of the differential equation.

In Figure 22, the relative difference calculation of Figure 21 is repeated for  $\varepsilon = .05$ . The solution as a function of time is displayed in Figure 22(c). Figure 22(a) shows the relative difference calculated for the initial coarse grid spacing,  $\delta t_i = .1$ ,  $\rho_0 = .01$ ,  $\Delta\rho = .01$ , and  $\rho_{max} = \rho_0(1 + \Delta\rho)^{j_{max}}$  with  $j_{max} = 1000$  or  $j_{max} = 2000$ . The calculation is repeated using an initial coarse grid  $\delta t_i = .01$ , and the results are shown in Figure 22(b).

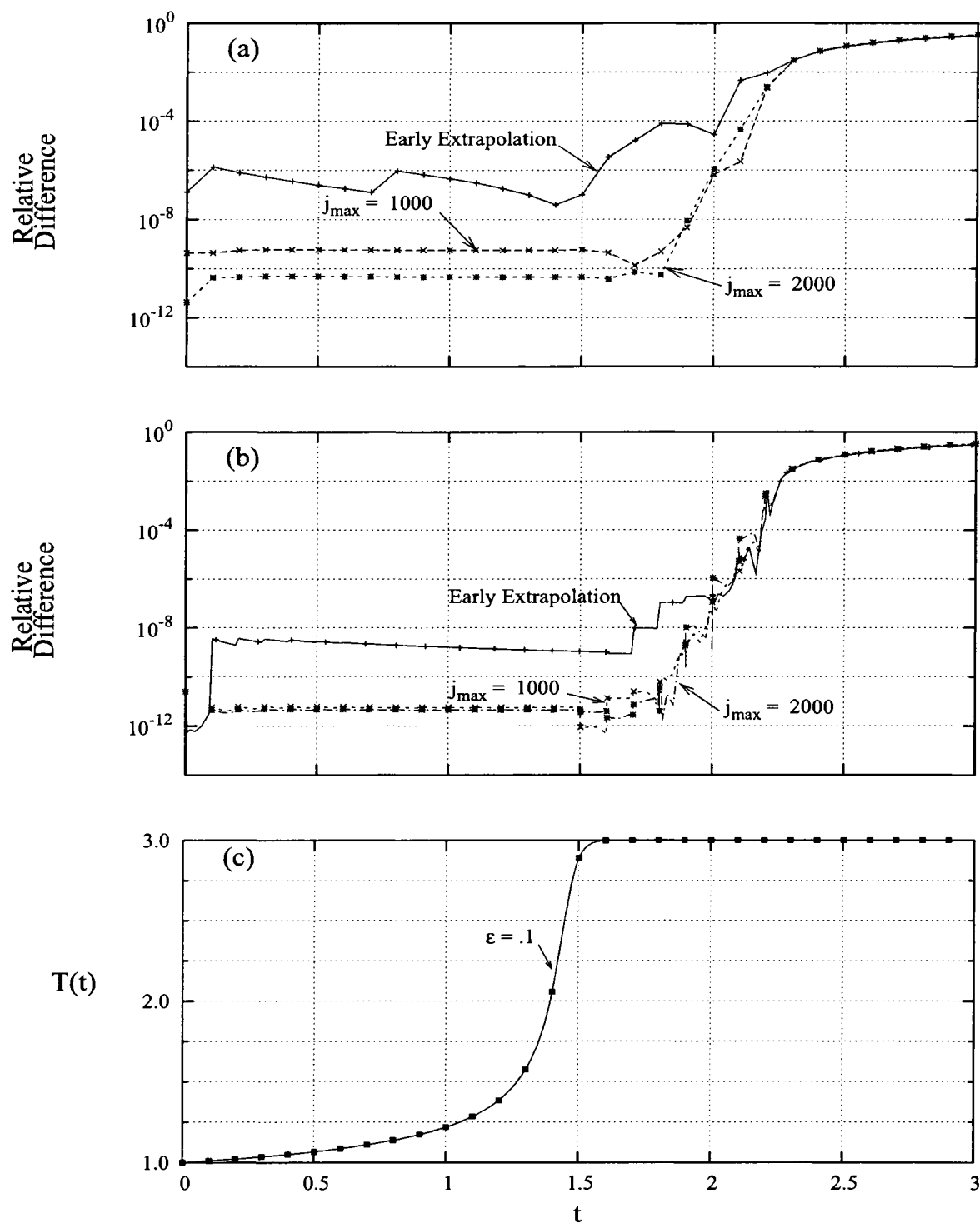


FIG. 21 Comparison of numerical and analytical solution to the Kassoy problem for  $\beta = 2, \epsilon = .1, \delta t_i = .1$ . (a) Relative differences vs time for  $\delta t_i = .1$  (b) Relative differences vs time for  $\delta t_i = .01$  (c) Solution for  $\beta = 2, \epsilon = .1, \delta t_i = .1$ .

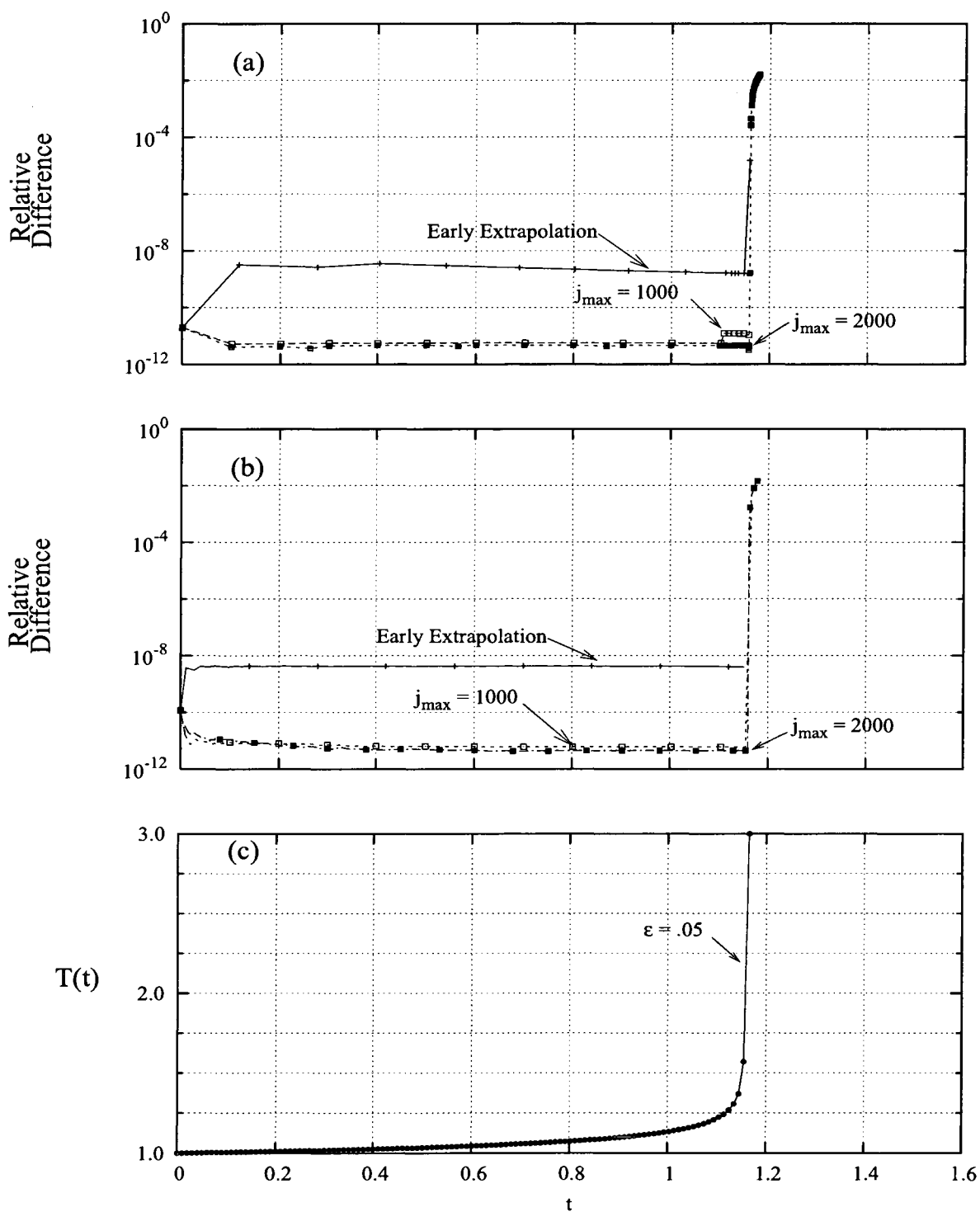


FIG. 22 Comparison of numerical and analytical solution to the Kassoy problem for  $\beta = 2$ ,  $\epsilon = .05$ ,  $\delta t_i = .1$ . (a) Relative differences vs time for  $\delta t_i = .1$  (b) Relative differences vs time for  $\delta t_i = .01$  (c) Solution for  $\beta = 2$ ,  $\epsilon = .05$ ,  $\delta t_i = .1$ .

## CHAPTER V

### CONCLUSIONS

The objective of this research is to develop a simple and consistent approach to determine numerically whether an equation has a singular or non-singular solution on a given interval without constructing an *ad hoc* method based on *a priori* knowledge of the solution. The investigation studied two types of equations: integral equations and ordinary differential equations (ODE's). First, three integral equations were solved using the developed method. The three integral equations are combustion type reaction-diffusion equations with Abel-type singularities in the kernel. In two cases, a parameter determined whether a blow-up solution at a finite value of the independent variable existed or whether a solution existed for all values of the independent variable. This is the first method proposed that is capable of determining both types of solutions with the same scheme.

The proposed method used the following integration criteria (IC):

- IC<sub>1</sub>: the integral is numerically approximated by existing software that accounts for the Abel-type singularity and adapts to a rapidly changing function;
- IC<sub>2</sub>: the singular or non-singular nature of the solution is unambiguously determined on a given time interval;
- IC<sub>3</sub>: if a point of singularity is determined to exist, the time step is adjusted in a straightforward manner to accurately approximate the solution near the singularity.

The first criteria (IC<sub>1</sub>) is satisfied by using quadrature schemes from QUADPACK [61] and by using a cubic-spline interpolation scheme to provide a reasonable approximation to the unknown function for all values of the independent variable. The second criteria (IC<sub>2</sub>) is satisfied by employing a specific change of variables. The third criteria (IC<sub>3</sub>) is satisfied by employing a two-grid method: a coarse grid and a fine grid.

The coarse grid proceeds in the original time variable  $\eta$  while the fine grid proceeds in a pseudo time variable  $\rho$ . Thus, for each new interval, the solution is calculated on the fine grid by time stepping in the  $\rho$  variable. Using the  $\rho$  variable in lieu of  $\eta$  provides a mechanism for satisfying integration criteria (IC<sub>2</sub>). If the blow-up time  $\eta^*$  satisfies  $\eta_i < \eta^* < \eta_{i+1}$ , then the second derivative with respect to  $\rho$  becomes positive on the interval. Otherwise, the second derivative remains negative for the entire interval, and the solution approaches a constant as  $\rho$  approaches infinity. If the solution is determined to

be singular on a given interval, the integration on this interval is discarded, and a smaller value of  $\delta\eta_i$  is chosen. The process continues recursively with the interval containing a singularity being found by using successively smaller  $\delta\eta_i$ . Thus, the time step is adjusted in a straightforward manner near the point of singularity which satisfies integration criteria (IC<sub>3</sub>).

The degree of accuracy possible with this approach was measured by investigating the following four issues:

- How accurate is the numerical integration near the point of singularity?
- How accurate are the cubic-spline interpolations in both the  $\eta$  and  $\rho$  variables?
- How accurate is the determination of second and third derivatives near the point of singularity?
- How does the extrapolation of the solution from the fine grid to the coarse grid affect the solution?

To demonstrate the flexibility of the proposed method, it is applied to ordinary differential equations with blow-up solutions or to ordinary differential equations which exhibit extremely stiff structure. Two of the ordinary differential equations tested are classic "blow-up" problems. The last ODE test equation is a problem with an extremely stiff structure without "blow-up." The proposed method was successful in determining and capturing numerically whether an integral equation or an ordinary differential equation contains a singularity or a region of extreme stiffness. The proposed method of solving the temporal blow-up problem is independent of the solution. If applied to a partial differential equation, the proposed method would be compatible with spatial mesh adaptation that is independent of the solution such as Wavelet Optimized Finite Difference [32]. Applying this method to partial differential equations will be the major focus of future work.



## REFERENCES

- [1] N. AKHMEDIEV AND A. ANKIEWICZ, eds., *Dissipative solitons, Lecture Notes in Physics*, vol. 661, Springer, Heidelberg, 2005.
- [2] R. S. ANDERSSEN AND F. R. DE HOOG, *Abel integral equations*, in Numerical solution of integral equations, vol. 42 of Math. Concepts Methods Sci. Engrg., Plenum, New York, 1990, pp. 373–410.
- [3] C. T. H. BAKER, *A perspective on the numerical treatment of Volterra equations*, J. Comput. Appl. Math., 125 (2000), pp. 217–249. Numerical analysis 2000, Vol. VI, Ordinary differential equations and integral equations.
- [4] J. M. BALL, *Remarks on blow-up and nonexistence theorems for nonlinear evolution equations*, Quart. J. Math. Oxford Ser. (2), 28 (1977), pp. 473–486.
- [5] C. BANDLE AND H. A. LEVINE, *Fujita type results for convective-like reaction diffusion equations in exterior domains*, Z. Angew. Math. Phys., 40 (1989), pp. 665–676.
- [6] ———, *On the existence and nonexistence of global solutions of reaction-diffusion equations in sectorial domains*, Trans. Amer. Math. Soc., 316 (1989), pp. 595–622.
- [7] J. W. BEBERNES AND D. EBERLY, *Mathematical problems from combustion theory*, vol. 83 of Applied Mathematical Sciences, Springer-Verlag, New York, 1989.
- [8] J. W. BEBERNES AND D. R. KASSOY, *A mathematical analysis of blowup for thermal reactions—the spatially nonhomogeneous case*, SIAM J. Appl. Math., 40 (1981), pp. 476–484.
- [9] J. W. BEBERNES AND K. SCHMITT, *On the existence of maximal and minimal solutions for parabolic partial differential equations*, Proc. Amer. Math. Soc., 73 (1979), pp. 211–218.
- [10] J. W. BEBERNES AND W. TROY, *Nonexistence for the Kassoy problem*, SIAM J. Math. Anal., 18 (1987), pp. 1157–1162.
- [11] H. BELLOUT, *A criterion for blow-up of solutions to semilinear heat equations*, SIAM J. Math. Anal., 18 (1987), pp. 722–727.

- [12] B. A. BEL'TJUKOV, *An analogue of the Runge-Kutta method for the solution of nonlinear integral equations of Volterra type*, *Diferencial'nye Uravnenija*, 1 (1965), pp. 545–556.
- [13] A. BLANCHET, J. A. CARRILLO, AND N. MASMOUDI, *Infinite time aggregation for the critical patlak-keller-segel model in  $\mathbb{R}^2$* , CPAMA, (2007), pp. 1–33 (electronic). Early View: online article in advance of print.
- [14] H. BRUNNER, *Collocation methods for Volterra integral and related functional differential equations*, vol. 15 of Cambridge Monographs on Applied and Computational Mathematics, Cambridge University Press, Cambridge, 2004.
- [15] H. BRUNNER, E. HAIRER, AND S. P. NØRSETT, *Runge-Kutta theory for Volterra integral equations of the second kind*, *Math. Comp.*, 39 (1982), pp. 147–163.
- [16] H. BRUNNER AND P. J. VAN DER HOUWEN, *The numerical solution of Volterra equations*, vol. 3 of CWI Monographs, North-Holland Publishing Co., Amsterdam, 1986.
- [17] C. J. BUDD, B. LEIMKUHLE, AND M. D. PIGGOTT, *Scaling invariance and adaptivity*, *Appl. Numer. Math.*, 39 (2001), pp. 261–288. Special issue: Themes in geometric integration.
- [18] C. J. BUDD AND M. D. PIGGOTT, *The geometric integration of scale-invariant ordinary and partial differential equations*, *J. Comput. Appl. Math.*, 128 (2001), pp. 399–422. Numerical analysis 2000, Vol. VII, Partial differential equations.
- [19] C. J. BUDD, V. ROTTSCHÄFER, AND J. F. WILLIAMS, *Multibump, blow-up, self-similar solutions of the complex Ginzburg-Landau equation*, *SIAM J. Appl. Dyn. Syst.*, 4 (2005), pp. 649–678 (electronic).
- [20] C. J. BUDD AND J. F. WILLIAMS, *Parabolic Monge-Ampère methods for blow-up problems in several spatial dimensions*, *J. Phys. A*, 39 (2006), pp. 5425–5444.
- [21] J. C. BUTCHER, *Numerical methods for ordinary differential equations*, John Wiley & Sons Ltd., Chichester, second ed., 2008.
- [22] I. FATKULLIN AND J. S. HESTHAVEN, *Adaptive high-order finite-difference method for nonlinear wave problems*, *J. Sci. Comput.*, 16 (2001), pp. 47–67.

- [23] G. E. FORSYTHE, M. A. MALCOLM, AND C. B. MOLER, *Computer Methods for Mathematical Computations*, Prentice Hall, Englewood Cliffs, NJ, USA, 1977.
- [24] D. A. FRANK-KAMENETSKII, *Diffusion and Heat Exchange in Chemical Kinetics*, Princeton University Press, Princeton, 1955.
- [25] A. FRIEDMAN AND A. A. LACEY, *The blow-up time for solutions of nonlinear heat equations with small diffusion*, SIAM J. Math. Anal., 18 (1987), pp. 711–721.
- [26] ———, *Blowup of solutions of semilinear parabolic equations*, J. Math. Anal. Appl., 132 (1988), pp. 171–186.
- [27] A. FRIEDMAN AND B. MCLEOD, *Blow-up of positive solutions of semilinear heat equations*, Indiana Univ. Math. J., 34 (1985), pp. 425–447.
- [28] H. FUJITA, *On the blowing up of solutions of the Cauchy problem for  $u_t = \Delta u + u^{1+\alpha}$* , J. Fac. Sci. Univ. Tokyo Sect. I, 13 (1966), pp. 109–124 (1966).
- [29] R. T. GLASSEY, *On the blowing up of solutions to the Cauchy problem for nonlinear Schrödinger equations*, J. Math. Phys., 18 (1977), pp. 1794–1797.
- [30] E. HAIRER, C. LUBICH, AND M. SCHLICHTE, *Fast numerical solution of weakly singular Volterra integral equations*, J. Comput. Appl. Math., 23 (1988), pp. 87–98.
- [31] K. HAYAKAWA, *On the nonexistence of global solutions of some semilinear parabolic equations*, Proc. Japan Acad. Ser. A Math, 49 (1973), pp. 503–505.
- [32] J. S. HESTHAVEN AND L. M. JAMESON, *A wavelet optimized adaptive multi-domain method*, J. Comput. Phys., 145 (1998), pp. 280–296.
- [33] T. HILLEN AND H. G. OTHMER, *The diffusion limit of transport equations derived from velocity-jump processes*, SIAM J. Appl. Math., 61 (2000), pp. 751–775 (electronic).
- [34] C. HIROTA AND K. OZAWA, *Numerical method of estimating the blow-up time and rate of the solution of ordinary differential equations—an application to the blow-up problems of partial differential equations*, J. Comput. Appl. Math., 193 (2006), pp. 614–637.
- [35] H. M. JONES AND S. MCKEE, *Variable step size predictor-corrector schemes for second kind Volterra integral equations*, Math. Comp., 44 (1985), pp. 391–404.

- [36] A. K. KAPILA, *Reactive-diffusive system with Arrhenius kinetics: dynamics of ignition*, SIAM J. Appl. Math., 39 (1980), pp. 21–36.
- [37] ASHWANI K. KAPILA, *Asymptotic treatment of chemically reacting systems*, Applicable Mathematics Series, Pitman (Advanced Publishing Program), Boston, MA, 1983.
- [38] S. KAPLAN, *On the growth of solutions of quasi-linear parabolic equations*, Comm. Pure Appl. Math., 16 (1963), pp. 305–330.
- [39] D. R. KASSOY, *Extremely rapid transient phenomena in combustion, ignition and explosion*, in Asymptotic methods and singular perturbations (Proc. SIAM-AMS Sympos. Appl. Math., New York, 1976), Amer. Math. Soc., Providence, R.I., 1976, pp. 61–72. SIAM-AMS Proceedings, Vol. X.
- [40] —, *The supercritical spatially homogeneous thermal explosion: Initiation to completion.*, Quart. J. Mech. Appl. Math., 30 (1977), pp. 71–89.
- [41] D. R. KASSOY AND A. LIÑÁN, *The influence of reactant consumption on the critical conditions for homogeneous thermal explosions*, Quart. J. Mech. Appl. Math., 31 (1978), pp. 99–112.
- [42] D. R. KASSOY AND J. POLAND, *The thermal explosion confined by a constant temperature boundary. I. The induction period solution*, SIAM J. Appl. Math., 39 (1980), pp. 412–430.
- [43] —, *The thermal explosion confined by a constant temperature boundary. II. The extremely rapid transient*, SIAM J. Appl. Math., 41 (1981), pp. 231–246.
- [44] E. F. KELLER AND L. A. SEGEL, *Initiation of slime mold aggregation viewed as an instability*, J. Theor. Biol., 26 (1970), pp. 399–415.
- [45] —, *Model for chemotaxis*, J. Theor. Biol., 30 (1971), pp. 225–234.
- [46] A. A. LACEY, *Mathematical analysis of thermal runaway for spatially inhomogeneous reactions*, SIAM J. Appl. Math., 43 (1983), pp. 1350–1366.
- [47] —, *The form of blow-up for nonlinear parabolic equations*, Proc. Roy. Soc. Edinburgh Sect. A, 98 (1984), pp. 183–202.

- [48] —, *Diffusion models with blow-up*, J. Comput. Appl. Math., 97 (1998), pp. 39–49.
- [49] D. G. LASSEIGNE AND W. E. OLMSTEAD, *Ignition of a combustible solid with reactant consumption*, SIAM Journal on Applied Mathematics, 47 (1987), pp. 332–342.
- [50] —, *Ignition or nonignition of a combustible solid with marginal heating*, Quart. Appl. Math., 49 (1991), pp. 303–312.
- [51] H. A. LEVINE, *The role of critical exponents in blowup theorems*, SIAM Rev., 32 (1990), pp. 262–288.
- [52] A. LIÑÁN AND F. A. WILLIAMS, *Theory of ignition of a reactive solid by constant energy flux*, Combustion Science and Technology, 3 (1971), pp. 91–98.
- [53] —, *Ignition of a reactive solid exposed to a step in surface temperature*, SIAM Journal on Applied Mathematics, 36 (1979), pp. 587–603.
- [54] C. LUBICH, *Fractional linear multistep methods for Abel-Volterra integral equations of the second kind*, Math. Comp., 45 (1985), pp. 463–469.
- [55] —, *Discretized fractional calculus*, SIAM J. Math. Anal., 17 (1986), pp. 704–719.
- [56] W. E. OLMSTEAD, *Ignition of a combustible half space*, SIAM Journal on Applied Mathematics, 43 (1983), pp. 1–15.
- [57] W. F. OSGOOD, *Beweis der existenz einer lösung der differentialgleichung  $dy / dx = f(x, y)$  ohne hinzunahme der cauchy-lipschitz'schen bedingung*, MMP, 9 (1898), pp. 331–345.
- [58] H. G. OTHMER AND T. HILLEN, *The diffusion limit of transport equations. II. Chemotaxis equations*, SIAM J. Appl. Math., 62 (2002), pp. 1222–1250 (electronic).
- [59] M. PARANG AND M.C. JISCHKE, *Adiabatic ignition of homogeneous systems*, AIAA Journal, 13 (1975), pp. 405–408.
- [60] C. S. PATLAK, *Random walk with persistence and external bias*, Bull. Math. Biophys., 15 (1953), pp. 311–338.

- [61] R. PIESSENS, E. DE DONCKER-KAPENGA, C. W. UBERHUBER, AND D. K. KAHANER, *QUADPACK A subroutine package for automatic integration*, Springer Verlag, 1983.
- [62] P. POUZET, *Étude en vue de leur traitement numérique des équations intégrales de type Volterra*, Rev. Franç. Traitement Information Chiffres, 6 (1963), pp. 79–112.
- [63] WILLIAM H. PRESS, SAUL A. TEUKOLSKY, WILLIAM T. VETTERLING, AND BRIAN P. FLANNERY, *Numerical recipes in FORTRAN*, Cambridge University Press, Cambridge, second ed., 1992. The art of scientific computing, With a separately available computer disk.
- [64] L. R. RITTER, W. E. OLMSTEAD, AND V. A. VOLPERT, *Initiation of free-radical polymerization waves*, SIAM J. Appl. Math., 63 (2003), pp. 1831–1848 (electronic).
- [65] C. A. ROBERTS, D. G. LASSEIGNE, AND W.E. OLMSTEAD, *Volterra equations which model explosion in a diffusive medium*, J. Integral Equations Appl., 5 (1993), pp. 531–546.
- [66] A. SCOTT, *Nonlinear Science Emergence and Dynamics of Coherent Structures*, Oxford University Press, Oxford, 2003. Second Edition.
- [67] A. R. SOHEILI AND J. M. STOCKIE, *An adaptive mesh method with variable relaxation time*, J. Franklin Inst., 344 (2007), pp. 757–764.
- [68] C. TURNER AND R. D. HAYNES, *A numerical and theoretical study of blow-up for a system of ordinary differential equations using the sundman transformation*, AEJM, 2 (2007), pp. 1–13.
- [69] S. N. VLASOV, V. A. PETRISHCHEV, AND V. I. TALANOV, *Averaged description of wave beams in linear and nonlinear media (the method of moments)*, Radiophys. and Quant. Electr., 14 (1971), pp. 1062–1070.
- [70] S. WANG, *Blowup in Nonlinear Heat Equations*, PhD thesis, University of Notre Dame, Notre Dame, Indiana, 2006.
- [71] M. I. WEINSTEIN, *Nonlinear Schrödinger equations and sharp interpolation estimates*, Comm. Math. Phys., 87 (1982/83), pp. 567–576.

- [72] F. B. WEISSLER, *Existence and nonexistence of global solutions for a semilinear heat equation*, Israel J. Math., 38 (1981), pp. 29–40.

## VITA

Charles F. Touron

Department of Computational and Applied Mathematics

Old Dominion University

Norfolk, VA 23529

### Education

Ph.D. Old Dominion University, Norfolk, VA, 2009.

Major: Computational and Applied Mathematics

M.S. Old Dominion University, Norfolk, VA, 2003.

Major: Computational and Applied Mathematics

M.A. East Carolina University, Greenville, NC, 1999.

Major: Pure Mathematics

B.S. Elon College, Elon College, NC, 1994.

Major: Mathematics

A.B. Elon College, Elon College, NC, 1994.

Major: Physics